People's Democratic Republic of Algeria
Ministry of Higher Education and Scientific Research
University of Oum El Bouaghi
Faculty of: Sciences and Applied Sciences

Thesis

Presented to obtain

3rd Cycle Doctorate

Branch: Electronic

Specialty: Microelectronics

Title :

Design of nanosized plasmonic structure for Biosensing applications

Presented by:

Hocine Bahri

Publicly defended on 06/12/2023 in front of the following committee members:

N°	First and last name	Grade	University	Quality
01	Mr. Mohamed LASHAB	Prof.	University of Oum El Bouaghi	President
02	Mr. Souheil MOUETSI	Prof	University of Oum El Bouaghi	Supervisor
03	Mr. Abdesselam HOCINI	Prof	University of M'sila	Co-reporter
04	Mr. Djamel Khedrouche	Prof	University of M'sila	Examiner
05	Mr. Remache Louardi	Prof	University of Oum El Bouaghi	Examiner
06	Mr. Skander ARIS	MCA	University of Constantine 1	Examiner

Année académique 2023-2024

Travaux réalisés au Laboratoire d'Electronique et des Nouvelles Technologies (LENT),
Faculté des Sciences et Sciences Appliquées, Département de Génie Electrique,
Université Oum El Bouaghi, Pôle d'Ain El Beida. Algéri

Dedicated

I dedicate this work to all who are dear to me.

To my dear parents, for all their sacrifices, their love, their tenderness, their support and their prayers throughout my studies,

To my dear wife, forl all her sacrifices, support, love

To my dear brothers and sisters,

To all the members of my family,

To all my friends, relatives and colleagues.

Acknowledgment

I wish to begin by expressing my profound gratitude to the Almighty Allah for bestowing upon me the strength, health, resilience, and determination that have sustained me through the challenging years of training and research.

It is both an honor and a privilege to extend my heartfelt thanks to Prof. HOCINI Abdesselam and to Prof. Mouetsi Souheil , my esteemed thesis advisors. Their unwavering guidance, invaluable advice, trust, and boundless patience have served as the bedrock of my research journey. Their moral support and encouragement have been an endless source of inspiration, and I hold them in the highest regard for their contributions to my academic and personal development.

I would also like to express my deepest appreciation to the distinguished individuals who have graciously agreed to serve on my thesis jury. Their expertise and thoughtful evaluation are absolutely crucial to the successful completion of this work, and I am profoundly grateful for their vital role in this important process.

To the members of the jury:

Mohamed LASHAB, Professor at the University of Oum elbouaghi, for doing me the honor of participating in my thesis jury as President. I am sincerely grateful for all the relevant comments and for his interest in this work;

Djamel Khedrouche, Professor at the University of M'sila, for his interest in this work and for agreeing to be an examiner for this thesis and for all the relevant comments;

Remache Louardi, Professor at Oum Elbouaghi University, for his interest in this work and for honoring me by agreeing to examine it and for all the relevant comments;

Skander ARIS at University of Constantine 1, for the interest he showed in my work and for the honor he did me by agreeing to examine it by participating in the thesis jury;

I would like to thank all the members of the electronics and new technology laboratory of the University of Larbi Ben M'hidi, as well as the signals and systems analysis laboratory of the University of M'sila;

My deep gratitude goes to all the professors and administrators of the sciences and applied sciences faculty at the university of Oum el bouaghi.

Furthermore, I extend my heartfelt thanks to Dr. Vivek Pachauri from RWTH Aachen University for his invaluable support, trust, and unwavering guidance throughout the course of my thesis research. His contribution has been pivotal to the successful completion of this research, and I am genuinely appreciative of his involvement.
To all those who have played a role in my academic and personal growth during this journey, I offer my profound thanks for their significant contributions and unwavering support.

List of acronyms and abbreviations

In this document, we have used some abbreviations of which we recall the meaning below:

$\boldsymbol{\omega_p}$: Plasma frequency.

$\boldsymbol{\lambda}$ **:** Wavelength.

$\boldsymbol{\lambda_m}$ **:** Resonance wavelength.

$\boldsymbol{\varepsilon_m}$ **:** Complex permissiveness of metal

n **:** Refraction Index.

$\boldsymbol{N_{eff}}$ ***:*** effective refraction index.

PS: Plasmons of the surface.

SPP: Polarity of surface plasmons.

K : vector of wave

.$\boldsymbol{k_{spp}}$**:** Wave vector of surface plasmon polarities..

TE: The transverse electricity.

TM: The magnetic transverse.

$\boldsymbol{L_{spp}}$ **:** The length of propagation.

FOM: Figure of Merit.

FWHM: Breadth at the height of the peak.

MIM : Metal-Isolating Metal.

FDTD: Method of Finite Time Differences.

PML: Perfectly Matched Layer

SPR: Surface Plasmon Resonance

BC: The boundary condition.

S: The sensitivity of the sensor.

List of figures

the transmission spectra versus the resonancewavelength for refractive index of the temper ambient from T=100 to -100 with a step of 400C.

Figure VI.20: (a) The schematic diagram of the proposed sensor structure with discontinue waveguide with a distance of C. (b) The transmission spectra versus the resonance wavelength for different states with continuum waveguide for g= 10–0 nm and discontinuewaveguide for g= 0 and C= 50, 200 nm.

List of Tables

Summary

Surface Plasmon polaritons (SPPs) are surface electromagnetic waves propagating along a metal-dielectric interface and have great potential applications in the realization of highly integrated optical circuits due to their capability to overcome the diffraction limit of light. Nano-plasmonic waveguides, supporting the propagation of SPPs and manipulating light on a sub-wavelength scale, can be regarded as an ideal optical element in an integrated plasmonic device. There are various SPPs-based waveguides, for instance, strip waveguides, semiconductor–insulator–semiconductor (SIS) waveguides, metal-insulator-metal (MIM) waveguides, and trench waveguides. Among these, the MIM waveguide has better properties, for instance, stronger confinement of light, shorter propagation length, smaller mode size, and low fabrication cost. To date a number of optical devices of the MIM waveguide structure have been extensively studied, for example, nano-sensors, demultiplexers and filters.

The introduction of cavities with defects in the conventional MIM waveguide ensured a longer interaction between the SPP modes produced and the molecules under test presented in the active region of the sensor. In all MIM structures, the plasmon resonator is the critical part that influences the detection and transmission characteristics of the devices.

In this context, this thesis aims the study and design of plasmonic nano-sensors based on two-dimensional metal-insulator-metal (MIM) waveguides made of silver for metal, for refractive index measurements (RI), for integrated optics application. The goal is to optimize the sensitivity and the transmission of these nano-sensors according to the physical and geometric parameters. To do this, we focus in our study on three concepts of RI nano-sensors with MIM plasmonic structures. The first structure concerns a MIM waveguide coupled by a hexagonal shaped ring resonator for a near infrared refractive index sensor. In this structure, the maximum linear sensitivity is S = 2220 nm / RIU and S = 3010 nm / RIU for mode 1 and mode 2 respectively. In the second structure, we propose a MIM waveguide coupled to intersected double cavity ring resonators for a refractive index sensor. In this structure, and after optimization of its structural parameters, the maximum linear sensitivity obtained is S = 4508 nm / RIU. The third structure concerns a simple design of mid infrared high sensitive metal-insulator-metal plasmonic sensor. In this structure, and after optimization of its structural parameters, the maximum linear sensitivity obtained is S = 5155 nm / RIU. In the three concepts of RI nano-sensors; the simplicity, the sensitivity of detection and the level of the transmission

spectrum which can be easily controlled by manipulating the structural parameters; are the main advantages of these structures.

Keywords: Surface plasmon polariton (SPP) – Metal – insulator – metal (MIM) waveguide - Refractive index sensor – FDTD.

Résumé

Les polaritons de plasmon de surface (SPP) sont des ondes électromagnétiques de surface se propageant le long d'une interface métal-diélectrique et ont un grand potentiel d'application dans la réalisation de circuits optiques à très haute intégration en raison de leur capacité à surmonter la limite de diffraction de la lumière. Les guides d'ondes nano-plasmoniques, favorisant la propagation des SPP et manipulant la lumière à une échelle de longueur d'onde inférieure, peuvent être considérés comme un élément optique idéal dans un dispositif plasmonique intégré. Il existe différents guides d'ondes basés sur les SPP, par exemple des guides d'ondes semi-conducteur-isolant-semi-conducteur (SIS), guides d'onde isolant-métal-isolant (IMI) et guides d'onde métal-isolant-métal (MIM). Parmi ceux-ci, le guide d'onde MIM a de meilleures propriétés, par exemple, confinement plus fort de la lumière, longueur de propagation plus courte, taille de mode plus petite, et facilité et faible coût de fabrication. À ce jour, un certain nombre de dispositifs optiques de la structure de guide d'ondes MIM ont été largement étudiés, par exemple, les nano-capteurs, les démultiplexeurs et les filtres.

L'introduction de cavités présentant des défauts dans le guide d'ondes MIM conventionnel a garanti une interaction plus longue entre les modes SPP produits et les molécules sous test présentées dans la région active du capteur. Dans toutes les structures MIM, le résonateur plasmonique est la partie critique qui influence les caractéristiques de détection et la transmission des dispositifs.

Dans ce contexte, cette thèse vise à étudier et à concevoir des nano-capteurs plasmoniques à base de guides d'onde métal-isolant-métal (MIM) bidimensionnels, constitués d'argent pour le métal, pour les mesures d'indice de réfraction (RI) pour des applications en optique intégrée. L'objectif est d'optimiser la sensibilité et la transmission de ces nano-capteurs en fonction des paramètres physiques et géométriques. Pour cela, nous nous sommes basés dans notre étude sur trois concepts de nano-capteurs RI aux structures plasmoniques MIM. La première structure proposée est un guide d'ondes MIM couplé à un résonateur annulaire de forme hexagonale pour un capteur d'indice de réfraction proche infrarouge. Dans cette structure, la sensibilité linéaire maximale est S = 2220 nm / RIU et S = 3010 nm / RIU, pour le *mode 2* et le *mode 1*

respectivement. La deuxième structure concerne un guide d'ondes MIM couplé à des résonateurs annulaires à double cavité intersectée pour un capteur d'indice de réfraction. Dans cette structure, et après optimisation de ces paramètres structurels, la sensibilité linéaire maximale obtenue est S = 4508 nm / RIU. La troisième structure concerne un simple capteur d'indice de réfraction plasmonique infrarouge moyen à haute sensibilité. Dans cette structure, et après optimisation de ces paramètres structurels, la sensibilité linéaire maximale obtenue est S = 5155 nm / RIU. Dans les trois concepts de nano-capteurs RI proposé ; la simplicité, la sensibilité de détection et le niveau de spectre de transmission qui peut être facilement contrôlé en manipulant les paramètres structurels, sont les principaux avantages de ces structures.

Mots clés : Polaritons de plasmon de surface (SPP) - Guide d'ondes métal– isolant–métal (MIM) - Capteur d'indice de réfraction – FDTD.

الملخص

بولاريتون البلازمون السطحي (SPP) عبارة عن موجات كهرومغناطيسية سطحية تنتشر على طول واجهة معدنية عازلة ولها تطبيقات محتملة كبيرة في صنع دوائر ضوئية متكاملة للغاية نظرًا لقدرتها على التغلب على محدودية انحراف الضوء. يمكن اعتبار أدلة الموجات النانوية ، التي تعزز انتشار SPP وتعالج الضوء على مقياس أطوال موجية أقل ، عنصرًا بصريًا مثاليًا في جهاز بلازمونيك مدمج.هناك أدلة موجية مختلفة تعتمد على SPP ، على سبيل المثال ، أدلة موجية لأشباه الموصلات - عازل - أشباه موصلات (SIS) ، أدلة موجية عازل – معدن - عازل (IMI) ، وأدلة موجية معدن- عازل - معدن (MIM). من بينها ، يتميز الدليل الموجي MIM بخصائص أفضل ، على سبيل المثال ، حبس أقوى للضوء ، طول انتشار أقصر ، حجم وضع أصغر وتكلفة تصنيع سهلة ومنخفضة. حتى الآن ، تم فحص عدد من الأجهزة البصرية لهيكل الدليل الموجي MIM على نطاق واسع ، على سبيل المثال ، مستشعرات النانو ، وأجهزة إزالة تعدد الإرسال والمرشحات.

كفل إدخال التجاويف التي بها عيوب في الدليل الموجي MIM تفاعلًا أطول بين أوضاع SPP المنتجة والجزيئات قيد الاختبار المعروضة في المنطقة النشطة من المستشعر. في جميع هياكل MIM ، يعتبر مرنان البلازمونيك هو الجزء الحاسم الذي يؤثر على خصائص الكشف والإرسال للأجهزة.

في هذا السياق ، تهدف هذه الأطروحة إلى دراسة وتصميم مستشعرات النانو البلازمية بناءً على أدلة موجية ثنائية الأبعاد (MIM) المكونة من الفضة للمعدن لقياسات معامل الانكسار (RI) للتطبيق في البصريات المتكاملة. الهدف هو تحسين حساسية هذه المستشعرات النانوية ونقلها وفقًا للمعايير الفيزيائية والهندسية. لهذا ، استندنا في دراستنا إلى ثلاثة مفاهيم لمستشعرات النانو RI مع هياكل البلازمونيك. يقدم الهيكل الأول؛ دليل موجي MIM مقترن بمرنان حلقة سداسية الشكل لمستشعر معامل الانكسار القريب من الأشعة تحت الحمراء. في هذا الهيكل، يكون الحد الأقصى للحساسية الخطية = S للوضع 2 والوضع 1 على التوالي. يقدم الهيكل الثاني ؛ دليل موجي MIM S = 2220 nm / RIU 3010 nm / RIU مقترن بمرنان حلقة تجويف مزدوجة متقاطعة لجهاز استشعار معامل الانكسار. في هذا الهيكل، وبعد تحسين المعلمات الهيكلية، يكون الحد الأقصى للحساسية الخطية التي تم الحصول عليها هوS = 4508 nm / RIU. يقترح الهيكل الثالث

تصميم بسيط لمستشعرMIM بلازمونيك عالي الحساسية للأشعة تحت الحمراء المتوسطة. في هذا الهيكل، وبعد تحسين المعلمات الهيكلية، يكون الحد الأقصى للحساسية الخطية التي تم الحصول عليها هو S= 5155 nm/RIU. في المفاهيم الثلاثة لمستشعرات النانو RI ؛ بساطة وحساسية الكشف ومستوى طيف الإرسال الذي يمكن التحكم فيه بسهولة عن طريق معالجة المعلمات الهيكلية ؛ هي المزايا الرئيسية لهذه الهياكل.

الكلمات المفتاحية :بولاريتون البلازمون السطحي (SPP) - دليل موجي معدن- عازل- معدن (MIM) -مستشعر معامل الانكسار- FDTD.

Table of Contents

Chapter II
Resonance sensor for surface plasmons

Chapter III
Guidance and sensing properties of a plasmonic guide MIM

CHAPTER IV

Results and Explanations

General introduction

General introduction

In the early 1980s, the emergence of nanotechnologies catalyzed a significant paradigm shift across scientific disciplines, particularly impacting optics. Modern optics, in stark contrast to its classical counterpart with macroscale mirrors and lenses, now centers on the manipulation of individual photons, leading to the domain of photonics. This transition underscores a notable departure from conventional optics.

Photonics has unlocked the ability to exert control over the propagation of light on a scale closely aligned with the guided wavelength, enabling the engineering of photonic structures. However, as electronic circuits continue to shrink to nanometric dimensions, the goals of photonics, especially in the near future, revolve around the creation of optical nano-circuits analogous to their electronic counterparts, designed to process information encoded in optical signals. Yet, a substantial challenge arises as optical component dimensions reduce, causing light diffraction. In essence, a light wave constrained within a photonic guide can disperse provided that the cross-sectional dimension of the guide is at least half the guided wavelength divided by the optical guide index [1]. This limitation imposes a fundamental constraint on the design of photonic nano-circuits.

To address this limitation, a promising discipline, known as plasmonics, has emerged in the last decade, acting as a derivative of nano-photonics. Plasmonics capitalizes on the unique physical properties of surface electromagnetic modes, specifically the surface plasmon-polariton (SPP).

Surface plasmon-polaritons (SPPs) represent electromagnetic waves that propagate along the interface between a metal and a dielectric. SPPs have the capability to transcend the constraints of light diffraction, thus facilitating the transport of energy and information. They are held in high regard as one of the most promising avenues for the development of highly integrated optical circuits within future nano-photonic systems. Among the architectures used for guiding SPPs, the Metal-Isolating-Metal Wave Guide Structure (MIM) stands as a popular choice. MIM features two closely spaced metallic-dielectric interfaces that guide SPPs along the interface. Due to their extended propagation distances and robust field confinement, MIM structures have found utility in various SPP optical components, encompassingfilters [2], switches [3], couplers [4], separators [5], nano-lenses [6] and sensors [7-8].

Plasmonic sensor technology harbors immense potential for overcoming issues related to sensitivity and accuracy. Moreover, the nanoscale realm of this plasmonic phenomenon paves the way for device miniaturization and offers compelling prospects for various applications, especially in the domain of biosensor technology. Integrated biosensors, characterized by their compact size, reduced weight, lower cost, and promise of parallel monitoring and analysis, open up new avenues for sensitive detection that were previously unattainable within macroscopic sensor configurations.

Since the refractive index of any substance is linked to different parameters, the manufacture of various sensors for measuring temperature, pressure, humidity and concentration of chemicals [9] are applicable.

Nevertheless, plasmonic sensors are currently grappling with the challenge of low sensitivity. Researchers are actively exploring strategies to surmount this limitation, which includes optimizing the geometric structure of the device by introducing cavities to facilitate the recirculation of optical and plasmonic resonance waves. It is envisaged that the judicious design of an MIM resonator structure in a sensor configuration will significantly augment the sensitivity of the resulting detection apparatus.

In recent times, scientific efforts have been directed towards the study of plasmonic nano-sensors based on MIM waveguides.

CHAPITRE I

Generalities on Surface Plasmons

I.1 Introduction

The term "surface plasmons" pertains to electromagnetic modes that propagate along the interface of a conductor and a dielectric medium. These modes exhibit distinctive properties that render them highly significant in the advancement of novel optoelectronic materials [1]. Their confinement to the conductor-dielectric boundary makes them particularly responsive to alterations in the surface structure, facilitating facile manipulation through material structuring. In the introductory chapter of this study, we shall elucidate the foundational principles necessary for comprehending surface plasmons, encompassing their diverse modes of observation and coupling.

A comprehensive understanding of surface plasmons necessitates an initial review of Drude's model for the dielectric constant of metals, as the unique characteristics of metals underpin the introduction of guided light modes at the conductor-dielectric interface, which we identify as surface plasmons. Within this chapter, an exhaustive analysis of the dispersion relationship governing surface plasmons will be undertaken, which prescribes specific geometric considerations for their observation. Furthermore, we shall provide a succinct overview of the physical attributes relevant to classical prisms [2] or network coupling, given their relevance to the manipulation and comprehension of surface plasmons.

The exploration of surface plasmons carries substantial implications for the field of optoelectronics, offering distinct opportunities for controlling and managing light at nanoscale interfaces.

I.2 Definition of plasma

Plasma is a highly energetic and electrically conductive state of matter. Unlike solids, liquids, and gases, which consist of atoms or molecules, plasma is made up of charged particles. These charged particles are primarily electrons and ions, which are atoms that have lost or gained one or more electrons.

The creation of plasma typically involves supplying a significant amount of energy to a gas, which causes its atoms to ionize. This can occur through various means, such as heating to high temperatures, exposing it to strong electromagnetic fields, or subjecting it to intense radiation.

Plasma exhibits several fascinating properties:

Conductivity: Plasma is an excellent conductor of electricity because of the presence of free-moving electrons. This property makes it crucial in various technological applications, including fusion energy research and some types of industrial processing.

Emission of Light: Many plasmas emit light, and this property is exploited in applications like neon signs, fluorescent lights, and certain types of lighting used in laboratories.

Magnetic Responsiveness: Plasma can respond to magnetic fields, and this characteristic is essential in magnetic confinement devices used in fusion research, such as tokamaks and stellarators.

Diverse Occurrence: Plasma is not just limited to man-made applications. It is the most abundant state of matter in the universe, found in stars like the Sun, lightning, and even the Earth's ionosphere.

Variability: Plasmas can exhibit different properties depending on their temperature, pressure, and the types of particles involved. These variations can range from low-temperature, weakly ionized plasmas to extremely hot and dense plasmas.

In summary, plasma is a high-energy, electrically conductive state of matter characterized by the presence of charged particles, making it a critical component of various natural and technological processes, from the stars in the sky to the devices we use on Earth

.I.2.1 Plasma waves in a metal

When an electromagnetic wave, like light, hits a metal, it causes the electrons in the metal to start moving back and forth. This movement is due to the influence of the electromagnetic field and is often described as oscillation.

A force called the Lorentz force affects these electrons, and they move within the lattice of positively charged metal ions. Imagine the metal ions as being much heavier and stationary compared to the lightweight and mobile electrons. As these electrons move away from their usual positions, the electromagnetic field pushes them back toward their starting points. This push is because opposite charges attract each other, so the negatively charged electrons are attracted back toward the positively charged ions.

If there were no energy loss or dissipation in this process, the oscillation of these electrons would be perfectly regular, like a swinging pendulum, and it would occur at a specific frequency known as the "plasma frequency," denoted by ωp.

In summary, when light interacts with a metal, it causes the electrons in the metal to move back and forth. These electrons experience a force that pushes them back to their original positions due to the attraction between positive ions and negative electrons. If there were no energy losses, this oscillation would be a regular and repetitive motion at a specific frequency called the plasma frequency (ωp).

I.2.1.1 Drude's Approach

In order to understand this oscillation and its consequences, we will quickly describe the Drude model [4]. The “q” charge of electrons is q= -e. The Lorentz force exerted on them by the electrical field E is thus written:

$$\vec{F} = -e.\vec{E} \qquad \text{(I.1)}$$

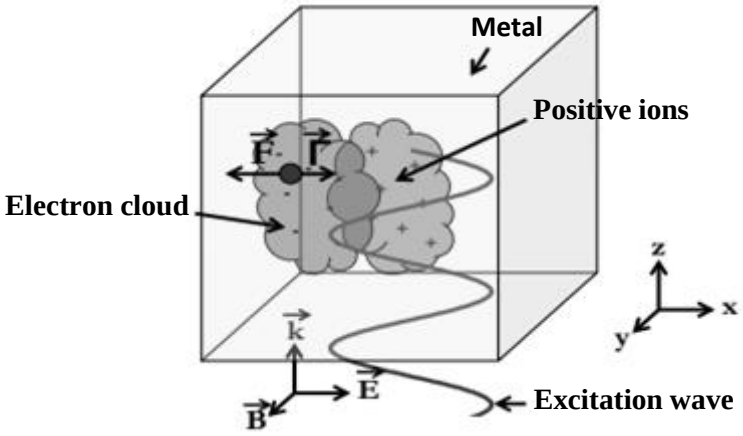

Figure I.1 *Scheme of the oscillation of the electronic cloud in a metal under electromagnetic excitation. Electrons are subject to two forces: the Lorentz force F and an amortization force.*$\vec{\Gamma}$

The Lorentz force induces a shift in the electron cloud. During its displacement, electrons can collide with each other, creating a viscous amortization. It is linked to the probability of "Y" encounter creating electron/electron couplings or electron/photon coupling, to the "m" mass and to the velocity of oscillation $\vec{v}$ of electrons. This force is noted $\vec{\Gamma}$, is directed in the opposite direction to the force of Lorentz (Figure 1.1) and has for equation:

$$\overrightarrow{\Gamma} = m.\Upsilon.\vec{v} \quad \text{(I.2)}$$

Υ define by the low de Mathieson [5]

$$\Upsilon = \frac{1}{\tau_{e-e}} + \frac{1}{\tau_{e-phonon}} + \frac{1}{\tau_{e-défauts}} + \frac{1}{\tau_{e-surface}} \quad \text{(I.3)}$$

It has been demonstrated that the oscillation of electrons subjected to an electrical field creates a polarization field $\overrightarrow{P}$ defined by the equation [5]:

$$\overrightarrow{P}(t) = \frac{-N.e^2}{m.(\omega^2+i.\Upsilon.\omega)} . \overrightarrow{E}(t) \quad \text{(I.4)}$$

With “N” the load density. The electrical susceptibility "χ" derives from this equation and is defined by the following equations:

$$\vec{P} = \varepsilon_0 x\vec{E} \quad \text{(I.5)}$$

$$x = \frac{-N.e^2}{\varepsilon_0.m.(\omega^2+i.\Upsilon.\omega)} \quad \text{(I.6)}$$

Electric susceptibility is a value defining the polarization induced by an electrical field in a given material. In the case of a low-intensity electric field, we can approximate the refraction index of the medium considered by the following expression:

$$n = \sqrt{1 + Re(x)} \quad \text{(I.7)}$$

Posons :

$$\omega_p = \sqrt{\frac{N.e^2}{\varepsilon_0.m}} \quad \text{(I.8)}$$

We can then rewrite the equation (1.6) based on the plasma pulse:

$$x = -\frac{\omega_p^2}{\omega^2+i.\Upsilon.\omega} \quad \text{(I.9)}$$

Finally, we define the complex permissiveness ε_m of the metal by the following equation:

$$\varepsilon_m = 1 - \frac{\omega_p^2}{\omega^2+i.\Upsilon.\omega} = 1 + x \quad \text{(I.10)}$$

According to the equation (1.7):

$$n = \sqrt{\varepsilon_m} \quad \text{(I.11)}$$

The complex permissiveness "ε_m" describes the response of a material to an electrical field and is a complex value that can be divided into two parts, notedε_m' and ε_m'' for the actual part and the imaginary part, respectively. Then we obtain:

$$\varepsilon_m(\omega) = \varepsilon_m'(\omega) + i\varepsilon_m''(\omega) \quad \text{(I.12)}$$

I.2.1.2 Optical properties of metals

Metals such as gold (Au), silver (Ag), copper (Cu) and aluminium (Al) are characterized by a strong presence of free electrons in the origin of their electrical and thermal conductive properties. The optical response of metals is heavily dependent on the frequency of the incident electromagnetic wave: reflective and poorly absorbing in visible/near-infrared and transparent in ultraviolet. It is then much less obvious to link the optical response (constants n_m andk_m) of metals to electrons. To solve this problem, the metal is assimilated to a cold gas or electron plasma [6] characterized by plasma pulseω_p.

A plasma wavelength can also be defined as$\lambda_p = 2\pi c/\omega_p$. The values of $\omega_p$and λ_p for metals are listed in Table I.1.

Table I.1 Drude model parameters: plasma frequencies, plasma wavelengths and relaxation times for Ag, Au, Al and Cu [7].

	ω_p (rad/s)	λ_p (nm)	T_0 (fs)
Ag	$1.36\ 10^{16}$	138	31
Au	$1.35\ 10^{16}$	139	9.3
Al	$2.58\ 10^{16}$	73	2.1
Cu	$1.64\ 10^{16}$	114	6.9

Table I.1 *Drude Model Parameters [7].*

However, the complete modelling of the optical response of the metal is difficult given the peculiarities of a solid: quasi-static positive ion network, outdoor surfaces, collisions... The Drude model then allows establishing an expression linking the complex permissivenessε_m of the metal to the two parameters that are ω_p and the average duration of collisions τ_0

$$\varepsilon_m = 1 - \frac{\omega_p^2}{\omega^2 + i\omega/\tau_0} \quad \text{(I.13)}$$

With ω the frequency of the incident wave and τ_0 the average time between two collisions, also called relaxation time (values listed in Table I.1).

The permissiveness of ε_m has a real part of the metalε_m', and an imaginary partε_m'', which is linked to the optical constants of metal ε_m' andk_m:

$$\varepsilon_m' = 1 - \frac{\omega_p^2 . \tau_0^2}{1+\omega^2\tau_0^2} = n_m^2 - k_m^2 \quad \text{(I.14)}$$

$$\varepsilon_m'' = \frac{\omega_p^2 . \tau_0}{\omega(1+\omega^2\tau_0^2)} = 2n_m k_m \quad \text{(I.15)}$$

The measured complex permittivity of Ag, Al, Au and Cu [7] are shown in Figure I.2. The k_m coefficient of metals increases with the wavelength, which is consistent with the behavior of the metal. (Absorbant dans le proche-infrarouge). The peak of the refractive index n_m at 800 nm of aluminium corresponds to an interband transition [7]. It can also be cited the simplified Drude model that neglects losses in the metal. The average time τ_0 between two collisions is considered infinite and the permittivity is then purely real:

$$\varepsilon_m \approx 1 - \frac{\omega_p^2}{\omega^2} \quad \text{(I.16)}$$

$$\varepsilon_m \approx 1 - \frac{\lambda^2}{\lambda_p^2} \quad \text{(I.17)}$$

The simplified Drude model is also easily accessible to explain the optical response of the metal: for example, ε_m tends towards one (transparent material) for extreme ultraviolet radiation such as$\lambda << \lambda_p$. By reaching the visible/near-infrared such as$\lambda >> \lambda_p$, the permittivity ε_m becomes negative and translates the refraction phenomena in this spectral field.

When this electron plasma oscillates at a Metal-Dielectric interface (MI for Metal-Isolating) and interacts with an incident wave under certain conditions, an electromagnetic wave can spread along the interface: then we speak of surface plasmon resonance.

I.2.1.3 Selection of Metal

The choice of metal is a pivotal factor in the development of a Surface Plasmon Resonance (SPR) system operating within the visible and near-infrared wavelengths. The complex permittivity (ε_m',ε_m'') of metals like silver (Ag), aluminum (Al), gold (Au), and copper (Cu) is determined based on their complex refractive indices (n_m,k_m). This analysis is crucial as it informs how these metals interact with incident light in the desired wavelength range.

Gold, silver, copper, and aluminium are often preferred for their unique plasmonic properties, and a thorough understanding of their complex permittivity aids in optimizing the SPR system's performance for applications such as Biosensing and surface-enhanced spectroscopy.

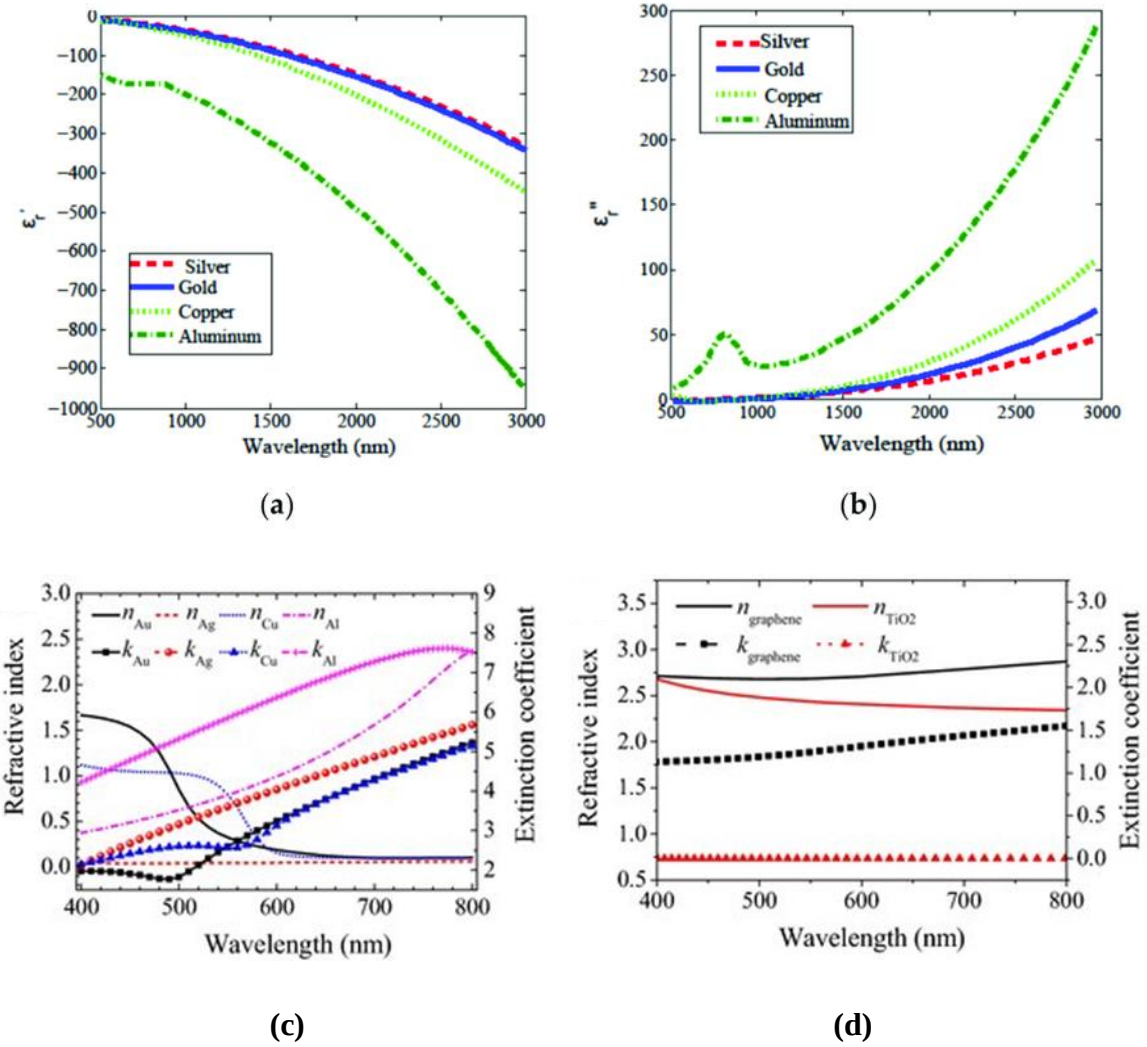

Figure I.2 *(a) (b) Calculation of the complex permittivity from (c) (d) the complex index of the metals Ag, Al, Au and Cu [7].*

In the field of plasmonics, gold and silver are commonly chosen metals for various reasons. First, both gold and silver can support surface plasmons in the visible part of the electromagnetic spectrum, primarily because their dielectric permittivity has a negative real part in this range. This property is essential for the generation and manipulation of surface plasmons.

Second, gold and silver are favoured in the visible spectrum because they exhibit relatively low losses and consequently have longer propagation lengths for surface plasmons. The propagation length is a critical parameter in plasmonics, as it determines how far the surface plasmon wave can travel while maintaining its intensity. In this aspect, gold and silver

outperform metals like aluminium and copper. However, the choice between gold and silver depends on the specific requirements and conditions of the plasmonic system. It often comes down to a trade-off between performance and durability. Silver, theoretically, offers better performance as it has much longer surface plasmon propagation lengths than gold. Moreover, silver allows for the excitation of surface plasmons at higher energies (up to 3.8 eV) before encountering interband transitions that limit plasmon excitation. This means that silver has a narrower plasmon resonance, which can lead to higher sensitivity in plasmonic devices.

On the other hand, gold, while not as performance-driven as silver, offers better durability. Gold does have a limitation related to the appearance of an electronic interband transition at around 2.5 eV (corresponding to a wavelength of 500 nm), which restricts the excitation of more energetic surface propagating plasmons. This limitation may not be a significant concern for applications operating within these limits. If the goal is to excite plasmons in the ultraviolet (UV) range, neither gold nor silver is suitable, as both encounter interband transitions that hinder plasmon excitation in this region. In such cases, other metals like aluminium must be considered.

The choice between gold and silver in plasmonics depends on the desired performance, sensitivity, and operating conditions of the plasmonic system. Silver offers superior performance but may have a shorter lifespan due to higher reactivity, while gold provides better durability but at the expense of some performance characteristics. Both metals excel in the visible spectrum, and the choice should be made based on the specific needs of the application.

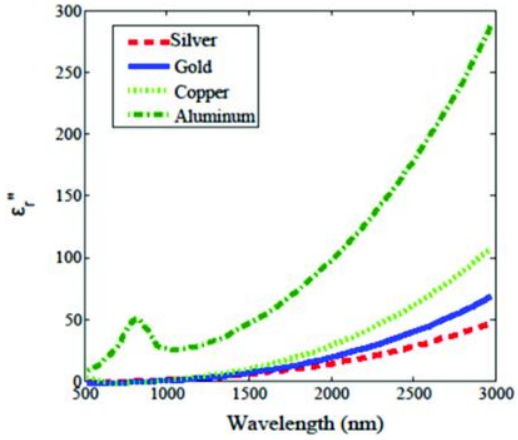

Figure I.3 *Theoretical propagation lengths of surface plasmons propagating to an air/metal interface for four metals supporting surface plasms in the field of visible (Silver: grey, Gold: yellow, Copper: red, Aluminium: purple).The values are calculated from the data of Johnson and Christy [9] for Ag, Au and Cu and Rakic for Al [10].*

On the other hand, with a standard Au^{3+}/Au torque potential of 1.52 V [11], gold is unbeatable in terms of chemical stability. It is a noble metal, which is therefore chemically very stable in the presence of both water and dioxide, and that reacts only with a few chemical species. For his part, silver is also considered a noble metal, but it is less than gold. Thus, the standard Ag^{+}/Ag couple potential is only 0.8 V [12], which is lower than the standard O2/H20 couple potential. (1, 23 V). Silver can therefore be stable in the presence of liquid water under certain conditions, but it oxidizes in the Presence of oxygen or airy water (containing dissolved dioxide). The main consequence is that over time, the performance of an air-driven, silver-based plasmonic device will deteriorate rapidly due to surface oxidation, not that of a gold-based device.

I.3 Plasmon-Polariton

When a material is exposed to an electromagnetic field, a coupling between that field and the induced local polarization in the material can occur. This coupled excitation is called polariton. When the polarized system is a gas of free electrons, that is, when that material is a metal or has a metallic character, the coupling that occurs with collective and quantified electronic oscillations. It is used the terme plasmon-polariton [1].

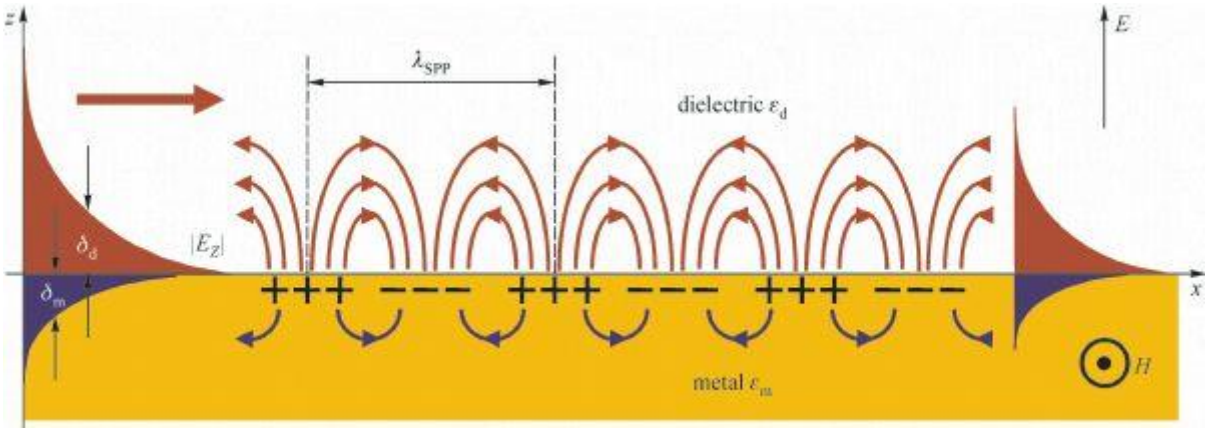

Figure I.4 *Schematic representation of the propagation of oscillations of the plasma of free electrons on the surface of the metal.*

I.3.1 Types of Plasmons

In the field of plasmonics, different types of plasmons are distinguished based on their location and behavior. These distinctions include volume plasmons, surface plasmons, and localized and delocalized surface plasmons:

I.3.2 Volume Plasmons:

Volume plasmons are collective oscillations of free electrons within the bulk or volume of a material, such as a metal or semiconductor. These plasmons typically occur in three-dimensional structures and involve the motion of electrons throughout the material. They are responsible for phenomena like the bulk plasmon resonance in metallic nanoparticles is defined by the equation (I.18)

$$\hbar\omega_p = \hbar\sqrt{\frac{ne^2}{m\varepsilon_0}} \tag{I.18}$$

This value of plasmon energy is therefore different depending on the metal considered, for example,

For Silver: $\hbar\omega_p = 8980$ meV.

For Gold: $\hbar\omega_p = 9030$ meV.

Volume plasmons can be excited when an electron passes through a thin metal film or reflects on that film, but cannot pair with light. It should be noted that volume excitations are not the subject of this study. Our study is limited only to surface plasmons.

I.3.3 Surface Plasmons

The peculiarity of evanescence associated with SPP is that the EM field decreases exponentially in the perpendicular direction of the two mediums of the interface[13], which is a specific feature of SPP waves such as the field takes maximum intensity on the interface. As illustrated by the figure. I.5, an electromagnetic wave trapped near a metal surface interacts only at a certain depth of penetration due to the energy dissipation phenomenon measurable intrinsically according to the optical functions of the metal. Surface plasmons are an important aspect of plasmon physics. According to Maxwell's theory, electromagnetic waves can propagate along the interface between a metal with a complex dielectric function and a dielectric material with a real permittivity. These waves are known as surface plasmons and are associated with the oscillations of free electrons on the surface of the metal. They represent a

unique combination of both collective electron excitations and electromagnetic waves existing at the metal's surface. Sometimes, they are referred to as surface plasmon polaritons (SPP) to emphasize this hybrid nature.

The most significant feature of surface plasmons is the localization of the electromagnetic field intensity at the metal-dielectric interface, with a rapid decrease in intensity as you move away from this interface in the direction perpendicular to it. This leads to the evanescent nature of these waves. In other words, the electromagnetic field intensity decreases exponentially as you move away from the interface in a direction perpendicular to it, making surface plasmons highly localized. As shown in Figure (I.5), the electromagnetic field associated with surface plasmons exhibits this exponential decrease, and it is confined to a certain depth of penetration near the metal surface. This limited penetration depth is a result of the inherent energy dissipation properties determined by the optical characteristics of the metal

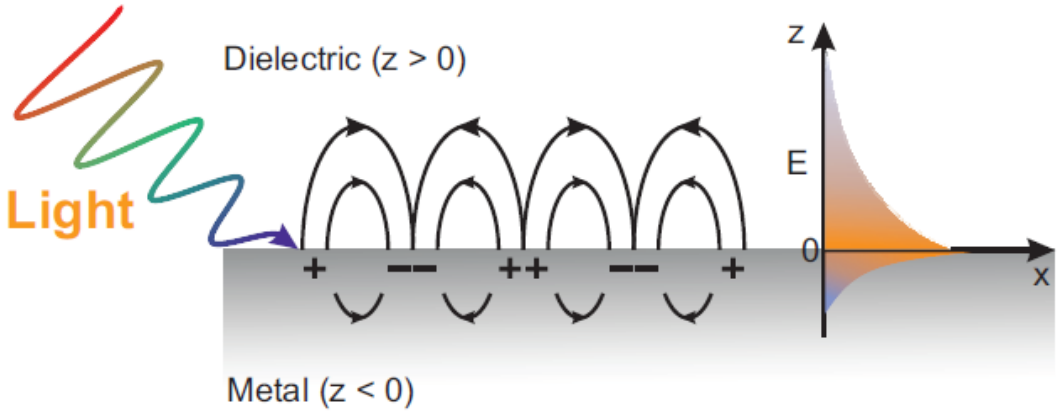

Figure I-5 *Oscillation of charges (surface plasmon) at the metal/dielectric interface. The exponential decay of the electromagnetic fields on either side of the interface is shown in the figure on the right.*

I.3.2.1 Types of Surface Plasmons

Surface plasmons can be categorized into two types based on how far they can spread localized surface plasmons and extended surface plasmons.

a. Localized surface plasmons

These plasmons are confined to a small region on the surface of a material or nanostructures. They have limited propagation and are mainly concentrated around the nanostructure or surface defect, resulting in strong local electromagnetic field enhancements. This property makes them useful for applications such as enhancing the sensitivity of sensors, improving the efficiency of photodetectors, and enabling localized spectroscopy.

b. Dislocated surface plasmons

Dislocated surface plasmons are plasmonic waves that extend across flat metal surfaces, covering distances of several micrometers. These plasmons can propagate over relatively long distances along the metal surface.

On the other hand, relocalized plasmon resonances (PSs) are generated at the interface of smooth metal films. They are termed "non-radiative" because they cannot spontaneously couple with an electromagnetic wave. In other words, they do not emit electromagnetic radiation on their own. To harness the energy or information carried by these relocalized PSs, a "coupler" is necessary. This coupler is a device or technique that allows the relocalized PSs to interact with electromagnetic waves, enabling their controlled manipulation and utilization. Further details about the coupler and its role in working with relocalized plasmon resonances will be discussed later in this chapter.

I.3.3.2 Conditions of existence of dislocated surface polarite plasmons

The simplest geometry supporting a surface plasmon (see Figure I.6) is a flat interface, between a non-absorbing dielectric (z > 0) with a real positive dielektric constant ε_d d and a metal (z < 0) which is described by the permittivity ε_m. Consider a polarized electromagnetic wave Transverse Magnetic (TM): the magnetic field H is strictly perpendicular to the incidence plane (y,z), that is, the components H_y, H_z and E_x are zero.

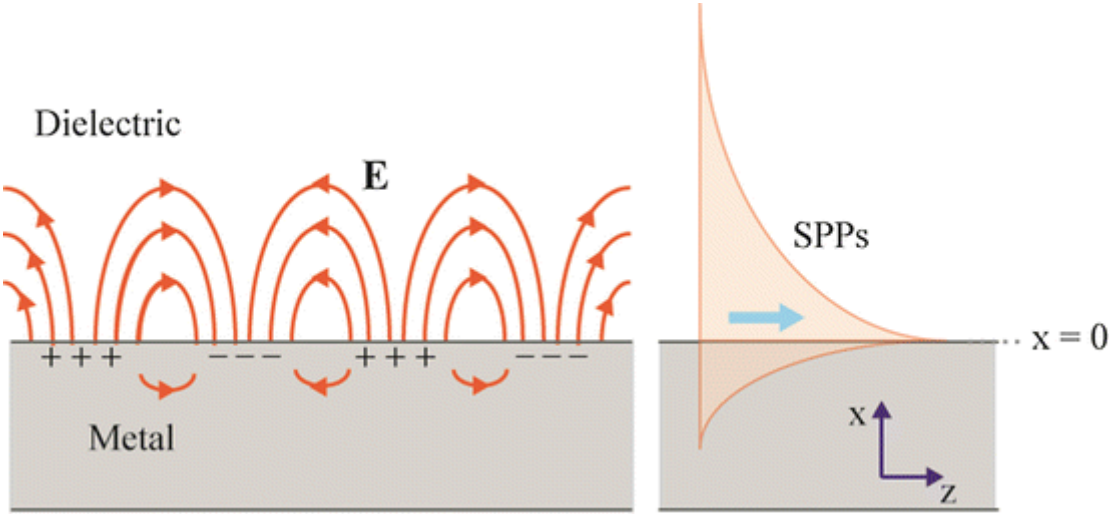

Figure I.6 *Diagram of a surface plasmon propagating along a dielectric/metal interface.*

The solution modeling a surface plasmon is a wave that spreads in the y direction, invariant in the x direction and has a decrease on both sides of $z = 0$. We have stated what the surface polarite plasmon is. We will now seek to find its conditions of existence from the equations of Maxwell.

For this, consider a flat interface between two environments: one consists of a Dielectric of a real dielectric constant ε_d , and the other of a non-magnetic metal $(\mu_m = 1)$ characterized by a complex dielectrical constant$\varepsilon_m = \varepsilon'_m + i\varepsilon''_m$. Figure I.7 shows the scheme of the system: the impact plane of the wave is $(yOz)$and the plasmon spreads according to the direction y. This means that the system studied is invariant following x.

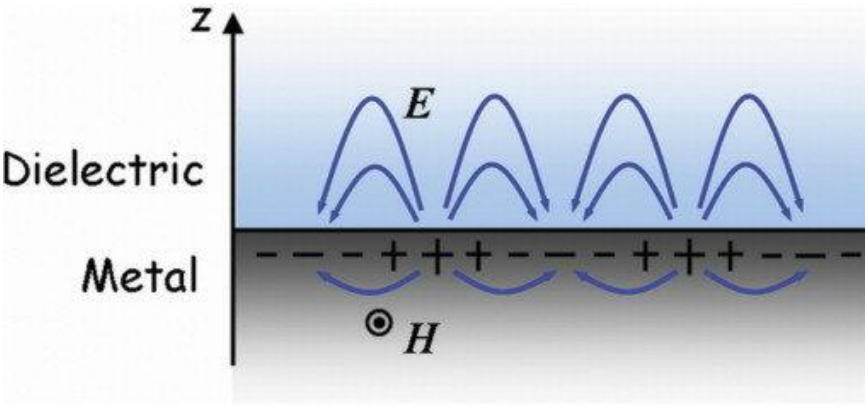

Figure I.7 *Geometry of the metal-dielectric interface we consider [14].*

Under these conditions, if we consider a linearly polarized wave TE or TM, we can define ψ_j as the transverse component of the field [14] :

$$\psi_j = \begin{cases} E_{jx} & cas\ TE \\ H_{jx} & cas\ TM \end{cases} \tag{I.19}$$

Where $j = d, m$, It is a dielectric or metal medium..

For both modes, Maxwell's relations give the propagation equation:

$$\Delta\psi_j + \frac{\omega^2}{c^2}\varepsilon_j\psi_j = 0 \tag{I.20}$$

Alternatively, ε_j is the dielectric constant of the environment$j$.

We have seen above that, in both mediums, the two fields are propagative following y and evasive in the perpendicular direction$z$.

$$\psi_m = A_m e^{\alpha_m z} e^{i(k_y y - \omega t)} \quad \text{In the metal for } z < 0 \qquad \text{(I.21.a)}$$

$$\psi_d = A_d e^{-\alpha_d z} e^{i(k_y y - \omega t)} \quad \text{The dielectric for } z > 0 \qquad \text{(I.21.b)}$$

Where a α_j are positive constants taking into account wave attenuation in the directions perpendicular to the interface. k_y is a non-zero real-part complex and translates spread according to the axis(Oy).

The boundary conditions for fields H and E between the two mediums give the following relationships:

$$\begin{cases} E_{xd}(z=0) = E_{xm}(z=0) \\ \frac{\partial E_{xd}}{\partial z}(z=0) = \frac{\partial E_{xm}}{\partial z}(z=0) \end{cases}$$

(I.22.a)

$$\begin{cases} H_{xd}(z=0) = H_{xm}(z=0) \\ \frac{1}{\varepsilon_d}\frac{\partial H_{xd}}{\partial z}(z=0) = \frac{1}{\varepsilon_m}\frac{\partial H_{xm}}{\partial z}(z=0) \end{cases} \qquad \text{(I.22.b)}$$

In the case of the polarized wave TE, by replacing in the equation (I.22.a) the form E_x d'après (I.21), We obtain:

$$A_d = A_m \qquad \text{(I.23)}$$

$$-\alpha_d A_d = \alpha_m A_m$$

We then get,$-\alpha_d = \alpha_m$ which is impossible because these two constants have been defined as positive. It is therefore inferred that a surface wave cannot be excited by a TE polarization.

In the case of TM, we get:

$$A_d = A_m$$

$$-\frac{\alpha_d}{\varepsilon_d} A_d = \frac{\alpha_m}{\varepsilon_m} A_m \qquad \text{(I.24)}$$

Consequently:

$$-\frac{\alpha_d}{\varepsilon_d} = \frac{\alpha_m}{\varepsilon_m} \qquad \text{(I.25)}$$

And since α_m et α_d are always positive, this relationship therefore imposes opposite dielectric constants on the two mediums. This condition is checked between a dielectric ($\varepsilon_d > 0$) and a metal ($\varepsilon_m < 0$).

A surface plasmon can only be excited by TM polarization and only if one of the two mediums is a metal [15].

From now on, we will only consider the case $\psi_j = H_j$.

The combination of the equation (I.21) with the equation (I.20), leads to:

$$-\alpha_j^2 + k_y^2 = \varepsilon_j \frac{\omega^2}{c^2} \tag{I.26}$$

The introduction of the continuity ratio (I.25) in the equation (I.26)

Leads us to the dispersion ratio of the k_{spp} wave vector surface plasmon polariton in the spread direction k_y..

$$k_y = k_{spp} = \frac{\omega}{c}\sqrt{\frac{\varepsilon_m.\varepsilon_d}{\varepsilon_m+\varepsilon_d}} = k_0\sqrt{\frac{\varepsilon_m.\varepsilon_d}{\varepsilon_m+\varepsilon_d}} \tag{I.27}$$

Where c defines the speed of light in the vacuum and k_0 the wave vector of light. By observing the typical dispersion diagram of an Air-Metal interface in Fig. I.8, it is noted that all the values taken by k_{spp} are below the light line lumière $\omega = ck_0n_d$ (n_d = the index of the medium of incidence): this means that the SPPs cannot be directly excited by the incident light of the middle. To excite a surface plasmon, the condition $k_{spp} > k_0n_d$ must be verified and then requires a coupling. We'll see later what coupling devices are for SPP excitement.

Since$\varepsilon_m = \varepsilon_m' + i\varepsilon_m''$ is complex, the dispersion equation (I.27) gives a complex component of the wave vector parallel to the interface. The wave vector is then written in the form of a sum of a real part and an imaginary part$k_y = k_y' + ik_y''$. In the case of a noble metal, for which$|\varepsilon_m'| > > |\varepsilon_m''|$, we obtain:

$$k_{spp}' = k_0\left(\frac{\varepsilon_m'.\varepsilon_d}{\varepsilon_m'+\varepsilon_d}\right)^{1/2} \tag{I.28}$$

$$k_{spp}'' = k_0\left(\frac{\varepsilon_m'.\varepsilon_d}{\varepsilon_m'+\varepsilon_d}\right)^{3/2} . \frac{\varepsilon_m''}{2\varepsilon_m'^2} \tag{I.29}$$

A new condition for the existence of surface plasmons is added here: In order for k_y^' to be real, it is necessary that $\frac{\varepsilon_m'.\varepsilon_d}{\varepsilon_m'+\varepsilon_d} > 0$ i.e. $\varepsilon_d < -\varepsilon_m'$ avec ($\varepsilon_m' < 0$) because the inequation $\varepsilon_d.\varepsilon_m < 0$ is already verified in the case of a metal-dielectric interface. After citing the conditions of existence of surface plasmons, we will now give some characteristic physical properties associated with these modes.

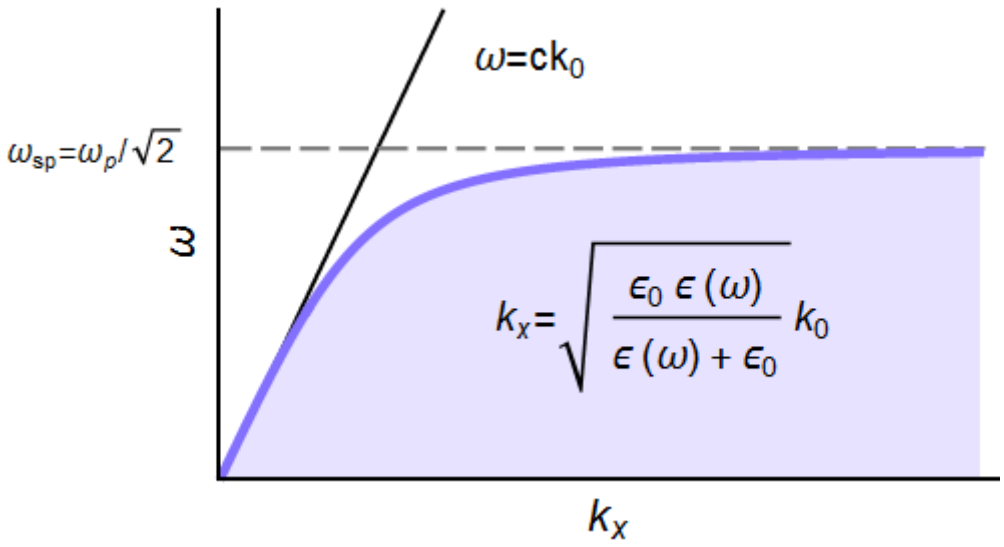

Figure I.8 *Typical dispersion diagram of a surface plasmon for an Air-Metal interface. Inspired by[16].*

I.4 Characteristics of the plasma wave

I.4.1 Spatial extension of the surface plasmon magnetic field

According to the field equation (I.20), the magnetic field of the surface plasmon in both mediums is written:

$$H_m = H_0 e^{\alpha_m z} e^{i[(k'_y + ik''_y)y - \omega t]} \quad \text{in the metal for } z < 0 \qquad \text{(I.30.a)}$$

$$H_d = H_0 e^{\alpha_d z} e^{i[(k'_y + ik''_y y - \omega t)]} \quad \text{in the dilectric for } z > 0 \qquad \text{(I.30.b)}$$

To determine the depth of penetration (or skin depth) of the wave in the dielectric and metal, we are interested in the terms in $e^{\pm\alpha_j z}$as they define evasiveness in both mediums. Thus, we can define in each of the two environments the expression of the penetration distance such as : $\tilde{z}_j = \frac{1}{\alpha_j}$

By combining the equations (I.25) and (I.26), we find the values of α_m et α_d :

$$\alpha_m = k_0 \left(\frac{\varepsilon_m'^2}{|\varepsilon'_m + \varepsilon_d|}\right)^{1/2} \qquad \text{(I.31.a)}$$

$$\alpha_d = k_0 \left(\frac{\varepsilon_d^2}{|\varepsilon'_m + \varepsilon_d|}\right)^{1/2} \qquad \text{(I.31.b)}$$

Therefore, the depths of skin in both mediums are written:

$$\tilde{z}_m = \frac{\lambda}{2\pi}\left(\frac{|\varepsilon'_m+\varepsilon_d|}{\varepsilon'^2_m}\right)^{1/2} \quad \text{(I.32.a)}$$

$$\tilde{z}_d = \frac{\lambda}{2\pi}\left(\frac{|\varepsilon'_m+\varepsilon_d|}{\varepsilon_d^2}\right)^{1/2} \quad \text{(I.32.b)}$$

For example, for a wavelength of 630 nm, on an air-gold interface, the penetration depths are of $\tilde{z}_{or}$= 29 nm in gold, and of $\tilde{z}_{air}$ = 242 nm in air. And in the case of an air-silver interface, $\tilde{z}_{argent}$ = 39 nm and $\tilde{z}_{air}$ = 262 nm for the same wavelength. By observing these values, we find that the skin thickness of the surface plasmon in the metal medium is much smaller than in the dielectric medium. This is entirely due to the last condition of existence of the surface plasmon, $\varepsilon_d < |\varepsilon'_m|$. This gives us an idea of the distances at which plasmons are likely to interact with their surroundings and in particular with transmitters located near the interface.

I.4.2 Surface plasmon propagation length

The imaginary part of k_{spp} is directly related to the length of SPP spread (in intensity) [14] :

The SPP spread length is defined as the distance at which the wave intensity decreases to $1/e$ of the initial intensity. It is given by:

$$L_{spp} = \frac{1}{2k''_{spp}} = \frac{1}{k_0}\left(\frac{\varepsilon'_m+\varepsilon_d}{\varepsilon'_m.\varepsilon_d}\right)^{3/2}.\frac{\varepsilon'^2_m}{\varepsilon''_m} \quad \text{(I.33)}$$

The propagation length of SPPs varies greatly with the wavelength.

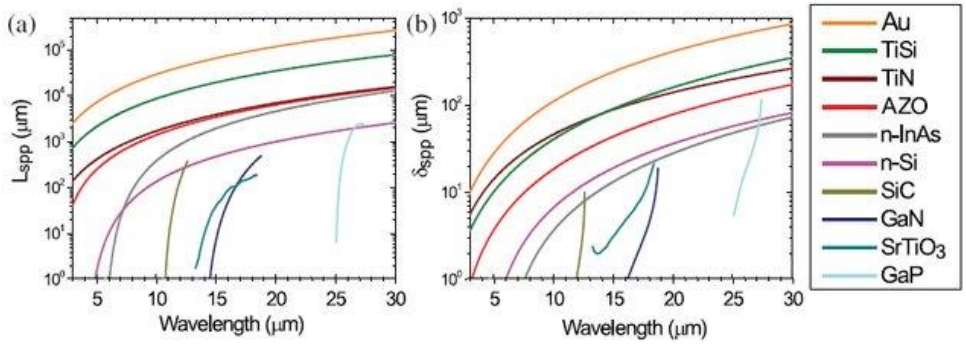

Figure I.9 *Diagram representing the propagation length of the SPPs, from the tabulated values of [7].*

I.5 Excitation of surface plasmons and Metal-Isolant-Metal structures

To excite a surface plasmon, we previously saw that it was necessary to use a coupling device to check the condition$k_{spp} > k_0 n_d$. Two main devices are to be distinguished: total internal reflection by a prisma and diffraction networks.

In the configuration suggested by Otto [2], an index prism, represented by 'n', is brought close to the top surface of the metal/air interface, specifically on the airside. This setup results in an air gap with a thickness roughly on the same scale as the wavelength of the excitation being used.

When total internal reflection occurs within the prism, the electromagnetic field in this narrow air gap allows for the excitation of surface plasmons. This happens when the wave vectors align properly, and when the distance between the prism and the metal is kept small enough.

I.5.1 coupling by prisma

There are two configurations of prisma coupling. The first was first described by Otto. The second was developed by Kretschmann.

a. Configuration of Otto

In the configuration described by Otto [2], an index prism "n" is brought close to the top of the metal/air interface, on the air side. This setup leaves a thin air gap, roughly on the same scale as the wavelength of the excitation, between the prism and the metal surface. When total internal reflection occurs within the prism, the electromagnetic field extends into the air gap. This field can stimulate the generation of surface plasmons under the right conditions, specifically when the wave vectors match and the distance between the prism and the metal surface is close enough.

b. Configuration of Kretschmann

The principle is to excite the surface plasmon using an index n prisma, higher than that of the dielectric of the metal/dielectric interface considered [2]. The base of the prisma is attached to the thin layer of metal. This thickness should be small, it is typically about fifty nanometers. For angles θ greater than that of total reflection, the evanescent field through the metal may pair a surface plasmon if the projection following the wave vector interface of the inciding light wave is equal to the surface plasmone wavevector k_{spp}.

$$k_{spp} = \frac{2\pi n}{\lambda} \sin(\theta), \tag{I.34}$$

with n the index of the prisma and θ, the angle of incidence of light. In this configuration, if a portion of the incident light pairs to the surface plasmon it is no longer reflected. The Kretschmann method is effective for obtaining the dispersion ratio of surface plasmons.

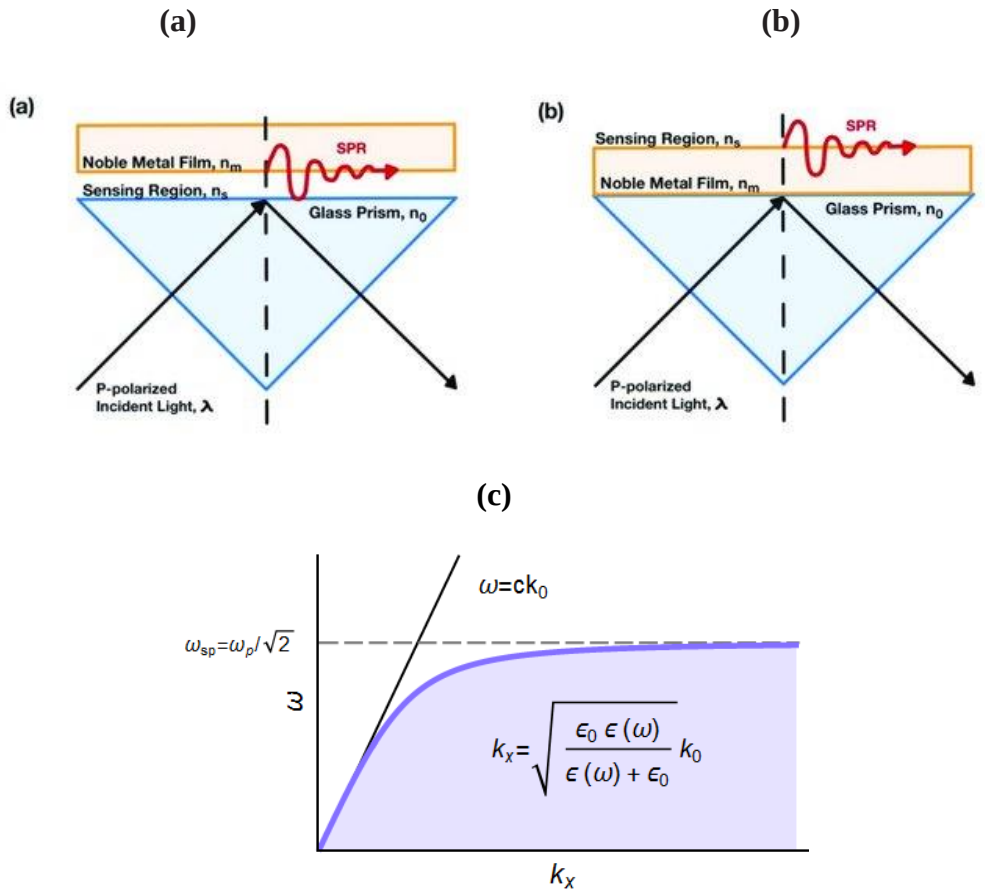

Figure I.10 *Coupling of surface plasmons by prism in the configuration of (a) Otto and (b) Retshmann with (c) the associated dispersion diagram.*

I.5.2 Excitation by a diffraction network

Another way to excite SPPs is by using a metal diffraction network (Figure I.11), when the parallel wave vector $k_{x,m}$ of an evasive network diffract order is identical to the SPP wavevector:

$$k_{x,m} = k_0 n_d \sin(\theta) + m\frac{2\pi}{p} = k_{spp} \tag{I.35}$$

with m a whole, that represents the order of diffraction and p the period of the network. The condition $k_{spp} > k_0 n_d$ an be verified according to the diffracted order and network parameters.

I.5.3 Special Cases of Metal-Isolating-Metal Structures

We have seen that SPPs are electromagnetic modes that spread and are confined along a Metal-Isolating interface. If you consider two close-knit interfaces that form a Metal-Isolating-Metal (MIM) structure, the SPPs of each interface will pair up and spread in the form of a guided mode. (Figure I.12). The dispersion ratio that makes it possible to calculate the β complex proliferation constant is then [17] :

$$tanh\left(\frac{w\sqrt{\beta^2-k_0^2}}{2}\right)=\frac{-\sqrt{\beta^2-k_0^2\varepsilon_m}}{\varepsilon_m\sqrt{\beta^2-k_0^2}} \quad \text{(I.36)}$$

with *w* the width of the insulation.

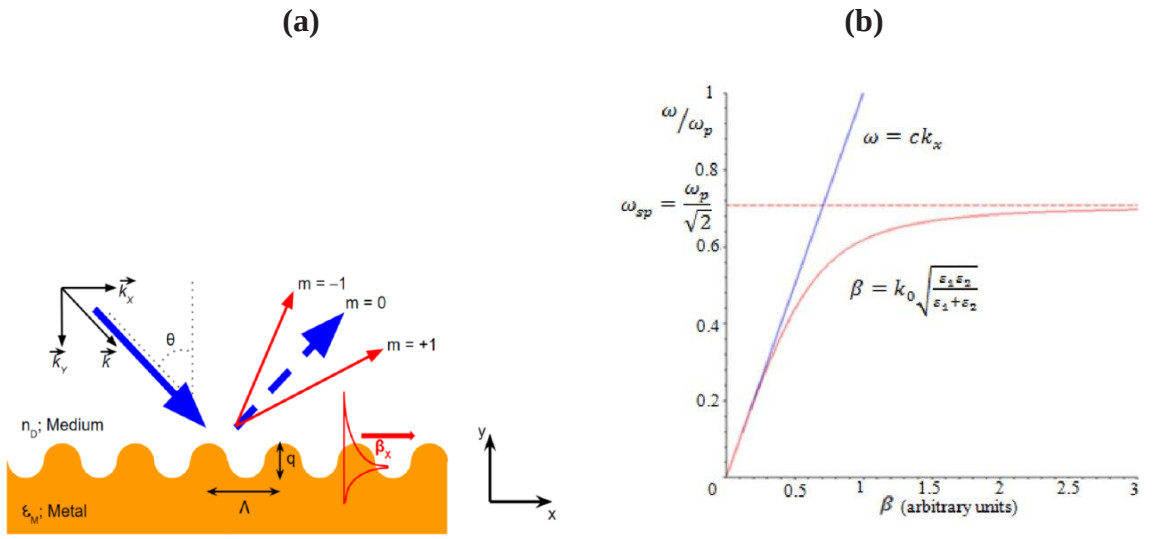

Figure I.11 *Coupling devices for the excitation of SPPs. (a) Use of a diffraction grating and (b) its associated dispersion diagram.*

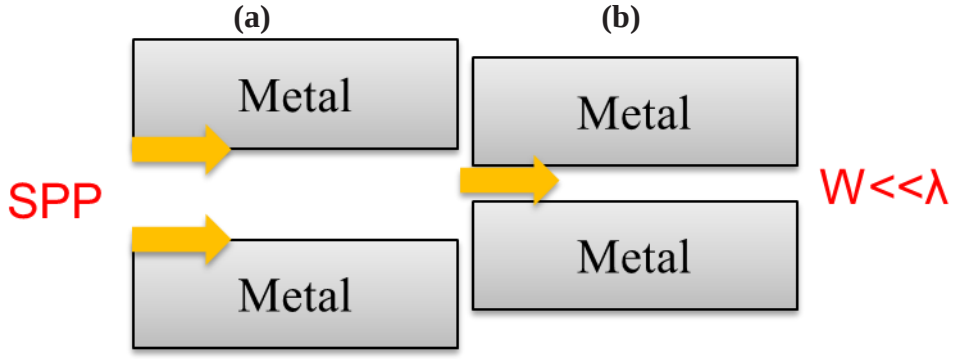

Figure I.12 *(a)(b) Representation of surface plasmons within a Metal-Insulator-Metal structure. (a) The thickness of the insulation is too great; the two SPPs do not couple. (b) Coupling of two SPPs for the generation of a guided mode.*

Generally, an effective refraction index n_{eff} is associated with the β propagation constant, which is the average index seen by the guided mode during its propagation:

$$n_{eff} = \frac{\beta}{k_0} \tag{I.37}$$

The actual part of the effective index n_{eff}, at λ = 1064 nm depending on the width of the MIM is represented in Figure I.13, in the Au-Air-Au structure configuration. These values were obtained by numerical simulation using the Reflection Pole Method (RPM) [18]. The effective index increases when the width of the MIM decreases: the closer the SPPs are, the stronger the coupling is and a higher effective index is produced.

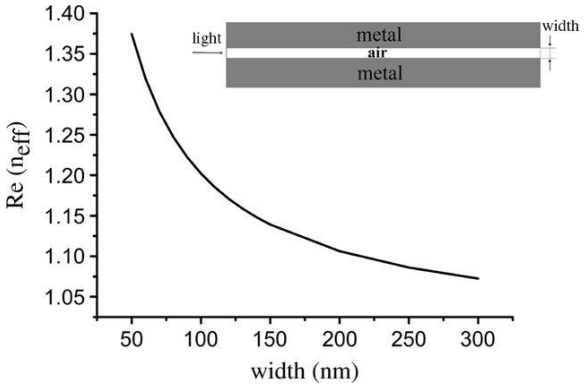

Figure I.13 *Numerical simulations of the real part of the effective index of an Au-Air-Au MIM, at λ = 1.064 µm as a function of the width w of the insulator [18].*

Conclusion

In this chapter, we have provided a comprehensive study of the phenomenon known as surface plasmon resonance. Initially, we defined surface plasmons as surface waves that propagate along the interface between a metal and a dielectric material. These waves exhibit an exponential decrease in the amplitude of the electromagnetic field as they move away from this interface, leading us to important characteristics such as the depth of penetration and spatial extension of these waves.

Based on our theoretical foundation, we discussed the selection of suitable metals for the applications explored in this thesis. Our choice primarily centered on silver due to its strong coupling with surface plasmons in the visible-near-infrared range. In a subsequent section, we delved into the conditions required for the resonant excitation of surface plasmons. Graphical representations of dispersion relations in a reference frame (k, ω) highlighted that the coupling between surface plasmons and electromagnetic waves can only occur in the presence of a coupler. We then introduced some of the most common coupling methods, which include prism couplings and diffraction network couplers.

CHAPTER II

Resonance sensor for surface plasmons

II.1 Introduction

Over the last two decades, research in the field of plasmonics has experienced a significant upsurge, opening the door to a multitude of potential applications across various sectors, including healthcare and energy. These applications encompass Raman spectrometers integrated into mobile phones for swift medical diagnostics, cancer therapy through phototherapy, the development of all-optical integrated circuits, high-resolution holographic displays, enhanced magnetic storage devices, and high-efficiency photovoltaic cells [1, 2,3]. Plasmonic devices have garnered substantial interest due to their unique ability to confine and amplify electromagnetic fields in the proximity of metal interfaces, offering innovative solutions to a wide array of challenges in diverse fields.

II.2 Plasmonics and Applications

The burgeoning field of plasmonics, as of my last knowledge update in September 2021, had seen a remarkable surge in patent activity. This uptrend can be attributed to several fundamental scientific and technological factors. Plasmonics, which involves the manipulation of plasmons (collective electron oscillations) at the nanoscale, provides a unique platform for interactions with light. Researchers, driven by the promise of its potential applications, have conducted extensive R&D. They have delved into a wide array of areas, such as sensing, energy harvesting, data storage, and medical diagnostics. Consequently, a substantial number of patents have been filed and granted, reflecting the concerted efforts to harness the fascinating and diverse properties of plasmonics.

Global collaboration and knowledge sharing also fuel this increasing number of patents. Plasmonics research transcends geographic boundaries, as researchers and inventors worldwide collaborate, exchange findings, and leverage shared knowledge. This global approach has accelerated innovation and contributed to the proliferation of patents. Moreover, technological advancements in nanofabrication and computational simulations have empowered scientists to design intricate plasmonic structures and devices, leading to novel inventions. These innovations are frequently patented to safeguard intellectual property and facilitate their potential commercialization. While I cannot provide specific figures, the robust scientific foundations and these key factors illustrate the dynamic growth of the plasmonics field and the substantial patent activity associated with it. For the most current and detailed patent statistics, I recommend consulting patent databases and academic literature that provide comprehensive insights into the evolving landscape of plasmonics research and innovation.

II.3 Surface Plasmon Resonance and Its Applications

Surface Plasmon Resonance (SPR) is a well-established optical phenomenon occurring at the interface of a metal and a dielectric, such as a gas or liquid. Extensive research efforts have been dedicated to exploring the applications of SPR, resulting in profound advancements in fundamental and instrumental domains. These applications can be succinctly categorized into three principal research themes:

- Biosensing
- Material Science and Nanotechnology:
- Analysis of Biomolecules and Biochemical Measurements

While comprehensively acknowledging the substantial body of work in this field is a formidable task, a select few applications have demonstrated notable industrial potential. (Source: [5])

II.3.1 Biosensing

The confinement of the electromagnetic field in the context of surface plasmon polariton (SPP) chips plays a pivotal role in their functionality for biosensing applications. SPP chips, which utilize the properties of surface plasmon polaritons, offer remarkable sensitivity to the conditions at the chip's surface, making them highly valuable for biosensing purposes. This sensitivity allows the detection and analysis of various biomolecules, including proteins, DNA, and other biological entities, as well as surface modifications or defects.

Surface Plasmon Resonance (SPR) microscopy, a technology that has been adapted for SPP chips, facilitates real-time surface interaction monitoring through SPP signals [6]. SPP chips are essential components for biosensing, as they enable the exploration of molecular binding events, biomolecular interactions, and other biosensing activities. When biomolecules bind to the SPP chip's surface, it induces changes in the SPP signal, which can be detected and quantified in real-time. This makes SPP chips a powerful tool for studying molecular interactions on the chip surface, an integral part of biosensing.

One aspect to consider in biosensing with SPP chips is the resolution limit, which is linked to the attenuation of SPPs in the metal layers of the chip. The choice of materials, such as gold or aluminum, for these chips can significantly influence the resolution. These metals have relatively low propagation lengths, which affect the resolution of the biosensor.

To address this limitation and enhance the biosensing capabilities of SPP chips, researchers have incorporated near-field optical microscopy techniques like Scanning Near-field Optical Microscopy (SNOM).

SNOM proves to be a promising approach for biosensing using SPP chips, offering the capability to probe biomolecules and their interactions at the nanoscale directly on the chip's surface as in Figure II.1. The fundamental concept of SNOM involves scanning the SPP chip's surface with an optical probe positioned just a few nanometers above the chip. The near-field interaction between the probe and biomolecules on the chip surface provides an optical image of the surface and the biomolecular activities taking place. In the context of biosensing with SPP chips, this allows for high-resolution visualization and quantification of molecular binding events, providing valuable insights into the biosensing process.

In summary, the confinement of surface plasmon polaritons and the integration of technologies like SPR, SPP chips, and SNOM are critical in advancing biosensing capabilities. These approaches enable the real-time Detaction.

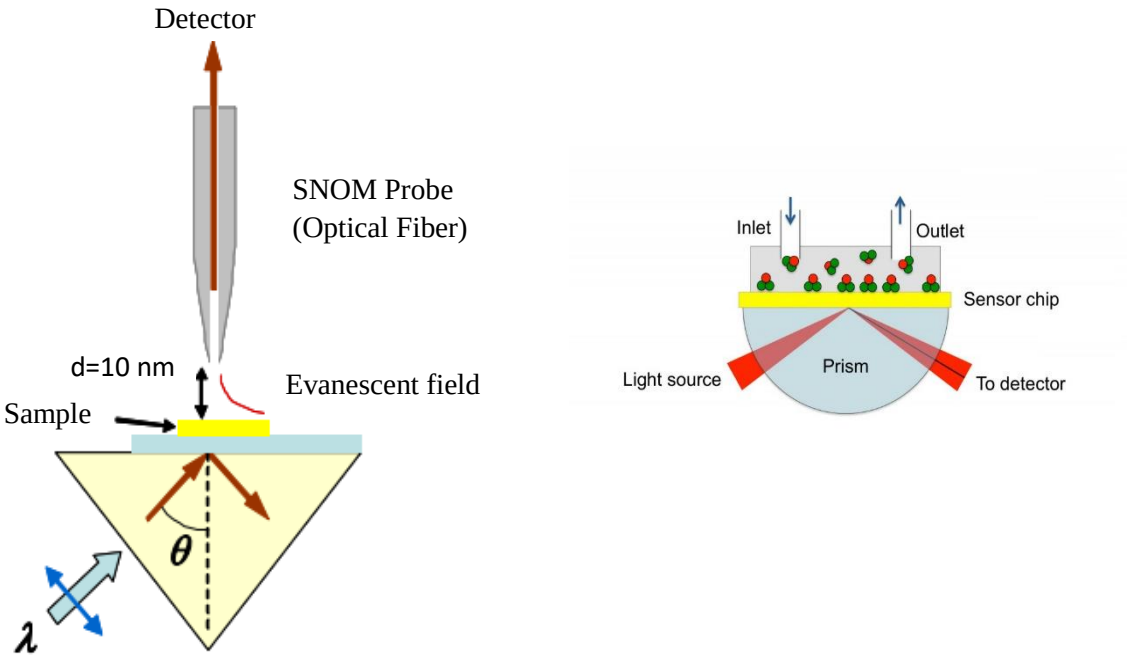

Monitoring and high-resolution imaging of biomolecular interactions on SPP chips, making them a valuable tool for biosensing applications..

Figure II.1 *Principle of the optical scanning tunneling microscope (PSTM) and the SPR chip. An evanescent field is created by total reflection.*

II.3.2 Material Science and Nanotechnology

Surface Plasmon Resonance (SPR) is indeed a versatile technique that extends beyond its well-known applications in biology[7]. In the realms of material science and nanotechnology, SPR plays a pivotal role in investigating surface modifications and interactions at the nanoscale. Here's an overview of how SPR is applied in these fields:

II.3.2.1 Surface Modification Studies

Surface Plasmon Resonance (SPR) finds extensive utility in material science and nanotechnology by allowing researchers to investigate and comprehend how surface modifications impact the properties of materials at the nanoscale. One significant area of application is the study of surface coatings and functional groups. Researchers can immobilize these modified surfaces on SPR sensor chips and monitor changes in the refractive index as various molecules or nanoparticles interact with the modified surface. This real-time, label-free monitoring provides valuable insights into the efficacy of different surface modifications in tailoring the material for specific applications. Whether it's enhancing the hydrophobicity of a material or creating a biocompatible surface for medical devices, SPR is an invaluable tool for optimizing and tailoring material surfaces to meet precise requirements.

Additionally, SPR is instrumental in understanding how different surface modifications influence the wettability, adhesion, and chemical reactivity of materials. For instance, in the development of superhydrophobic or superoleophobic surfaces, which are crucial in self-cleaning materials or oil-repellent coatings, SPR can provide insights into the effectiveness of various surface treatments. By immobilizing these modified surfaces on SPR sensors, researchers can quantitatively assess changes in contact angles, hysteresis, and surface energy, aiding in the design of advanced materials for specific industrial or commercial purposes.

Furthermore, in the context of nanotechnology, SPR is essential for optimizing the properties of nanomaterials. Nanoparticles, nanowires, and nanoscale structures often undergo surface modifications to tailor their electronic, optical, or catalytic properties. Researchers can use SPR to analyze how these modifications influence the interaction of nanomaterials with other substances, such as gases or molecules, which is critical for applications in catalysis, sensing, and nanoelectronics. This knowledge allows for the precise control and customization of nanomaterials for a wide range of applications, from enhancing catalytic activity to improving the sensitivity and specificity of nanoscale sensors. SPR serves as a versatile and

indispensable tool in material science and nanotechnology, offering in-depth insights into the effects of surface modifications on the properties of materials. This knowledge is pivotal for tailoring material surfaces to meet specific requirements, whether it's creating superhydrophobic surfaces, enhancing material adhesion, or optimizing the properties of nanomaterials. SPR's real-time and label-free monitoring capabilities make it an essential technique for researchers aiming to design advanced materials and devices that meet the evolving demands of various industries.

II.3.2.2 Nanoparticle Interactions

Surface Plasmon Resonance (SPR) is a powerful technique used to study the interactions of nanoparticles with various surfaces and molecules. This technology plays a crucial role in the field of nanotechnology, particularly in the design and development of nanoparticles for applications such as drug delivery and catalysis.

SPR works by detecting changes in the refractive index near the surface of a thin metal film, typically gold or silver, when molecules or nanoparticles bind to it as in Figure II.2. This interaction can provide valuable insights into several aspects of nanoparticle behavior:

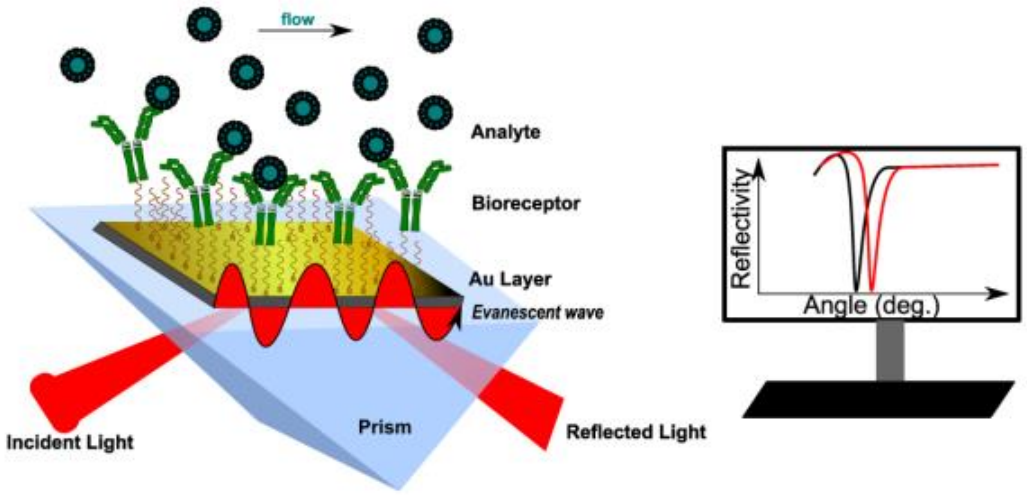

Figure II. 2 *Principle of conventional SPR biosensor with Kretschmann configuration. The analyte binding to the immobilized bioreceptor causes a change in RI near the surface, recorded as the shift of the resonance angle (here, measured at a fixed wavelength). RI reaches a constant value at equilibrium [9].*

Adsorption Kinetics: SPR can be used to measure how quickly nanoparticles bind to a surface. Understanding the rate of adsorption is essential when designing drug delivery systems, as it affects the release of therapeutic agents at the target site.

Quantifying Binding Affinities: SPR allows researchers to determine the strength of interactions between nanoparticles and specific molecules or surfaces. This information is crucial for tailoring nanoparticles to bind selectively with particular receptors or substrates.

Studying Multivalent Interactions: Nanoparticles often have multiple ligands or binding sites. SPR can reveal how these nanoparticles interact with surfaces or molecules with multiple binding partners, providing insights into complex binding behaviors.

Monitoring Surface Modifications: When nanoparticles are coated with ligands or functionalized to enhance their properties, SPR can track changes in the surface chemistry of nanoparticles. This is vital for optimizing nanoparticles for various applications, such as catalysis, where surface modifications can influence reactivity.

Competitive Binding Studies: Researchers can use SPR to study how nanoparticles compete for binding sites on a surface. This is valuable in drug delivery, where nanoparticles may need to displace other molecules to deliver their cargo effectively.

Dynamic Studies: SPR can provide real-time data on nanoparticle interactions. This is useful for understanding the kinetics of nanoparticle binding and release, which can be critical in drug delivery to control release profiles.

In nanotechnology, the information obtained through SPR can guide the engineering of nanoparticles with specific properties, enabling them to function as carriers for drugs or catalysts with enhanced selectivity and efficiency. It helps in tailoring nanoparticles to interact with target molecules or surfaces in a precise and controlled manner, ultimately improving their performance in various applications.

II.3.2.3 Thin Film Characterization

Surface Plasmon Resonance (SPR) is a powerful and versatile technique used in the characterization of thin films [10]. It is particularly valuable for studying various properties of thin films, including their thickness, refractive index, and quality. This capability plays a crucial role in optimizing coatings and films across a wide range of industries, from electronics to optics.

SPR operates on the principle of surface plasmon resonance, which occurs when light of a specific wavelength strikes a thin metallic film, typically gold or silver that is in contact with

a dielectric medium. This phenomenon results in the resonant oscillation of electrons on the metal's surface, leading to changes in the reflectance of incident light. By carefully monitoring these changes, scientists and engineers can extract valuable information about the thin film under investigation. Here is how SPR is utilized in the characterization of thin films:

Measuring Thickness: SPR can accurately determine the thickness of thin films by monitoring the angle or wavelength at which the resonance occurs. As the film thickness changes, the resonance angle or wavelength shifts accordingly. This feature is essential for ensuring that thin films meet specific design requirements in industries like microelectronics, where precise thickness is critical for performance.

Determining Refractive Index: The refractive index of a material is a key parameter in optics and photonics. SPR can be employed to deduce the refractive index of a thin film by observing changes in the resonance angle or wavelength as a function of refractive index. This is useful for selecting materials with desired optical properties in applications like anti-reflective coatings and waveguide fabrication.

Assessing Film Quality: Thin film quality is essential for ensuring the performance and durability of coatings. Imperfections, defects, or changes in film quality can be detected through SPR. Deviations from the expected resonance patterns can indicate issues with film uniformity or the presence of contaminants, allowing for quality control and optimization.

II.3.2.4 Spectral analysis of plasmon resonance in an optical fiber

Jorgenson and Yee initially introduced the concept of utilizing an optical fiber as a surface plasmon sensor [12]. In parallel, Yee conducted research on a structure that combined the principles of the Kretschmann prism and a multimodal optical fiber. This surface plasmon fiber probe comprises a sensitive region located at the tip of a multimodal optical fiber with a typical step change in refractive index, often referred to as PCS (Plastic Cladding Silica). This sensitive region was symmetrically coated with a layer of 50 nanometers of either silver or gold, as

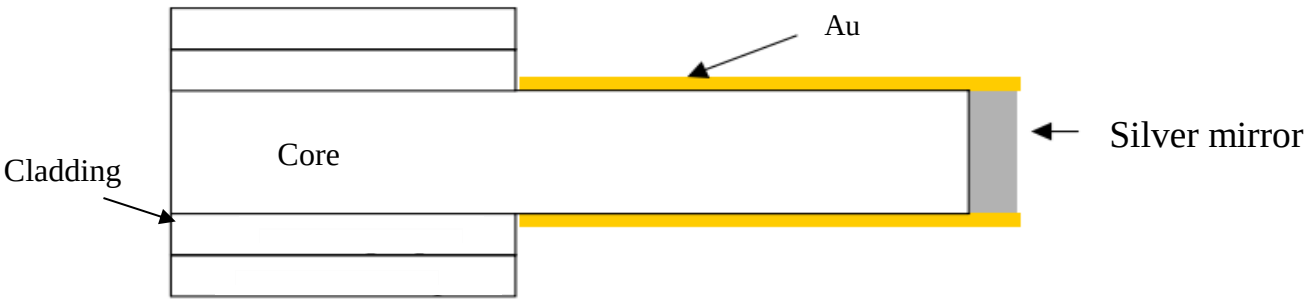

illustrated in Figure II.3. This innovative approach paved the way for the development of optical fiber-based surface plasmon sensors with valuable applications in various fields.

Figure II.3 *Schematic of the optical fiber surface plasmon sensor with "optrode" configuration (After Jorgenson [12]).*

In this setup, light emitted from a white source is introduced into the optical fiber and, within the fiber, experiences multiple reflections in the active region where specific wavelengths are absorbed by surface plasmon waves, as depicted in Figure II.4. Positioned on the fiber's output

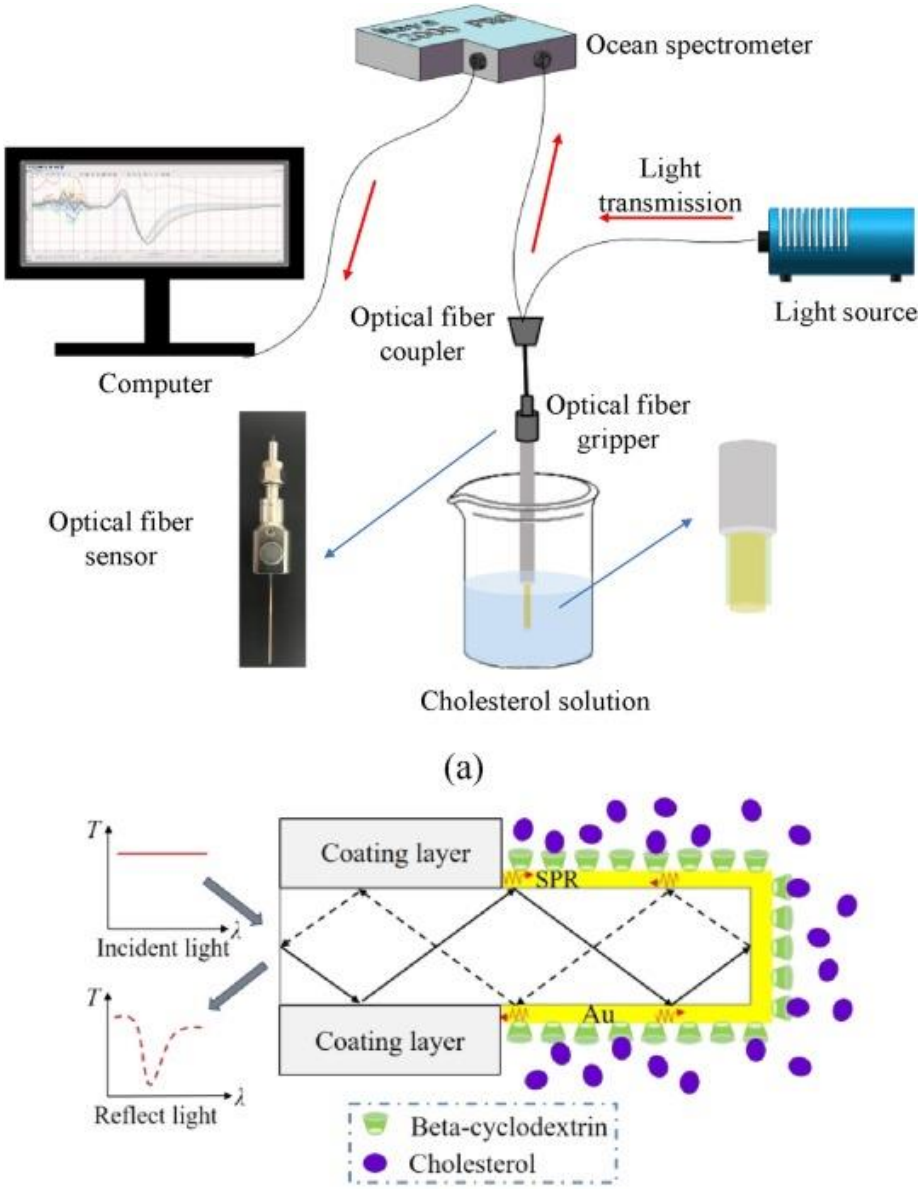

side is a mirror, which reflects the light. This reflected light is subsequently directed into a spectrometer for analysis. Through spectral analysis, it becomes possible to determine the refractive index in the vicinity of the fiber's active surface. When the refractive index increases,

the minimum resonance wavelength shifts towards longer wavelengths, as illustrated in Figure II.4. Notably, this configuration differs from the conventional prism-based setup where the wavelength remains fixed, and the interrogation is performed through angular changes.

Figure II.4 *Illustration of the complete multimodal optical fiber sensor (After Jorgenson [12]).*

II.3.2.5 Plasmonic Wave Guides

Plasmonic waveguides are a type of waveguide that utilizes metal structures to guide and confine surface plasmons. These structures have been extensively studied in the literature, and several types of plasmonic waveguides have been proposed. Here, we will explore some of the most widely researched plasmonic waveguides and discuss their key properties.

a- The Metal Film

The spread length of a surface plasmon on a flat interface is extremely small, making it impractical for integration into optoelectronic circuits. This is because the strong confinement of the electromagnetic field results in substantial absorption in the metal. To address this issue and reduce losses in plasmonic waveguides, it is necessary to modify the distribution of the field within the structure. The most straightforward solution to alter the propagation of a surface plasmon is to employ a metal film positioned between two dielectric media, creating a sandwich-like structure (as depicted in Figure II.5). Research on these waveguides has revealed the existence of modes that spread with minimal losses along the metal film [13]. In essence, the use of a metal-dielectric-metal (MDM) waveguide structure offers a practical way to mitigate the high losses associated with surface plasmons, allowing for more efficient and low-loss guidance of plasmonic modes along the metal film. This has significant implications for the development of optoelectronic circuits and plasmonic devices, as it enables the realization of compact and high-performance components for various applications in photonics and nanophotonics.

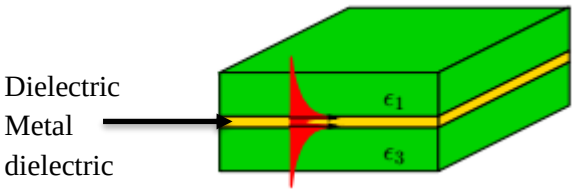

Figure II.5 *Metal film: surface plasmons, shown schematically in red, propagate along the metal between the two dielectric media.*

If the metal film is thick enough in front of the skin thickness in the metal, the fields associated with the surface plasmons of each interface do not overlap and spread independently from each other. By decreasing the thickness of the film, the modes supported by each interface match up.

b- Chains of Metal Nanoparticles

The strong interaction between individual metal nanostructures and light makes it possible to transfer energy over short distances and create waveguides. Specifically, when light interacts with metal nanostructures, it can excite volume plasmons within them, causing them to act like dipoles. When these metal nanoparticles are placed in an orderly, fashion a few dozen nanometers apart from each other (as shown in Figure II.6), they exhibit collective behavior, and light can propagate along this guide [14]. This is one of the few plasmonic guides in the literature that features a periodic structure. However, the low coupling between particles and excessive radiative losses severely restrict the ability of this system to effectively guide light.

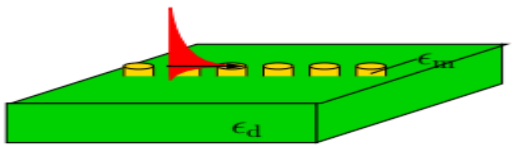

Figure II. 6 *Chain of metal nanoparticles deposited on a dielectric substrate.*

c- waveguide Metal / Dielectric / Metal (MIM)

An alternative approach to achieving strong mode confinement involves inserting a dielectric material between two thick metal films, as depicted in Figure II.7. In this structure, the fundamental mode comprises a coupled mode that combines the two surface plasmons at each interface. When the two metal films are adequately separated, the effective index of the guide (expressed as $n_{eff} = k_x/k_0$ closely approximates the actual surface plasmon index at a single metal/dielectric interface. As the distance between the metal films decreases, both the actual index and mode confinement increase. However, this heightened confinement comes at the expense of mode spreading, meaning that the electric field penetrates deeper into the metal, leading to increased absorption losses [15].

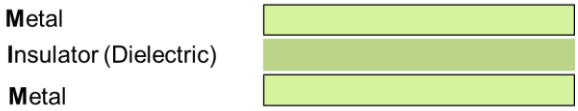

Figure II.7 *Dielectric layer between two metal layers. Surface plasmons propagate at dielectric and metal interfaces with excellent confinement and an increase in effective index.*

II.3.3 Detection of biomolecules and biochemical measurements

Bio-detection through Surface Plasmon Resonance (SPR) and the utilization of biosensors were first explored by Liedberg and his research team [16]. Presently, biosensors based on SPR principles have found a limited but significant niche within the biochemical control market. These biosensors have demonstrated their competitiveness when compared to other technologies. They offer advantages such as cost-effectiveness, ease of operation, high sensitivity, and the ability to provide real-time measurements.

The core concept of SPR is instrumental in the detection and quantification of various molecules and in the biophysical analysis of interactions among biomolecules.

In 1902, Robert Wood conducted experiments that revealed sudden fluctuations in the intensity of light produced by a continuous-profile light source when it was reflected by a metal grid, a phenomenon famously known as "Wood anomalies" [16]. Notably, these fluctuations only occurred when the light possessed magnetic transverse polarization [16]. Theoretical underpinnings for these anomalies were not provided until 1941 when Ugo Fano contributed a theoretical framework, explaining them as the result of quasi-stable waves propagating along the surface of the metal. In 1958, R. Ferrell extended this theoretical understanding by describing the coupling between an electromagnetic wave and surface modes at the interface between a metal and an electrical medium. However, it was only in 1968 that SPR was introduced as an official exhibition [20].

II.4 Biosensor with surface plasmon resonance

II.4.1 1 History of biosensors in SPR

In 1902, the scientist Robert Wood made an intriguing discovery while conducting experiments. He observed sudden variations in the intensity of light when a metal grid, a phenomenon

famously known as “Wood anomalies”, reflected it. What made this observation particularly remarkable was that these fluctuations exclusively manifested when the incident light exhibited a specific attribute known as magnetic transverse polarization [16].

Substantiating this phenomenon came later, in 1941, when Ugo Fano provided a theoretical foundation for Wood's experiments. Fano's work elucidated that the anomalies were a consequence of quasi-stable waves propagating along the surface of the metal [18]. Building upon this theoretical understanding, in 1958, R. Ferrell delved deeper into the coupling between an electromagnetic wave and surface modes occurring at the interface between a metal and an electric medium.

The year 1968 saw two significant developments in this field. First, Otto proposed an experimental demonstration of the phenomenon by utilizing a technique called Attenuated Total Reflection (ATR) [20]. This method involved employing a high-index dielectric prism to enhance the momentum of the incident wave, generating an evanescent wave, which, in turn, excited the metal surface placed in close proximity to the prism's base. Concurrently, in the same year, Kretschmann and Raether introduced a similar configuration where the metal was directly deposited on the prism's base [21]. This configuration subsequently became the most widely adopted setup in applications related to surface plasmon resonance, primarily due to its ease of installation. For approximately three decades, surface plasmon resonance remained a compelling theoretical concept, intriguing from a scientific standpoint but with limited practical utilization.

The concept of employing surface plasmon resonance as a biosensor began to take shape in 1983. It was in this year that B. Liedberg, C. Nylander, and I. Lundstrom pioneered the development of a system based on the Kretschmann configuration. Their system was designed to detect low concentrations of anesthetic gases. Additionally, in an experimental endeavor, they explored the adsorption of γ-globulins onto the metal surface through specialized surface chemistry, and the subsequent interaction of these γ-globulins with anti-γ-globulin antibodies. These interactions led to changes in thickness and alterations in the surface refractive index, resulting in shifts in the resonance angular curve.

From the early 1990s, the field witnessed a transformation as the first commercial systems, such as the inaugural Biacore system in 1990, were manufactured. This milestone sparked a surge in research activity. In 1990, the number of publications stood at around fifty as depicted in Figure II.8; however, by 2010, it had soared to more than 3000 [16]. This exponential growth in

publications signified the escalating interest and research dedication in the realm of surface plasmon resonance.

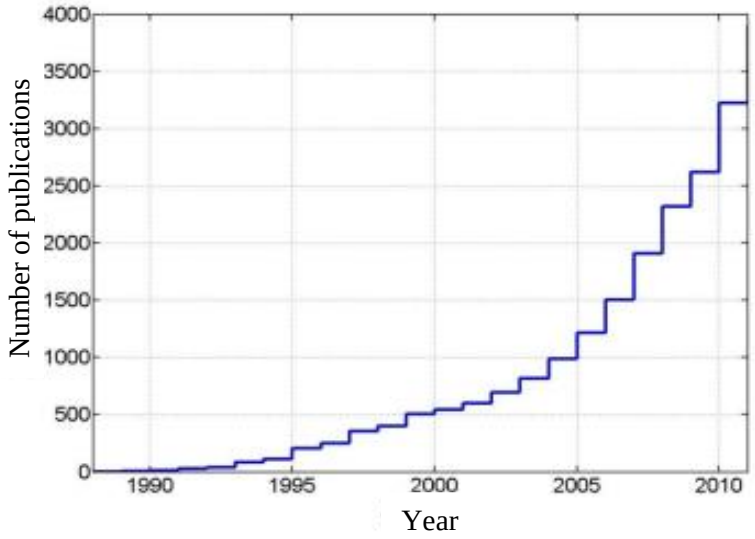

Figure II.8 *Number of publications per year between 1988 and 2010 provided by the ISI Web of Knowledge database (keywords used "plasmonic(s)"+"biosensors"+"surface plasmons resonance") [22].*

II.4.2 Principle of detection of a SPR sensor

II.4.2.1 1 Principle of a SPR sensor

The rapid progress of technology has led to the availability of various sensor types, which can primarily be categorized based on the properties of the substances they analyze or the mode of transduction employed, such as optical, electrochemical, mechanical, or thermal sensors. Among these, optical sensors utilizing Surface Plasmon Resonance (SPR) and local Surface Plasmon Resonance (LSPR) have become the most prevalent and commercially accessible.

Surface plasmon resonance is a non-discriminatory detection method, as it does not differentiate between the natures of the molecules it is detecting. Instead, the selectivity of sensors employing this method relies on the immobilization of receptors on a metal surface, allowing interaction solely with the specific molecule one intends to identify [24]. These sensors can then be employed in the identification of substances exhibiting distinct interactions with recognition elements that have been previously attached to the metal surface as it shown Figure II.9, such as in antibody-antigen or protein-DNA interactions.

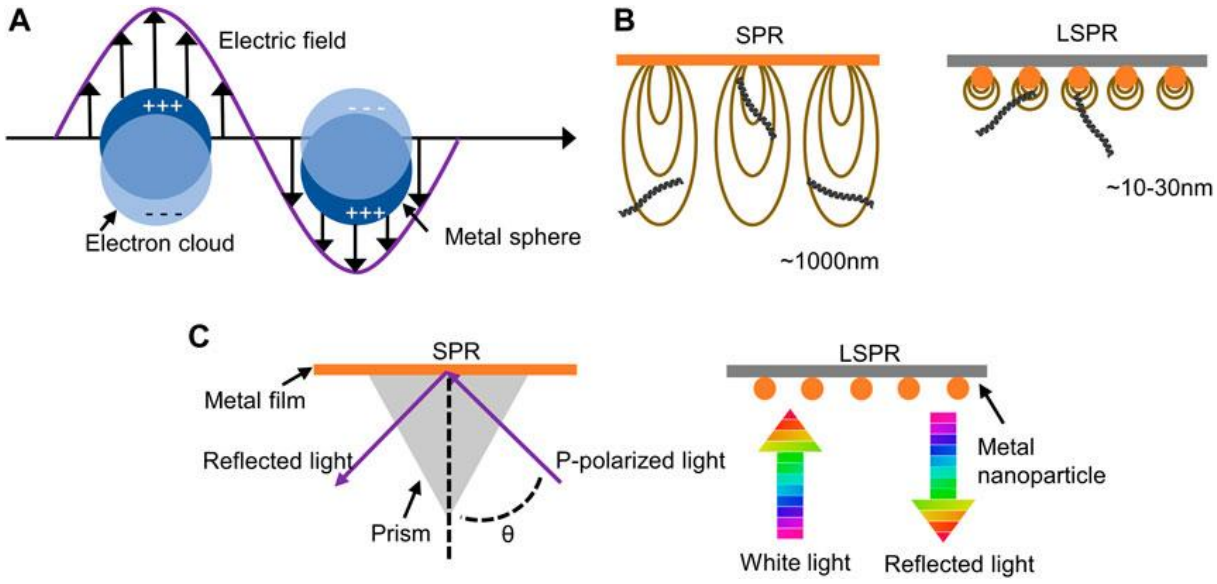

Figure II.9 *Operating principle of an SPR biosensor.*

II.4.2.2 Methods of Detection

The main methods of detection are

- to measure the intensity of the optical wave (reflected or transmitted) around the resonance.
- To measure variations in the minimum resonance in angular interrogation (Figure II.9 (c).
- To measure variations in the minimum resonance depending on the wavelength.

The most widely used configuration currently is the measurement of the variation of the minimum resonance (in wavelength and angular interrogation) because it offers a better signal/noise ratio compared to measuring the light intensity.

a. Interrogation The Angular

Surface plasmon waves serve as probes for disturbances occurring on the metal surface. Indeed, a disturbance in the vicinity of the surface generates a variation in the coupling conditions that concretely translates into the variations in the properties of the fall of reflectivity: an angular

shift in the curve of reflection. (Figure II.10) In other words, angular interrogation allows the resonance angle to be tracked at a fixed wavelength and thus to go back to information about the evolution of the biomolecular interaction studied by quantifying the disturbances at the metal/dielectric interface [25].

b. Spectral Questions

As we have already mentioned, coupling between the incident wave and surface plasmons can also be achieved by fixing the incidence angle and variing the incident wavelength. An absent spectral band thus characterizes the spectrum of reflectivity. In this case, the resonance wavelength corresponds to the minimum of the reflection signal. Spectral interrogation thus allows the spectral position associated with the minimum of reflectivity to be tracked at a fixed angle (Figure II.10) [26]. This variation, similar to the angular query, makes it possible to quantify disturbances at the metal/dielectric interface.

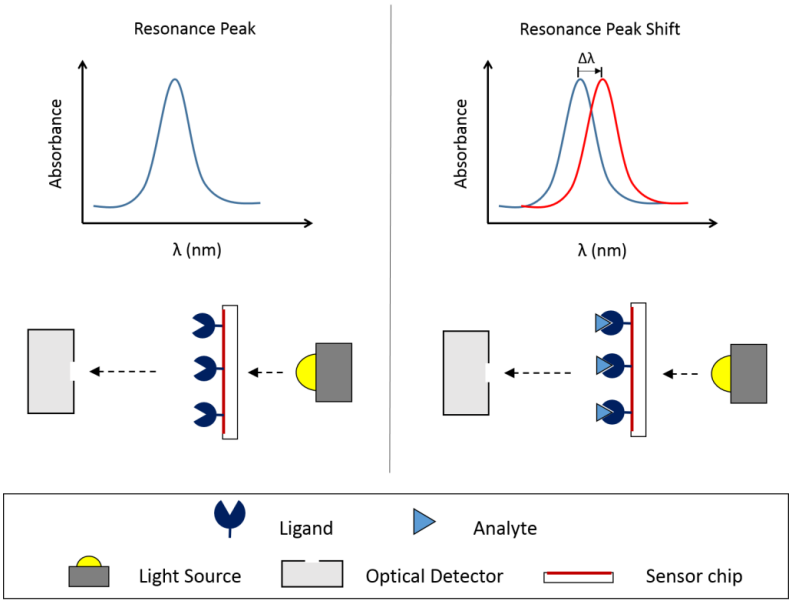

Figure II.10 *The detection principle of SPR sensors.*

II.4.3 Performance characteristics of a SPR sensor

The main performance characteristics of a SPR effect sensor are sensitivity, resolution and detection limit. These three characteristics play a very important role in determining sensor performance in the detection of target molecules.

II.4.3.1 The sensitivity

Sensitivity in the context of SPR sensors pertains to the capability of the instrument to discern minute variations in the refractive index near the sensor surface. Refractive index, a measure of how much a material alters the velocity of light passing through it, plays a central role in SPR sensing. This sensitivity characteristic determines the instrument's ability to detect low concentrations of analytes, establishing its utility in applications like molecular interaction studies, environmental monitoring, and medical diagnostics.

The sensitivity of an SPR sensor is contingent on several influential factors, including:

Surface Properties: The nature of the surface coating on the sensor affects sensitivity. A well-designed coating should be optimized to attract specific analytes effectively, enhancing the sensor's responsiveness to their presence.

Optical Components: The optical components within the sensor system, such as the light source, prisms, and detectors, contribute to sensitivity. High-quality optical components can reduce signal noise and boost sensitivity.

Instrument Precision: The precision of the instrument itself, including the alignment of optical components and the stability of the system, can impact sensitivity. Careful calibration and alignment are essential to maximize the instrument's performance.

Achieving high sensitivity in an SPR sensor is a primary goal in sensor development, as it empowers the detection of even trace amounts of analytes, thereby broadening the range of possible applications.

The sensitivity *S* is a very important parameter for studying the performance of a SPR sensor. It is defined as being the ratio between the variation of the plasmon resonance parameter ΔY taken into account (the resonant angle θ, the resonancy wavelength λ, etc.) and the corresponding variation in the magnitude to be measured which is in our case the refraction index variation Δn_d. (Figure 12).

$$S = \frac{\Delta\lambda}{\Delta n_d} \qquad \text{(II.1)}$$

However, in order to better assess the sensitivity of the detection, it is necessary to consider another parameter: the SPR signal mid-height width of *FWHM*. This increases with the value of the dielectric (nd) refractive index, inducing a wider SPR signal. By dividing the

value of *S* by the *FWHM*, we introduce the concept of the "Figure of Merit" *FOM* Merit Factor, a factor used to analyze, overall, the performance of a SPR sensor [27].

$$FOM = \frac{S}{FWHM} \qquad \text{(II.2)}$$

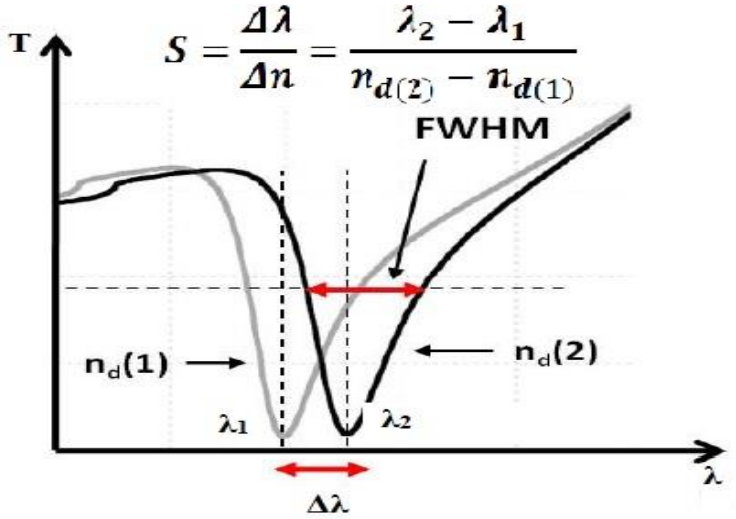

Figure II.11 *Shift of the SPR signal with a change in the refractive index of the dielectric* n_d.

Thus, for the same variation Δnd, if the FOM is high this indicates a significant spectral shift of the signal or a narrower plasmonic signal (less error in determining the resonance wavelength). In both cases, this results in a better performance of the sensor.

II.4.3.2 Limit of resolution

The resolution is the detection of a small variation in the refraction index Δn_d by a visible shift in the resonance wavelength λ of the plasmonic signal. This parameter is determined by measuring the LD detection limit, expressed by:

$$LD = \frac{(\Delta\lambda)_{min}}{S} \qquad \text{(II.3)}$$

$(\Delta\lambda)_{min}$ is the minimum spectral variation in resonance wavelength (often equal to the value of the sensor noise level) and S sensitivity.

Today, a high-resolution optical spectrum analyzer can reach a resolution wavelength of dλ = 0,01 nm. The detection resolution of the refraction index is defined by $SR = (\Delta n_d / \Delta\lambda) \times d\lambda$ [28]. The literature data shows the resolution limits by dividing the accuracy of each method

and device used by the sensor sensitivity. Detection limits of the order of 10^{-6} are obtained by angular study as well as for spectral interrogation, of 10^{-5} for the measurement of light intensity.

In order for a SPR sensor to perform, its sensitivity must be as high as possible with low measurement noise. This results in a very low-resolution value reflecting a high ability to probe external disturbance (deposition of a biological layer, index variation).

II.5 Conclusion

The significant attention that the phenomenon of surface plasmon resonance (SPR) has garnered in recent years can be attributed primarily to two key factors. Firstly, SPR enables the confinement of light at the nanometer scale, and secondly, it facilitates the amplification of incident light intensity at the interface between a metal and a dielectric material. This amplification serves as an effective means to allow surface plasmons to propagate over extended distances. The ability to achieve substantial propagation lengths, typically on the order of micrometers, is in high demand across various applications, including photonic devices, optical imaging, surface characterization tools, and techniques for the detection and characterization of biochemical molecules.

In this chapter, we have elucidated the operational principles of SPR sensors. Additionally, we have expounded on their performance characteristics, notably sensitivity, and detection limits. These aspects are pivotal in understanding and harnessing the capabilities of SPR technology for a diverse range of applications, such as biosensing, material analysis, and advanced imaging systems.

CHAPTER III

Guidance and sensing properties of a plasmonic guide MIM

III-1 Introduction

The incorporation of the Drude model into Finite Difference Time Domain (FDTD) simulation codes, specifically for the representation of metallic materials, marks a significant milestone in the progression of plasmonics research. Within the domain of integrated nanophotonics, a central objective is the achievement of confined light propagation at the nanoscale. This confinement is made possible through the interaction between incident light waves and the free electrons present at the interface between a metal and a dielectric medium, giving rise to surface plasmon polaritons (SPPs).

The phenomenon of SPPs has ignited substantial interest in the development of novel nanometric waveguiding structures. Various innovative structures have been proposed, including metal nanowires [1], V- or W-shaped channels etched onto metallic substrates [2], and networks of metal particles [3]. Among these configurations, some are based on the concept of focusing incident light within the dielectric core of a sandwich-like structure known as 'Metal-Isolating-Metal' (MIM). These MIM-based devices have demonstrated exceptional potential in achieving extended-range propagation and sub-wavelength confinement of light [4]. Consequently, waveguides of the MIM type exhibit considerable promise in the development of all-optical devices at the nanometer scale. They offer several advantages, including strong field localization, minimal loss resulting from curvature, and a relatively straightforward manufacturing process employing state-of-the-art techniques [5]. This makes MIM-type waveguides particularly appealing for applications in nanophotonics and the creation of high-performance nanoscale optical devices.

In this thesis, all electromagnetic simulations were conducted using the FullWAVE simulator [6], which is based on the Finite-Difference Time-Domain (FDTD) algorithm. The initial portion of this chapter is dedicated to elucidating the fundamental principles of FDTD, the modeling of dispersive materials, and the boundary conditions relevant to the computational domain.

The latter part of this chapter delves into an examination of the characteristics of a two-dimensional plasmonic Metal-Isolator-Metal (MIM) waveguide coupled with nanocavities [7, 8]. Our study reveals that the physical phenomenon of coupling results in the emergence of transmission peaks, particularly when the nanocavity is positioned outside the waveguide. We provide a comprehensive analysis of the choices made regarding physical and geometric parameters within the MIM structure, which significantly influence its optical properties.

III-2 the tool of simulation

III-2-1 Rsoft CAD software

The RSoft CAD is a core program from RSoft Photonic; it allows users to create systems for the design of several types of devices; cavities, wave-guide, optical circuits and other photonic devices. It acts as a management program for the device simulation modules. *RSoft*: *BeamPROP, FullWAVE, BandSOLVE, GratingMOD, DiffractMOD, ModePROP, FemSIM,* et defines the important contributions required by these programs, the properties of the materials and the structural geometry of the device to be studied [9].

III-2-1- Full Wave Simulator

This is an integrated module in the software developed by the company RSoft, based on FDTD [6], this module allows us to study the spread of light for a wide variety of photonic and plasmonic structures as well as the calculation of the quality factor from any cavities to photonic and plasmonic structures. It is fully integrated into the Rsoft CAD environment, which allows the user to define the properties of materials and the geometry of the structure of any plasmonic device. The FullWAVE module can accurately model dielectric and magnetic materials, as well as anisotropic, dispersive, and non-linear materials [10], the use of this module requires defining the materials that make up the structure using electrical permittivity.

A key element of a FullWAVE simulation is the launch field of the structure. The excitement must be properly chosen to match the type of simulation results required. For example, a CW (Continuous Wave) excitation should be used when the permanent mode operation of a structure is desired, and a pulsed signal may be considered when the spectral characteristics of a structure are needed. The excitator field is defined via a dialog box of launch settings, which can be accessed through the “Edit Launch Field” button in the CAD interface [11].

III-2-2 Method of finite time differences (FDTD)

The method of finite differences in the time domain or FDTD, the English acronym of Finite-Difference Time-Domain, allows to accurately and reliably studying many problems belonging to electromagnetism. It is a useful tool for exploring the optical properties of metal nanoparticles because it allows to model highly heterogeneous systems, i.e. containing materials with different dielectric functions (dielectric, metal, plasma...) and complex geometric

shapes. Moreover, as this is a temporary method, a single simulation is needed to obtain the response of the system studied on a broad frequency band via the Fourier transform.

The FDTD was born from Yee's pioneering work in 1966 [12] and continued to be developed by Taflove's in the 1975s [13], its main advantage lies in the simplicity of its principle of operation. The basis of a FDTD code is based on two equations: the equations of Maxwell-Faraday and Maxwell - Ampère in their form and in the time domain.

The, the components of the electromagnetic field in each parallel epiped cell of the three-dimensional volume. (Figure III.1).

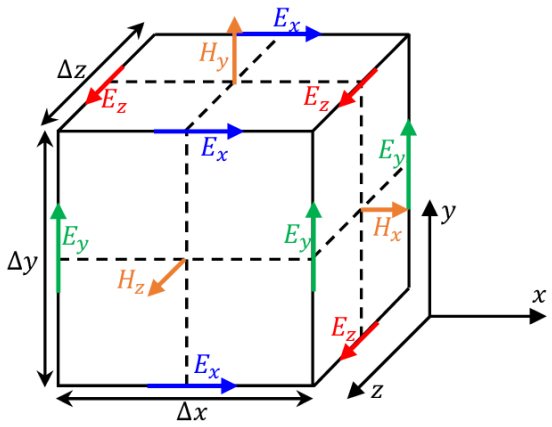

Figure III.1 *Spatial decomposition of the calculation volume [14].*

The principle is based on the division of space into elementary cells (*mailles élémentaires*). Each of these meshes is characterized by the physical properties of the element (*permittivité, perméabilité, conductivité*). Within which the six orthogonal components of electromagnetic fields are calculated (*Ex, Ey, Ez et Hx, Hy, Hz*). The particular form of Maxwell's equations leads to the calculation of the components of the electrical field in the middle of the edges of the mesh. The components of the magnetic field are determined at the center of the faces. (Figure III.1).

III-2-2-1 Conditions of stability

The choice of spatial and temporal steps is not arbitrary. It has an impact on both the accuracy and stability of the FDTD algorithm. FullWAVE supports both uniform and non-uniform space grid. In order to produce a precise simulation, the spatial grid must be small enough to simulate the smallest element of the field.

First, the spatial discretion must be fine enough to describe the geometry of objects belonging to the correctly studied system, as well as the distance between these objects. Furthermore, the transition from a physical problem in a continuous space-time to a discreet problem in an sampled time space creates a parasitic effect called numerical dispersion. This effect comes from errors made on estimating the wave spread speed in the calculation field. In order to minimize the distortion of signals due to digital dispersion, the spatial value is set according to the minimum wavelength present in the FDTD grid [15]:

$$Max\ (\Delta x, \Delta y, \Delta z) \leq \frac{\lambda_{min}}{10} \tag{III.1}$$

Ou, Δx , Δy, Δz : Discretion in Space.

In the case of a uniform $= \Delta y = \Delta z = \Delta$:

$$\Delta \leq \frac{\lambda_{min}}{10} \tag{III.2}$$

It follows from the equation (III.2) that it is necessary to have at least 10 cells per wavelength to obtain correct results.

Fullwave will provide a smart choice for these parameters, but the user is strongly encouraged to refine the grid sizes in order to produce an effective and accurate simulation.

Second, iterative time algorithms such as the FDTD can generate an erroneous, most often exponential, increase in the values of the electromagnetic field leading to the divergence of the calculation. In order to address this problem, it is necessary to ensure that when choosing the time increase it meets a criterion called digital stability [13]:

$$\Delta t \leq \frac{1}{c\sqrt{\frac{1}{\Delta x^2}+\frac{1}{\Delta y^2}+\frac{1}{\Delta z^2}}} \tag{III.3}$$

where :

c: The speed of light in the vacuum.

Δt: The time sampling step.

In the case of a uniform grid with $= \Delta y = \Delta z = \Delta$, the inequality (III.3) is simplified and becomes:

$$\Delta t = \frac{\Delta}{c\sqrt{3}} \quad \text{(III.4)}$$

III-2-2-2 Boundary Conditions

For obvious reasons of computing volume and therefore time and amount of memory used, we are forced to limit the volume of simulation. To reproduce the "illusion" of an open domain, the conditions at the limits commonly used are the absorbing conditions. (Absorbing Boundary Conditions). A first solution is to fix the field components to a zero value on the edges of the domain and not to apply the basic algorithm. Non-physical reflections then appear on these edges and severely disrupt the behavior of the structure. It is therefore necessary to create an algorithm to illustrate those edge components that aim to reduce reflections. The use of performance limit conditions is ultimately the major difficulty of implementing this calculation technique.

The Fullwave module uses the so-called PML (Perfectly Matched Layer) [16] limit conditions based on the absorbent layer model discovered by J.P. Confusing [17] and perfectly suited to the modeling of absorbing boundaries in electromagnetism.

The PML-type absorption condition is an artificial domain created for digital computing to address wave spread problems in infinite environments. Knowing that in digital simulation the fields conceived cannot be infinite, the idea is to set up conditions with absorbing limits at the borders of the field studied to prevent the wave from reflecting at the level of these borders. (figure III.2). The waves that thus cross the interface between the non-PML domain and the PML domain are absorbed at the level of the latter [18].

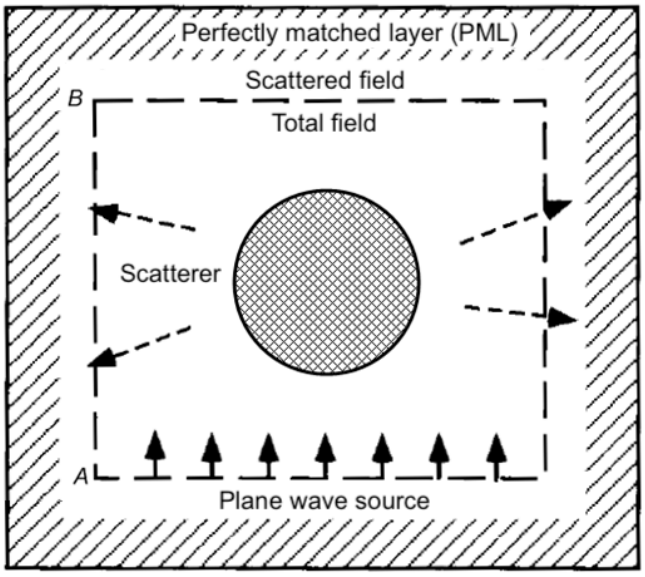

Figure III.2 *The PML technique.*

III-3 Modeling of Dispersive Materials and Conditions at Source

III-3-1 Modeling of Dispersive Materials

Within the FullWAVE simulator, the modeling of material dispersion, which entails the frequency-dependent permittivity (ε), is achieved through the implementation of the Drude and Drude-Lorentz models. These models are tailored to characterize the electrical (dielectric permittivity) and magnetic (magnetic permeability) properties of materials, respectively.

Dielectric permittivity encompasses the material's response to induced polarization when subjected to the propagation of an electromagnetic wave [19]. Metals, in particular, exhibit dispersive characteristics, wherein their permittivity becomes complex and varies with the frequency of the incident electromagnetic wave. To accurately represent the dispersion of metals, microscopic phenomenological models, such as the Drude model [20] and the Lorentz-Drude model, are employed. The selection between these models is contingent upon the specific metal being investigated and the spectral range of interest. It is worth noting that within the near-infrared spectrum, significant absorption of incident electromagnetic waves is observed in only metals and silicon. This information holds significant relevance when determining the appropriate dispersion model for conducting precise simulations within this spectral range.

III-3-2 Conditions on Source

All electromagnetic simulations in this thesis contain a source that produces a flat wave. It can be monochromatic by choosing a wavelength representative of the near-infrared spectrum. Spectral studies were conducted using a Gaussian source of $\lambda = 0.8$ μm to $\lambda = 1.2$ μm.

III-4 Theoretical study of plasmonic MIM structures with cavities

III-4-1 nanogide plasmonic MIM

Nanoplasmic waveguides, promoting SPP spread and manipulating light on a lower wavelength scale, can be considered an ideal optical element in an integrated plasmonic device.

There are different wave-guides based on SPPs, for example semi-conductor-isolant-semiconductor (SIS) waveguides, insulant-metal-isolating (IMI) wavelength guides, and metal-isolating-metall wave Guides. (MIM). Among these, the MIM wave guide has better properties, for example, stronger confinement of light, shorter spread length, low band loss, smaller mode

size, and easy and low manufacturing cost [9,10]. To date, a number of optical devices of the MIM wave guide structure have been extensively studied, for example, nanocapters [21-22], filters [23], separators [24] and demultipliers [25].

III-4-2 Differences in topologies for the realization of plasmonic devices

Micro-resonator-based devices have recently received special attention due to their potential for application in integrated optical circuits [26]. In the field of signal processing, resonators have marked their sensing capability in transfer functions.

Among the many possible configurations for the realization of plasmonic devices, metal-insulating-metal (MIM) topologies can be used to transport electrical and optical signals in an integrated circuit. Due to the unique optical characteristics of MIM configurations, they have received a lot of attention for the design of optical devices.

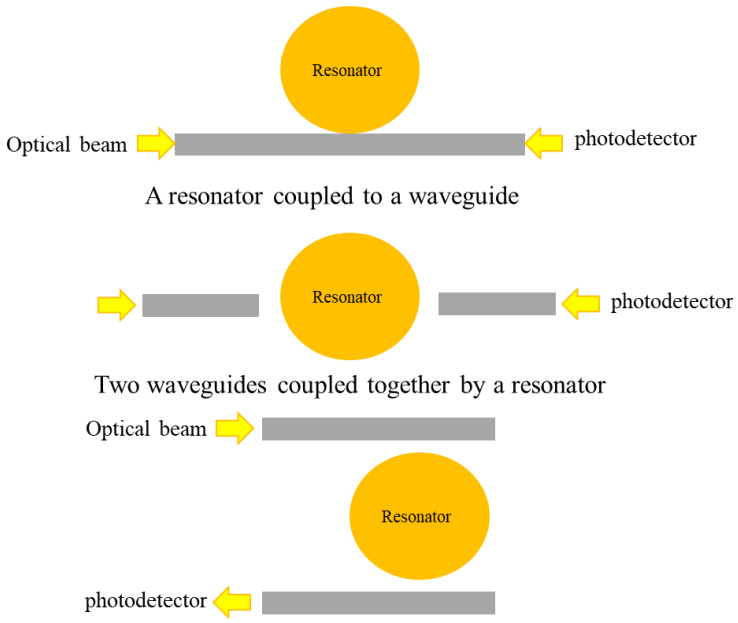

Figure III.3 *Different topologies for the creation of plasmonic devices. (a) A cavity coupled to a waveguide. (b) Two waveguides coupled together by a resonator. (c) Ring resonator topology.*

As shown in Figure III.3 there are several mechanisms for the design of an optical device. These devices consist of optical wave-guides and a resonator. The figures (III.3.a, b and c) are the conventional configurations that are referred to in the various publications in this regard. The figure (II1.3.a) shows a cavity coupled side by side with a wave-guide. This means that the resonance wavelength will be reflected towards the input port. Figure (III.3.b) shows a cavity located between two wave-guides, only the resonance wavelength will reach the output port.

Another solution that is widely used is to use the ring resonator topology represented on the figure. (III.3.c).

III-5 Numerical study of plasmonic MIM structures with cavities

III-5-1 Study of MIM waveguide

III-5-1-1 Description of the studied MIM wave-guide

Figure (III.4) shows a two-dimensional plasmonic wave-guide made of metal insulating. The grey and white areas represent the silver (m) and dielectric (d) layers respectively. In this structure, SPP modes spread through the common interface between the insulating metal along the Z direction.

Figure (III.4) shows a two-dimensional plasmonic wave-guide made of metal insulating. The grey and white areas represent the silver (m) and dielectric (d) layers respectively. In this structure, SPP modes spread through the common interface between the insulating metal along the Z direction.

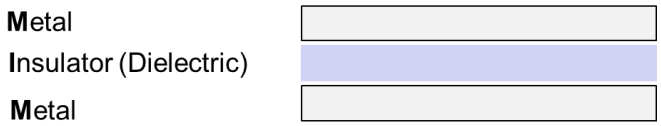

Figure III.4 *The structure of a metal-insulator-metal plasmonic waveguide.*

La figure III.5 présente la distribution de l'indice de réfraction d'une structure plasmonique MIM constituée d'argent pour le métal et d'air pour le diélectrique.

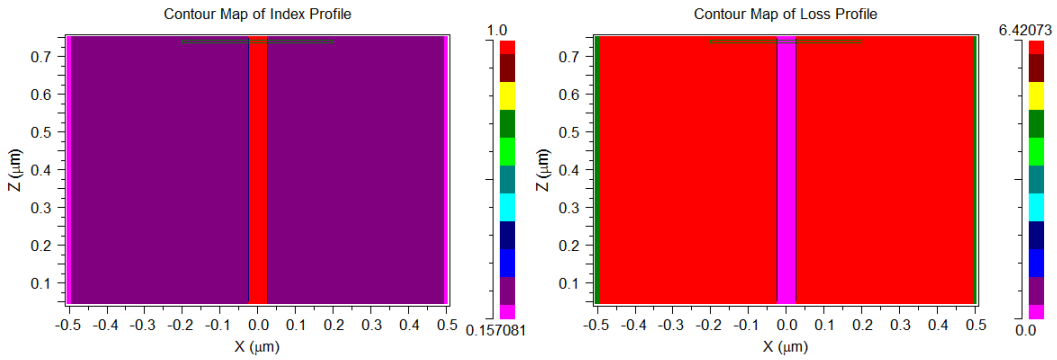

Figure III.5 *Distribution of the refractive index of a MIM plasmonic structure. a) The real part of the refractive index. b) The imaginary part of the refractive index.*

III-5-1-2 Analysis of the MIM waveguide studied

In this MIM structure, when the wave guide width becomes smaller than the wavelength of the incident light applied to the structure, the SPP waves are excited by the transverse magnetic mode (TM) inside the MIM. In this case, the dispersion ratio in TM mode is expressed by the equation (III.5) [27] :

$$\varepsilon_m\sqrt{n_{eff}^2-\varepsilon_d}\ tanh\left(\frac{W\pi\sqrt{n_{eff}^2-\varepsilon_d}}{\lambda}\right)+\varepsilon_d\sqrt{n_{eff}^2-\varepsilon_m}=0 \qquad \text{(III.5)}$$

In the equation (III.5), λ is the wavelength of the incident light, W is the wave guide width, $n_{eff}$is the effective refraction index, ε_d is the dielectric permissivity and ε_m is the metal permissiveness.

The complex relative permissiveness depending on the ε_m frequency of silver is characterized by the Lorentz-Drude model with its dielectric constant[28] :

$$\varepsilon_m(\omega)=\varepsilon_\infty-\frac{\omega_p^2}{\omega(\omega+i\gamma)} \qquad \text{(III.6)}$$

When :

- ε_∞ is the dielectric constant at the infinite angular frequency with a value of 3.7.
- ω_p is the frequency of the near-free electron gas of the metal, with a value of $1.38\times10^{16}Hz$,
- $\gamma=2.73\times10^{13}\ Hz$ is the frequency of collision of electrons,
- ω is the angular frequency of the incident wave in the vacuum[29].

The numerical resolution of the equation (III.5) allows to obtain the variation of the actual index according to the width of the guide. Its actual part, n'_{eff}, informs us about the rate of propagation of the plasmonic mode,

$$V_{SPP}=\frac{C}{n'_{eff}} \qquad \text{(III.7)}$$

and its imaginary part, n''_{eff} informs us about the L_{SPP}, defined as the length at the end of which the intensity of the wave is reduced by a factor 1/e [30]:

$$L_{spp} = \frac{\lambda_0}{4\pi . n''_{eff}} \quad \text{(III.8)}$$

The actual part of the effective refraction index for different wavelengths with W = 40, 50, 60 nm according to the equation (III.6) is shown in Figure III.6. It can be observed that when the width of the wave guide increases,, n_{eff} decreases [31].

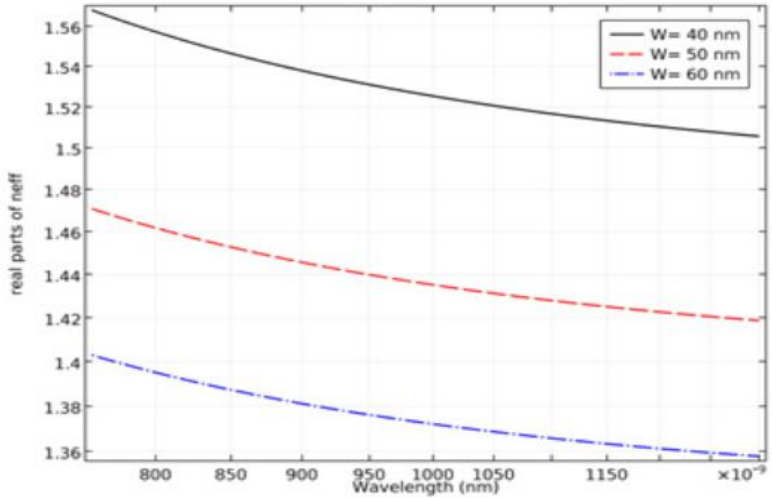

Figure III.6 *Effective refraction index for different wavelengths with a wave guide width of 40, 50 and 60 nm [31].*

Figure III.7 illustrates the evolution of the L_{SPP} spread length in $W/2$. We observe a quasi-linear evolution reflecting the decrease in propagation length with the confinement of the wave. Finally, for larger wavelengths (from 500nm to 700nm), the spread length increases significantly.

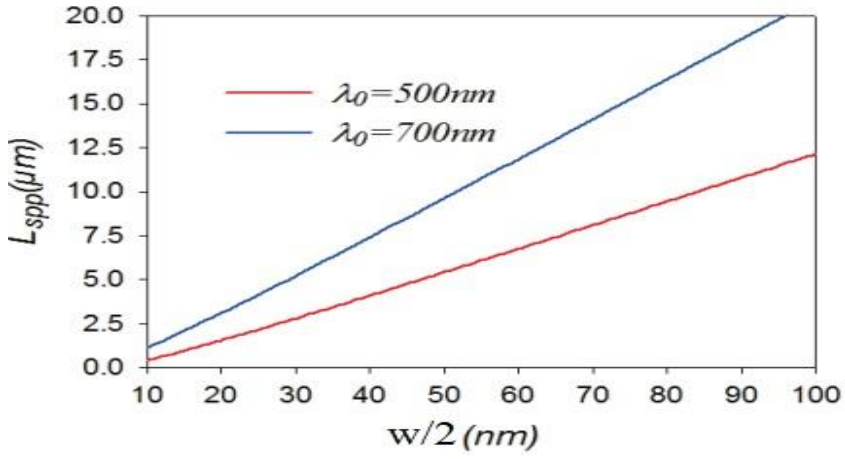

Figure III.7 *Variation in plasmonic signal propagation length in the MIM guide [32].*

The actual portion of the β propagation constant is represented by the effective index $n_{eff} = real\ (\beta/k_0)$, ($k_0 = 2\pi/\lambda_0$ is the free-space wave vector) of the wave guide for SPP. The actual part of the effective index n_{eff} based on the refractive index n of the detected material in a MIM slit wave guide structure for different incidental wavelengths, with W = 50 nm, is represented in Figure III.8. Obviously, n_{eff} is almost linear with the refraction index n in the range of 1.0 to 1.6 at all wavelengths [33].

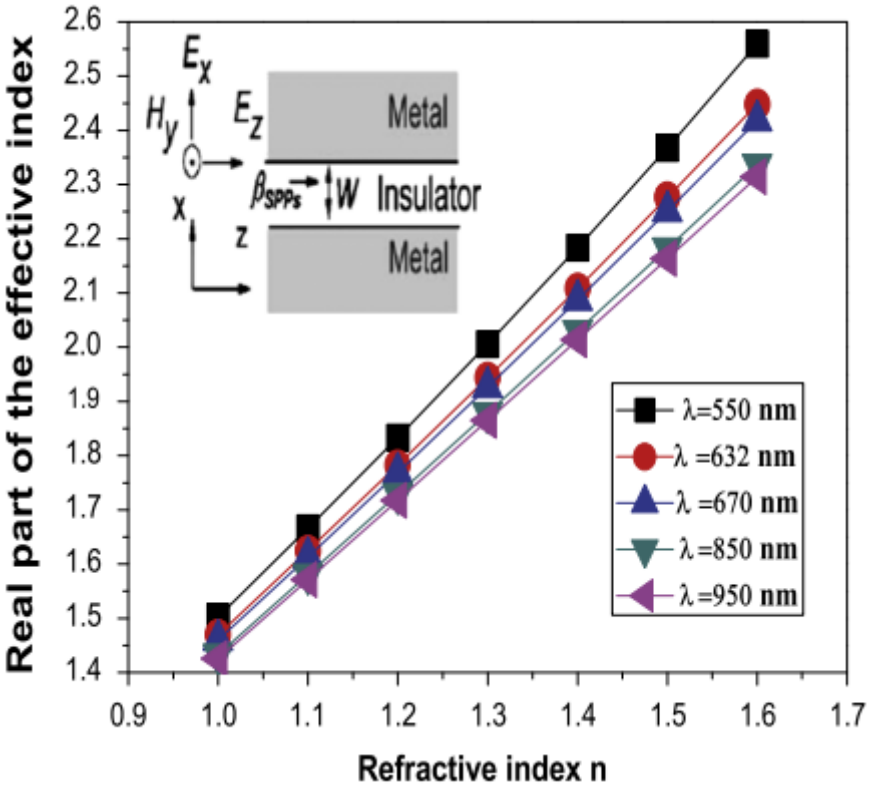

Figure III.8 *Actual portion of the effective index neff relative to the refractive index n of the detected material in a MIM slit waveguide structure for different incident wavelengths [33].*

III-5-2 Study of the MIM waveguide coupled to a nanocavity

III-5-2-1 Condition and results of the simulation

The FDTD method implemented using RSoft's commercial FullWave software [6], with the imposed condition of perfectly suited layers (PML) as the absorbent limit condition for all sides of the calculation window in order to absorb outgoing waves, is applied to the structure to simulate its transmission characteristics. The size of the grid in the x and z directions is chosen as $\Delta x = \Delta z = 5$ nm [21]. The input type is a continuous Gauss modulated wave of polarisation field TM. The transmitted light was collected on the right side of the waveguide

which is defined as T = Pout / Pin. Both the Pin incident power and the Pout transmitted power are observed at positions A and B.

Figure III.9 shows the transmission spectrum according to W_{t1} = 50 nm, *by adding a* material cavity.

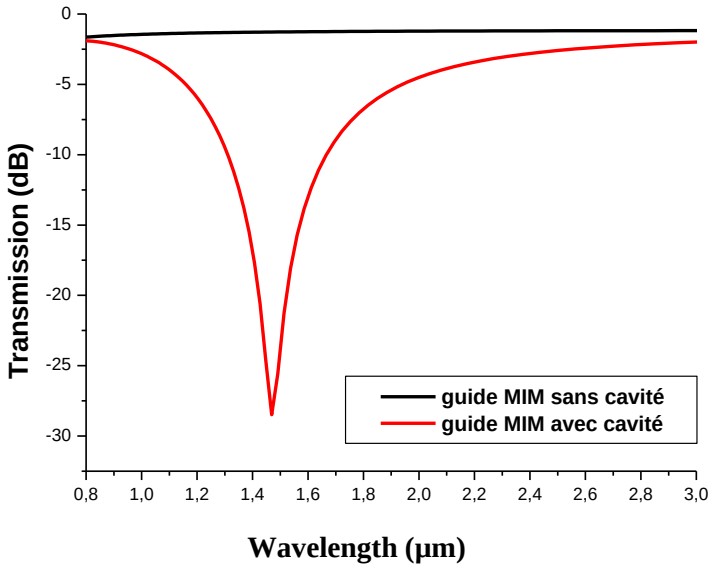

Figure III.9 *The transmission spectrum of the MIM waveguide with a cavity and no cavity.*

Such a cavity has several SPP modes, the number and position of which depends on the cavity geometry [34].

III-5-2-2 Analysis of the influences of construction physical parameters on the MIM rejection sensor response

III-5-2-3-1 Nature of the metal

The response of the MIM refractive sensor is strongly influenced by the nature of the metal in question. Thus, an analysis of the effect of variation of permissiveness m on the position and shape of the resonant peak is carried out. For this study, we will use the most commonly used metals for making surface plasmon resonance systems such as gold, silver, copper or aluminum.

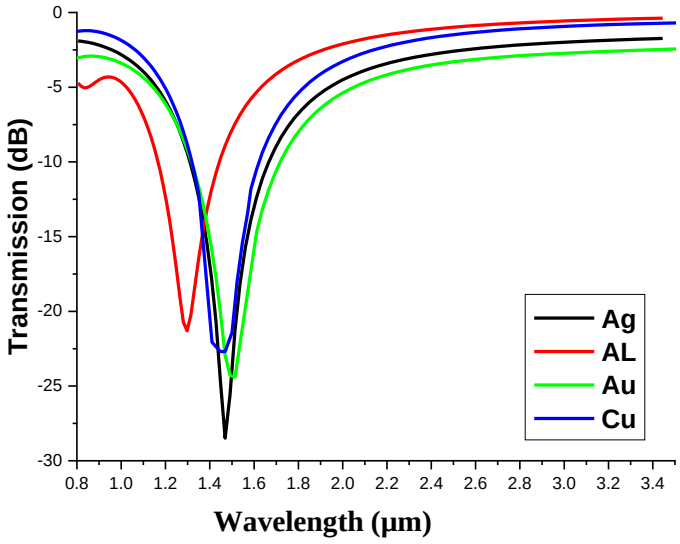

Figure III.10 *The transmission spectrum of the MIM sensor depending on the nature of the metal.*

Figure III.10 illustrates the influence of the nature of the metal on the MIM sensor response, this influence is determined by two main elements:

- Spectral Position of Resonance
- Spectral Selectivity of Resonance

Silver has the narrowest resonant peak, and it has the best transmission level and thus the best theoretical sensitivity.

III-6 Conclusion

In this chapter, we presented, first, the basic principles of the FDTD method. This technique is a well-suited method for the modelling of plasmonic structures mainly because it allows access to the dynamic characteristics of structures (transmission, reflection, field localization, resonator quality factor, etc.). It also allows the use of different and varied spatial profile sources (guided modes, flat waves, point source) and time profiles (harmony, impulses). PML-type boundary conditions are suitable for strong diffraction that occurs in plasmonic structures. It is therefore a tool of choice for the experimentator who wants for a better understand the physical meanings of the experimental spectrum of transmission or reflection.

The extension of the FDTD code to the simulation of real metals has paved the way for studies related to plasmonics. Based on our experience in the study of dielectric wave-guides, we have become interested in plasmonic metal-insulating nano-guides (MIM). Plasmonics finds its strength in the confinement of light in sub-wave-length guiding structures. In this work, we detailed the case of a MIM structure consisting of silver for metal and air for dielectric. The linear plasmonic nanowire was then coupled to a nanocavity, also in the air, located next to it

CHAPTER IV

Results and Explanations

IV.1 Introduction

Optical sensors are of great interest in various areas of research and industry, such as food safety, environmental monitoring and medical diagnostics [1, 2]. Advances in surface plasmon polarite (SPP) structures and devices, as well as research in this field, have shown extensive applications in chemical sensors and biosensors.

As for our work, we focused on plasmonic nano-sensors using a metal-isolant-metal wave guide (MIM). This type of device has been considered one of the most popular structures for the SPP wave guide because it has a long spread distance and strong field confinement.

MIM plasmonic nano-sensors for refraction index (RI) measurements have been a very engaging subject of research in recent years, and until today new technologies are being proposed. The application of RI sensors includes measurements of parameters such as temperature, humidity, chemical composition, DNA detection, proteins, cells and bacteria.

This work includes three proposals for plasmonic refraction index nano-sensor with MIM wave guide. The first proposal based on a slit and a hexagon ring resonator. In order to determine the impact on sensor functionality and refractive index sensitivity, we have varied the length of the inner side of the hexagonal resonator with the distance between the six-point ring resonador and the wave guide. The second proposition is based on a slit and two identical intersecting rings. We varied the distance between the center of the two ring resonators and their inner radius to study the effect of changes in parameters on its detection characteristics and its sensitivity to the refraction index. The third proposal is based on a MIM wave guide coupled to double teeth and a rectangular shape defect inside the first dental cavity. In this proposal the design and improvement of a highly sensitive metal-insulating-metal plasmonic sensor in the medium infrared spectral region are presented.

IV.2 The effect of the interaction between the MIM guide and nanocavity on sensor sensitivity

The effect of the interaction between the MIM guide and nanocavity on sensor sensitivity

Sensor sensitivity is one of the most critical merits in evaluating sensor functionality for various substances based on the variation in the refractive index. The aim is to improve the sensitivity aspect by using various designs in a limited space and to evaluate the most efficient sensibility and transmission characteristics.

Incorporating a MIM resonator could be a viable option to overcome challenges and can enhance sensitivity through increased field confinement. The introduction of defective cavities in the conventional MIM wave guide ensures a longer interaction between the produced SPP modes and the test molecules presented in the active area of the sensor. This improvement in interaction length can theoretically improve the sensitivity of the SPP products. To establish the fully desired confinement and minimize the complexity of the spread length, (which is common in the case of MIM designs), the sensor size should be as small as possible with an acceptable size [3]. A change in the resonator resonance wavelength, where the material to be tested is mounted, can identify the change in refraction index as a result of a change in material, temperature or molecular concentration.

Recently, efforts have been made to study plasmonic nano-sensors based on MIM wave guides or structures coupled with wave guidance. These nano-sensors include a plasmonic wave guide with ring resonators [4], a tooth-shaped structure [5], a slit cavity [6], a nano-disk resonator [7], and a single-defect MIM waveguide [8]. In all the previous structures, the plasmonic resonator is the critical part that influences the detection characteristics and transmission of devices.

IV.3 Conditions for simulation of proposed plasmonic nanocapters based on MIM structures

In this work; we have proposed three MIM structures; including Figure IV.1 (a, b et c). The thickness of the proposed MIM structures in the third dimension is much larger than the size of the entity in the calculation plan. (2D). So the effect of the thickness of the substrate on the results obtained can be neglected by mathematically assuming that the structure is infinite in the third dimension [9–10]. Thus, our simulations are all carried out in 2D because of the significantly feasible reduction of calculation time without compromising the accuracy of the calculation.

(a) **(b)** **(c)**

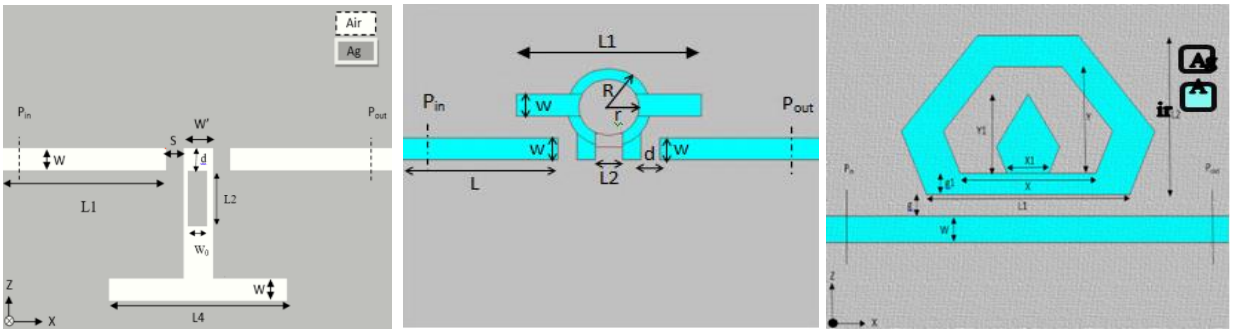

Figure IV.1 *Proposed MIM structures.*

In the three proposed structures, the grey and white zones represent the silver layer (ε_m) and the dielectric ((ε_{in}). respectively. The complex relative permissiveness based on the m frequency of silver is characterized by the Lorentz-Drude model.

The incidence light for excitation in our SPP mode simulation process is polarised TM, this leads to the magnetic field being parallel to the y axis [11]. Only the basic mode (TM_0) can spread along the wave guide because the waveside width is much smaller than the incident wave length.

The two-dimensional FDTD method using RSoft's FullWave software with perfectly matched layers (PML) is applied on all sides to simulate the transmission spectrum of the structure. The grid sizes in the x and z directions are chosen as $\Delta x = \Delta z = 5nm$, based on the size of our structures, it should be below the minimum of our small gap which we used here 10 nm, and the time pass, derived from the current condition is $\Delta t = 0.95/c\sqrt{(\Delta x)^2 + (\Delta z)^2}$ [12] where c is the speed of light in the free space. The input type is a Gaussian modulated continuous wave of the polarisation field TM. Two power monitors are set to A and B to detect emitted and incident power. To calculate the transmittance of the wave guide, $T = P_{out} / P_{in}$, P_{in} incidence power and P_{out} transmitted power are controlled at positions A and B, respectively. The effect of simulation grids on the simulation is achieved. The above FDTD calculations are repeated for smaller grid sizes and precision is compared: if comparable accuracy is obtained, the results are accurate. If there is a big difference, successively smaller grids are used until accurate results are found. This convergence process is done with the stop time to ensure accurate spectral results.

IV.4 Design and analysis of high-sensitivity near-infrared plasmonic biosensor MIM

IV.4.1 Description of the first structure studied

The proposed plasmonic structure based two sharp Fano resonances are achieved by employing rectangular cavities ; we placed a perpendicular cavity between the MIM waveguides, while another horizontal one is integrated to the bottom of the first one. Due to the interactions, the Fano resonances dual with asymmetrical line shapes ; wherefore, double sharp peaks are obtained with high sensitivity. Besides, to enhance the sensitivity, an additional cavity is added to the middle of the perpendicular cavity. The structure's performances are investigated using the finite-difference time-domain (FDTD) method.

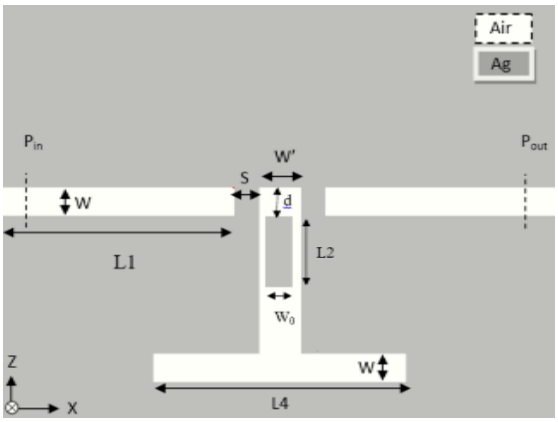

Figure IV.2 *The MIM plasmonic structure.*

Figure IV.3 shows the distribution of the refraction index of a plasmonic MIM structure consisting of silver for the metal and air for the dielectric.

When the SPP wave spreads along the wave guide, part of the energy is coupled inside the cavity, producing static waves that would create a resonance in specific wavelengths.

The resonance wavelength λ_m of the rectangular plasmonic cavity can theoretically be obtained by [16]:

$$\lambda_m = \frac{(6L_{eff})x\ \mathrm{Re}(n_{eff})}{m - \varphi 2\pi} \qquad \text{(IV.1)}$$

where L_{eff} is the lateral length of the rectangular cavity, Re (n_{eff}) is the real part of the effective refraction index of the cavity of the rectangular form. The positive integer m represents the order of the stationary SPP wave in the cavity; φ also presents the total defase in the corners of the rectangular cavity.

IV.4.2 study the transmission and sensitivity

The proposed structure's geometrical parameters L1, L3, L4, S, W', are set as 455 nm, 500 nm, 450 nm, 15 nm and 70 nm, respectively, the width W of the MIM is set as 50 nm, we chose this width according to the previous researches and our simulation results [7–10]. First, the MIM and the cavities' structure filled with nothing ; this means that the insulator is air (n = 1).

The rectangular-shaped cavity structure shown two sharp Fano resonance appears according to Figure. ***IV.3***, with a maximum transmission value of 98 and 67 %, was named mode 1 and mode 2 at the resonance wavelength of 1062 nm and 2272 nm, respectively

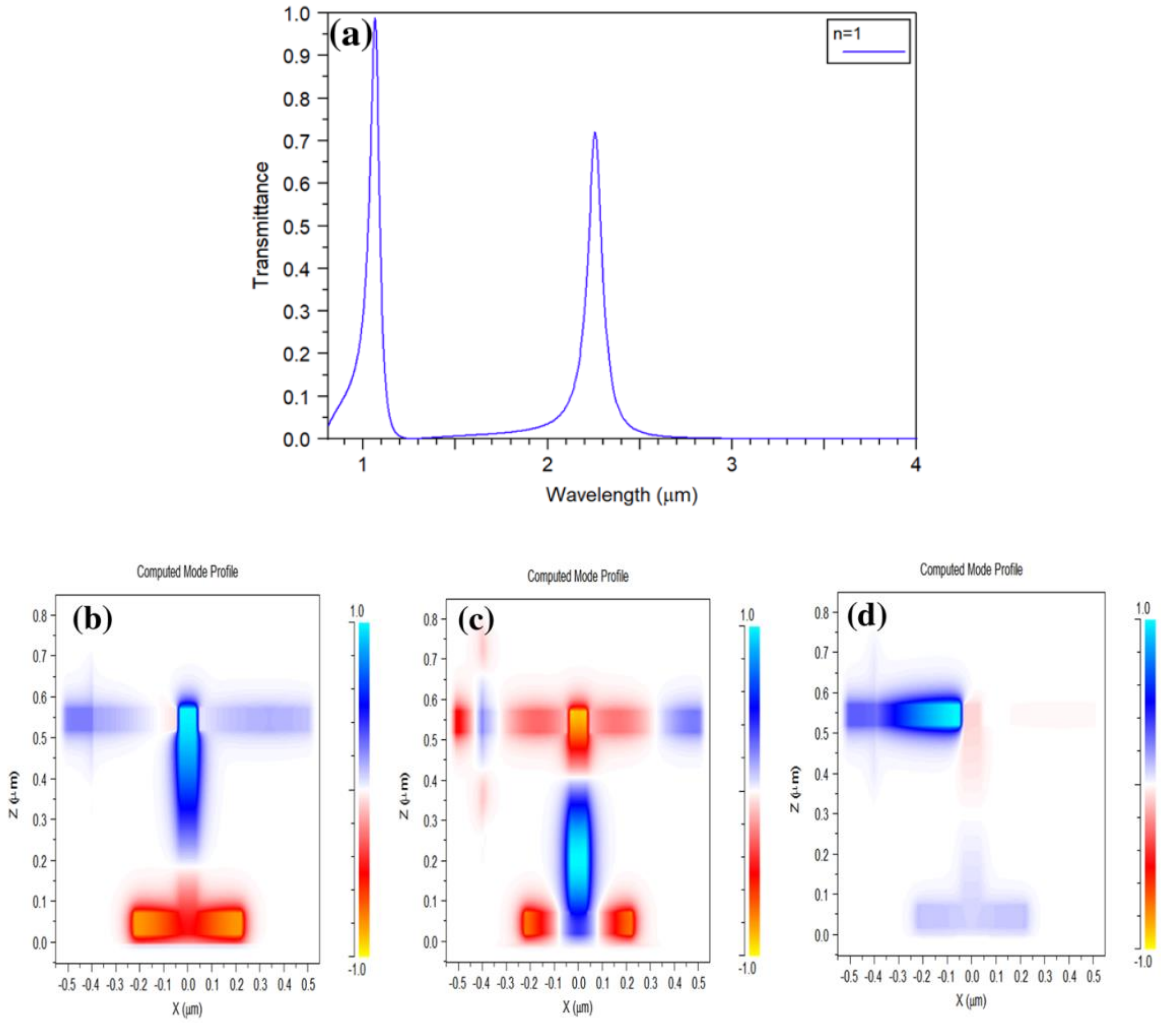

Figure IV.3. *The transmission spectra of the MIM waveguide(a). The contour profiles of field |Hz| of the resonator for(b) at 1.098µm, for (c) at 1.297µm, for (d) at 3µm.*

In such cases, the waveguide output exhibits a high energy distribution, as seen in Figs. ***IV.3*** a and b. We can clearly see an increase in the resonance wavelength at 1098 nm and 1297 nm, which correspond to the resonant peak wavelengths at modes 1 and 2, respectively. At the resonance wavelength, the power transmission spectrum and Hy field pattern are obtained. In contrast, no SPPs waves flow through the output waveguide at 3000 nm in Fig. ***IV.3*** c, showing that the wavelength cannot transfer in this structure, which is consistent with what we discovered in Fig. ***IV.3*** a.

In Figs. ***IV.4,*** when the structure's refractive index changes from 1 to 1.08 with a step of 0.02 to be able to calculate the shift and study the sensitivity of the structures, This shift in the resonant wavelength ($\Delta\lambda$) tells us about the RI shift (Δn). As a result, the spectrum sensitivity of such sensors is commonly defined as $S = \Delta\lambda / \Delta n$ [21]. According to the definition, the

plasmonics sensor's sensitivity value in mode 1 is 1155 nm/RIU, whereas mode 2 is 2360 nm/RIU. The sensitivity of all sensors must be evaluated [22].

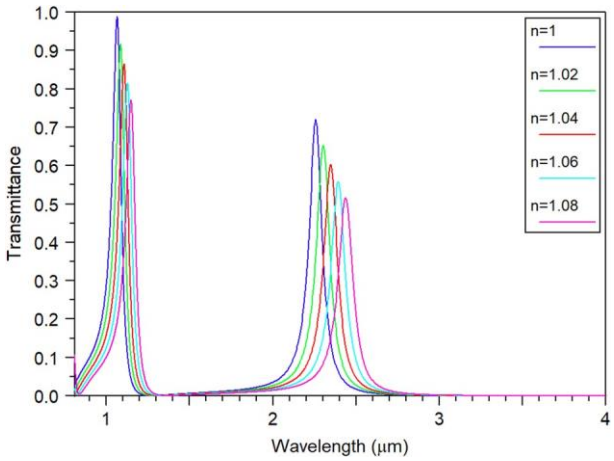

Figure IV.4 *The structure transmission spectrum for different refraction indices n,*

IV.4.3 Geometric Optimization

IV.4.3.2 Influence of the cavity on the transmission spectrum and sensitivity of the biosensor

We use a new cavity C inside cavity A with unique characteristics to improve sensitivity. We fix S in Fig. ***IV.5 and*** set L2, L3, and L4 to 15nm, 100nm, 500nm, and 450nm, respectively. Modes 1 and 2 have a linear green shift in the transmission spectrum of both structures with and without cavity C, as shown in Fig. ***IV.6*** and the variations of resonant wavelengths of modes 1 and 2 are 293 nm and 229 nm, respectively.

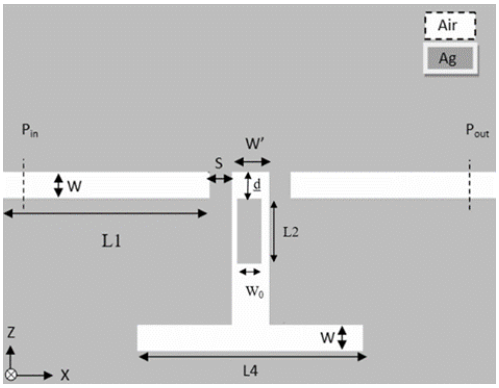

Figure IV.5 *Schematic* diagram of the plasmonics sensor with cavity C

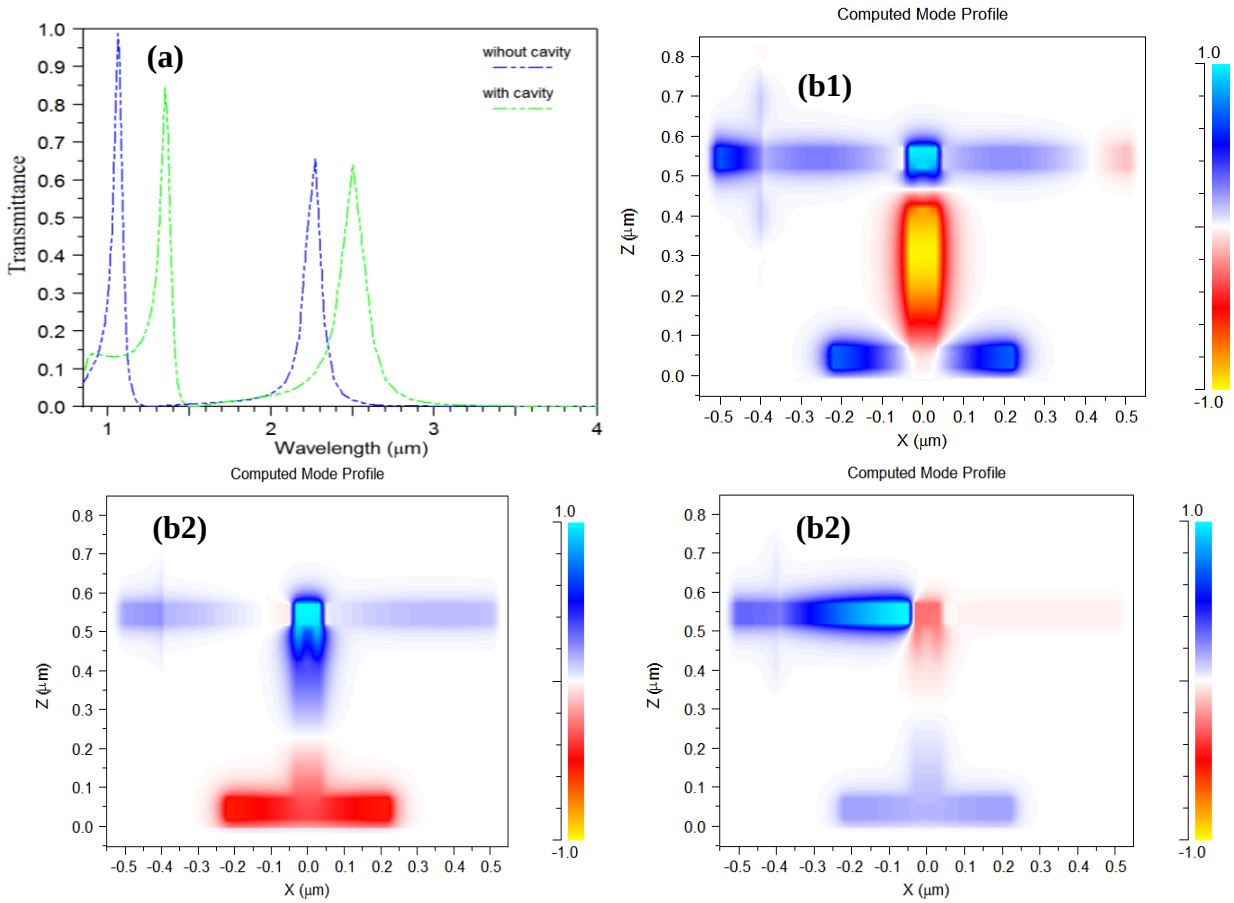

Figure IV.6 *The transmission spectra of the MIM waveguide.*

The results imply that with cavity C we decrease transmission from mode 1 and mode 2 by 14.14% and 2.6%, respectively, however we improve and increasing the sensitivity with cavity C. To gain a better understanding of the inner mechanism of SPRs in the MIM and the change in the transmission spectra, the magnetic field distribution of the spectra applied at the resonance presented in Figure. 5(b, c), a strong energy distribution can be observed shown in c1 and c2 correspond the resonance of mode 1 at 1.393µm and 2.587µm for mode 2, however, for b3 at 3µm we notice that there is no resonance in output and this conform with what we found in Figure. IV.6.

IV.4.3.1 Influence of coupling distance the gap on the behavior of transmission peaks

In order to further investigate the performance of the cavity C on the proposed structure of the plasmonic sensor, we studied the effect of the length d on the transmittance characteristics, by changing length d from 0 to 200nm with step of 50nm, we notice that the position of cavity C has an effect on the narrow and the transmission on both modes as shown in Figure. IV.7 (a). Clearly it is observed that the transmission spectra of the peak for d=100nm

become better and narrow and when we increase the length d=150, 200nm, we decrease the transmission of both modes, however, by using the value of d=0 the Fano resonance loss their narrow and transmission. Therefore, we used d of 50 nm for the rest of our studies to have a narrowest resonant peak for better resolution. Next, we focus on the influence of the refractive indices by increasing n from 1.00 to 1.04 with step of 0.02, as it displayed in Figure. IV.7 (b), we notice a redshift in the resonance wavelength by increasing the refractive index, this change in the resonant wavelength $\Delta\lambda$ provides a highly sensitive for both modes, therefore we achieved the sensitivity for mode 1 and mode 2 as 1166 nm/RIU, 2220 nm/RIU, respectively [18].

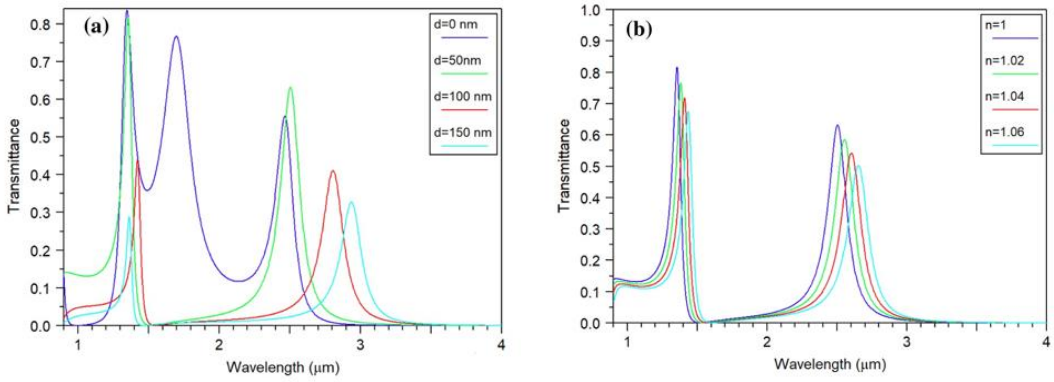

Figure IV.7 *The Shift of the resonance wavelength with cavity C by changing length d from 0 to 150 nm (a). The transmission spectra of the structure for different refractive indices n.*

IV.4.4 The design and performance improvement of a plasmonic biosensor

For better characterization of the performance of a plasmonic sensor, the sensitivity (S), are considered as the most important parameters, and should be, preferably, as high as possible for a more performing sensor [19].

Using a secondary cacity inside the main retangular, (as illustrated in Figure IV.5), To improve the performance of the sensor, we investigate how the length L4 affects on the sensing characteristics and the dependence of resonance wavelength, we varied the value of L4 from 100 to 700 nm with a step of 100 nm and 70nm as W', Indeed, we noticed a significant linear relation between the sensitivity and the value of the length L4, by increasing L4 we also increase S for both modes as shown Figure 7(a). Further, the sensitivity for mode 1 increased from 1166 to 1650 nm/RIU, then we archive highly sensitivity from 2220 to 3010nm/RIU for mode 2,

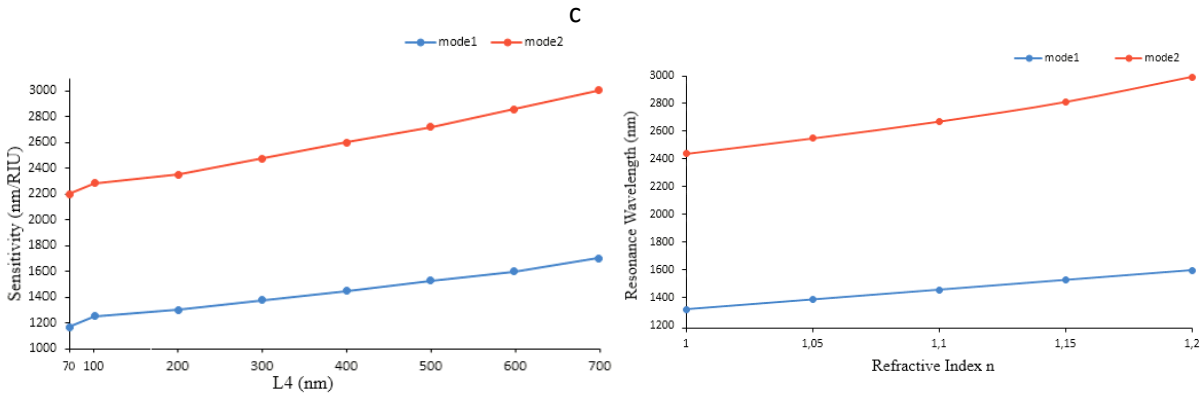

***Figure IV.8**. The sensitivity versus the length L4 (a). The resonance wavelength versus the effective length L4. The resonance wavelengths versus different refractive indices n by varying n from 1 to 1.2 with a step of 0.1(b).*

IV.5 High-sensitivity sensor based on double-ring resonators intersected in a metal – insulating – metal structure

IV.5.1 Description of the second structure studied

The MIM plasmonic structure pattern is shown in Figure IV.9. It consists of a slit and two identical intersecting rings. The wave-guide width, the distance between the ring resonator and the wave guide, and the gap between the centers of the two ring resons, are noted respectively w, g, and D. The inner and outer rays of the ring are defined by r and R, respectively. Structural parameters are defined to be w=50 nm, R = 450 nm, r = 120 nm, g = 10 nm and D = 100 nm respectively. The resonance wavelength of the ring resonator can be given approximately by the following (20):

$$\lambda_m = \frac{2Re(n_{eff})L_{eff}}{m}, m = 1,2,3,\ldots \qquad \text{(IV.2)}$$

Or $L_{eff} = \pi(r+R)$ *is the effective resonance length*, Re (n_{eff}) is the real portion of the effective SPP refraction index.

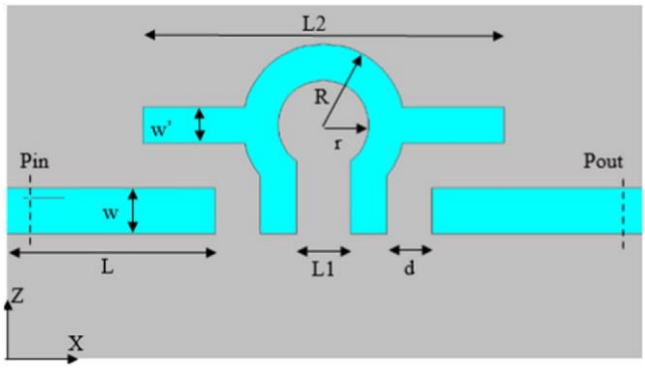

***Figure IV.9** Principle scheme of the plasmonic structure MIM.*

IV.5.2 Transmittance and Sensitivity Study

First, the refraction index n of the insulant in the dielectric core and cavities is assumed to be equal to 1. As we can see from Figure IV.10, We start by choosing to fill the insulator with nothing; this means that the insulator is air (n = 1) than the output characteristics of the structure has been calculated as showing in Fig. 2a, we achieve one sharp peak with high power of transmission in mid-infrared (mid-IR) rang at λ = 2860 nm. The mid-IR range is particularly wellsuited for biosensing as it encompasses the molecular vibrations that uniquely identify the biochemical building blocks of life2 and 12.5% for mode 1.

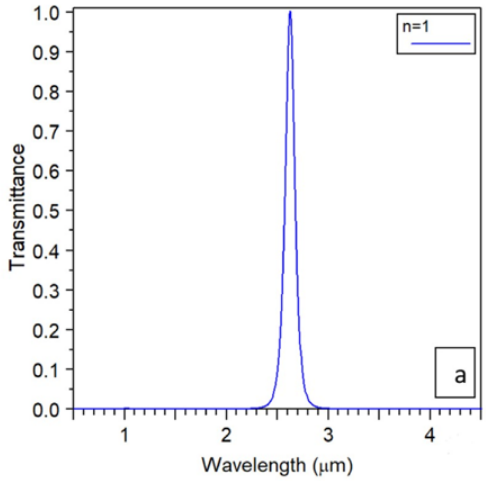

Figure IV.10 the transmission spectra of the MIM waveguide

Further, to gain a deeper understanding of the change in the transmission power mechanism, Figure IV.11 presents the resonance's magnetic field. Figure IV.11(a) there is no resonance at 1700 μm. Nevertheless, in the resonance of 2860 nm, a vital energy distribution can be observed in the output waveguide, as shown in Figure IV.11(b). The proposed structure is applied for the refractive index sensor.

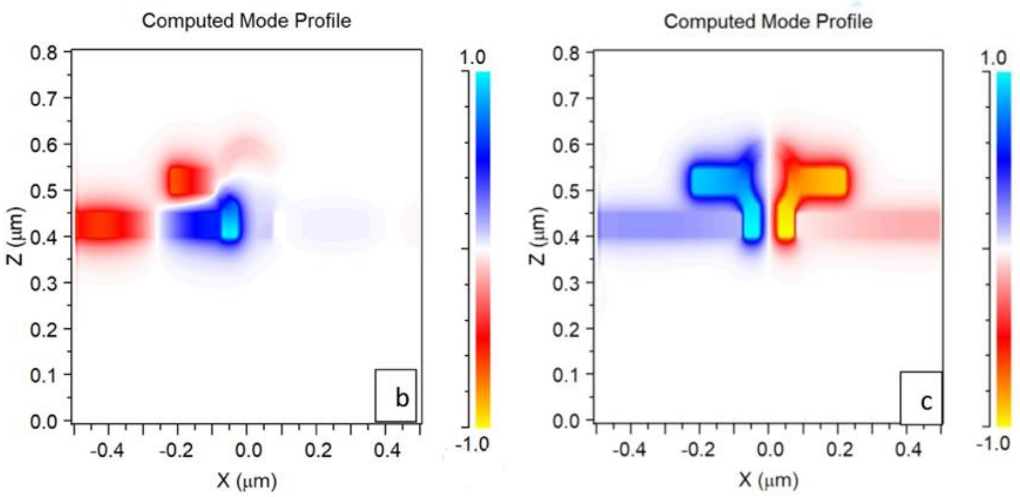

Figure IV.11. *(a) : The contour profiles of field /Hz/ of the resonator at 1.700 µm, (b) at 2.6275 µm.*

While keeping the other existing parameters fixed and increasing the refractive index from n = 1 to 1.2; The proposed structure is applied for the refractive index sensor. Therefore, the transmission spectra of the structure with different refractive indexes are studied by changing the refractive indexes from 1.00 to 1.08 with a step of 0.02, and the results are displayed in Figure IV. 12, its clear can be seen that the wavelength is shifting as we increase the RI.

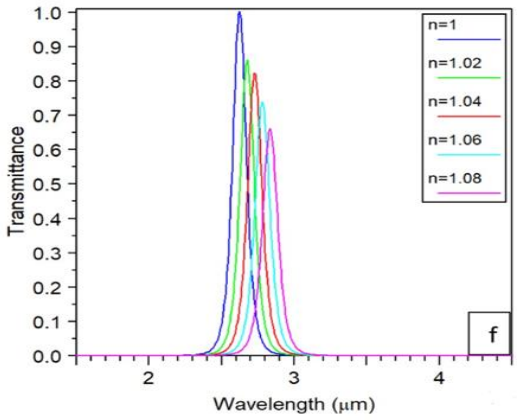

Figure IV.12 *The transmission spectra of the structure for different refractive indices ranged from 1.00 to 1.08 with a step of 0.02.*

IV.5.3 Geometric Optimization

IV.5.3.1 Influence of rectangular cavity's L_2 on the behavior of transmission peaks

To optimize this plasmonics structure characteristic parameters', we studied the rectangular cavity's influence. We varied the length of L2 from 440 to 940 nm with a step of 100 nm as shown in Figure IV.13. It is evident that by increasing the length from 440 nm to 900 nm, we

decrease the power of transmission from 98% to 26% because as we increase the length L2, the SPPs come to contact with the increment lossy metallic part affecting the lossy transmission with a shift in the resonance wavelength occurs. According to Eq. 3, a proportional relationship between the effective length of the surface plasmon SP (L2) and the resonance wavelength conforms to the resonance wavelength shift in Figure IV.13 [18].

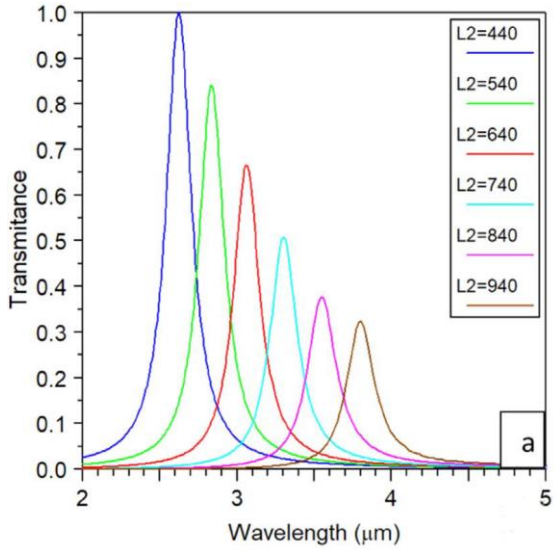

Figure IV.13 *The transmission spectra for different L2.*

IV.5.3.2 Influence of the the inner (r) and outer (R) radius and the shap of the cavity on transmission spectrum and sensor sensitivity

Figure IV.14(a) illustrates the influence of the inner (r) and outer (R) radius as depicted in Fig. 3b, with R = 180 nm, r = 120 nm, and R0 = (R–r) from 60 to 30 nm with a step of 10 nm by fixing the length L2 to 440 nm from Figure IV.13 for better transmission. Indeed, we noticed that for R0 = 30 nm, we lose the power of transmission. At the same, by decreasing the radius R0, we decrease The transmission. However, for the radius of 50 nm, we achieve a sharp and narrow peak wavelength with high transmission power. To further investigate the performance and explain our choices to this structure, we studied the main design with circle and notch cavity, without notch cavity (ring cavity) and without notch and circle cavity (circle) on the plasmonic sensor as shown in Figure IV.14(b), by using the optimum value of the parameters we found in Figs. 3a,3b as L2 = 440 nm and R0 = 60 nm, and keeping the same other parameters fixed, it is clear that with the main design, we achieve a high transmission with a sharp and single-mode of resonance wavelength in the mid-IR range with is the range we use in biochemical applications, for ring cavity and circle we achieve in NIR range a

resonance wavelength coupled with to peaks, wich used in communication application, i.e. (filer…).

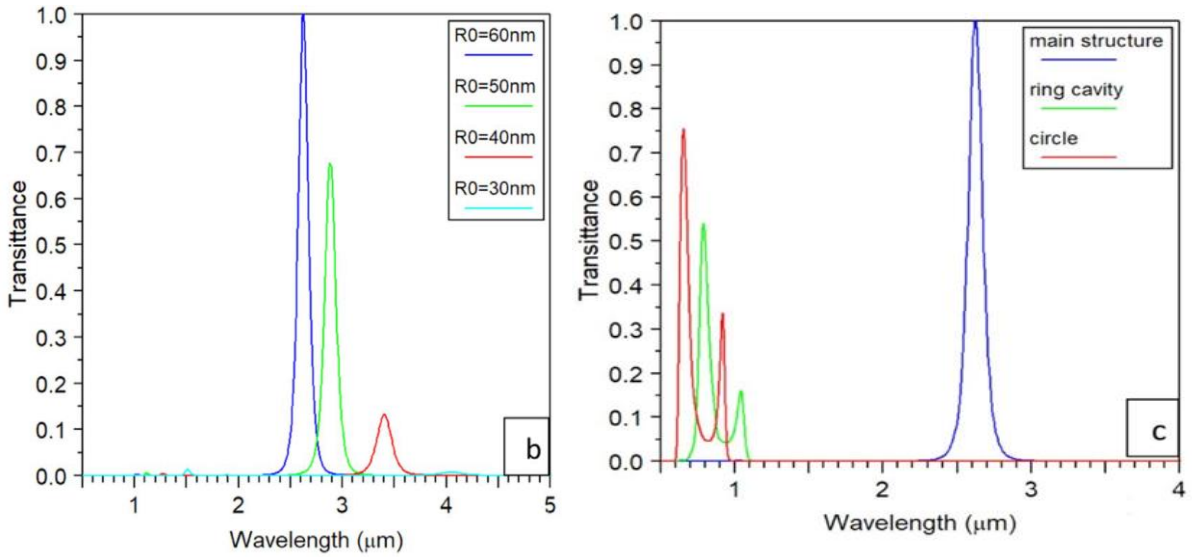

Figure IV.14 *(a) the transmission spectra for different radius R0, (b)the transmission various the wavelength for a different structure without cavity (ring cavity), without the ring (circle), and the main design with L2 = 440 nm and R0 = 60 nm.*

IV.5.3.3 Influence the rectangular cavity length L2 on the sensitivity and the refractive index for sensor sensitivity

We have also studied the effect of the rectangular cavity length L2 on the sensitivity for that purpose. We achieved linear improvements from 440 to 740 nm and maximum increases From 740 to 940 nm of the sensitivity concerning the rectangular length L2 by changing the length L2 from 440 to 940 with a step of 100 nm by keeping the same parameter as mentioned before. As we can see in Figure IV.15 (a), clearly we notice an increase in sensitivity as we change the length from 440 to 740 nm, this increase get a high from 840 nm till the maximum value as L2 = 940 nm, with high sensitivity, reach to 4572 nm RIU^{-1}. We can explain this improvementas we increase the length of L2 we increase the interaction between the surrounding medium and the SP. Figure IV.15 (b), by varying the refractive index n from 1 to 1,4 with an interval of 0.1, a linear relationship between the refractive index and the resonance wavelength was achieved, in the sensitivity due to the length of the surface plasmon (SP).

we use unique parameters (n = 1.3 and varying L2 from 400 to 300 with W’ = 40 nm) to investigate the perfect length of L2 to obtain a sharp peak with a high transmission as possible as we can. Figure IV.15 (c) depicts the change in transmission spectra for different rectangular length L2, as we notice for the length L2 = 400 nm with W’ = 50 nm w lose the transmission peak. On the other hand, according to section 3, the rectangular cavity is the key parameter to

improve the sensitivity ; as we increase the length L2 of the cavity, we achieve high sensitivity. However, we lose the transmission spectra as an effect of the loss of metallic parts with SPPs. Therefore, to enhancing the transmission, we should decrease the length L2, which in Figure IV.15 (a) confirms that, by varying the width W'from 50 nm to 40 nm, the results show that as we decrease the width W' we increase the transmission spectra. To thus, we choose L2 = 300 nm as the optimum value for the next analyses.

Moreover, the refractive index sensor in biomedical applications has been investigated, as shown in Figure IV.15 (d)for n = 1.3 to 1.4, which makes the sensor suitable for biochemical and medical diagnostic applications.

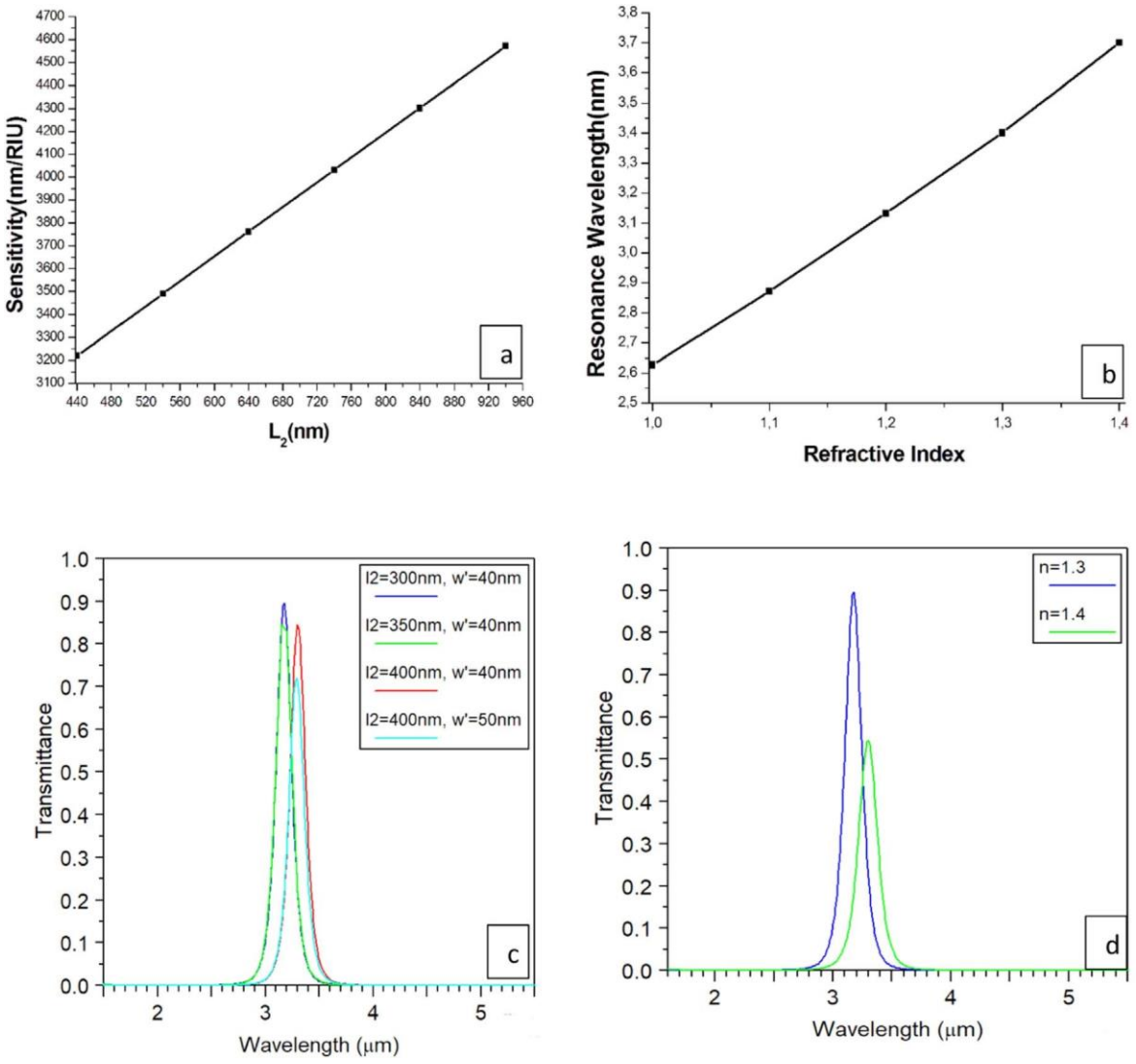

Figure IV.15 *(a) the sensitivity vs different length L2 from 440 to 940 with a step of 100 nm. (b) The resonance wavelengths for different refractive indices n by varying from 1 to 1.4 with a step of 0.1. (c) The transmission spectra for different L2 with n = 1.3. (d) The transmission spectra of the structure with l2 = 300 nm and w' = 40 nm for different refractive indices n = 1.3 and 1.4.*

IV.6 A high-sensitivity biosensor based on a metal–insulator–metal diamond resonator and application for biochemical and environment detections

IV.6.1 Description of the third structure studied

The pattern of the third structure of the proposed MIM sensor is shown in Figure IV.16. A MIM waveguide structure and the sensor geometry parameters are depicted in Figure IV.16 (a). The surface plasmon (SP) can focus and impinge the light using the subwavelength scale metallic structure. For this reason, due to the long side interaction, hexagonal resonators have high importance compared to circular and disc resonators. So they can effectively eliminate many constraints on the gap between the waveguide and resonator, and achieve a high value of sensitivity by decreasing the radiation loss of SPP propagation.

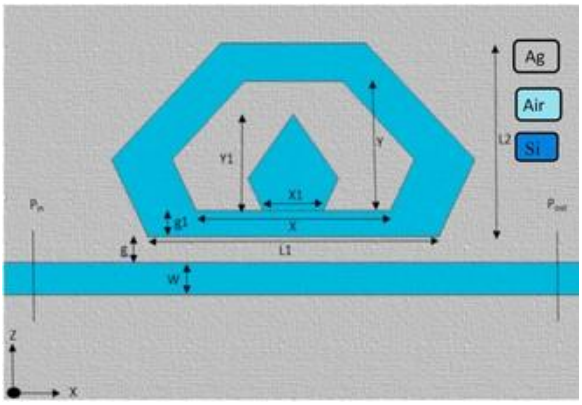

Figure IV.16 *2D schematic diagram of the proposed sensor structure.*

Figure IV.17 shows the distribution of the refraction index of a plasmonic MIM structure consisting of silver for the metal and air for the dielectric.

In IV.17 (a), we achieve one sharp peak with high transmission at a wavelength of 1982,6 nm. To get a better knowledge of the inner magnetic field process. As a result, IV.17 (b) depicts the magnetic field pattern of Hy at the wavelength of the peak, as we can see a strong energy distribution inside the cavities but nothing in the output waveguide. However, in IV.17 (c) outside the peak's resonance wavelength, the robust energy can be seen in the output, which agrees with the results shown in Fig. 1. Next, In IV.17 (d), the transmission spectrum has been studied versus wavelength for different refractive index. The RI ranges from n =1–1.08 with a 0.02 step, while the other parameters remain constant. As we increase the RI, the resonance wavelength shifts, this redshift phenomenon is caused by the proportional relationship between the Re (neff) and the wavelength λm. The refractive index shift Δn is revealed by a change in the resonant wavelength. Hence, it is conventional to define the most important parameters to characterize its performance. The values of these parameters are preferred to be much higher

for biosensor devices, which is the spectral sensitivity of such sensors as S =Δλ/Δn. For this structure, the sensitivity is 2260 nm/RIU.

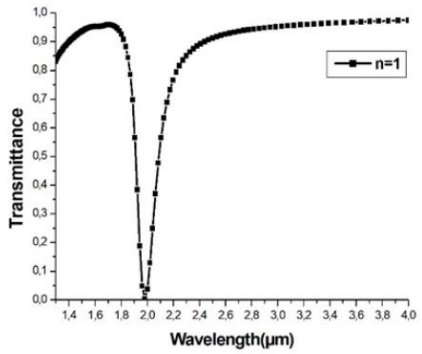

(a)

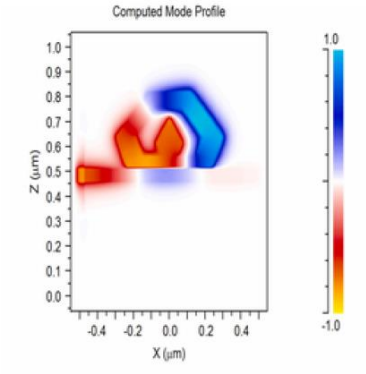

(b)

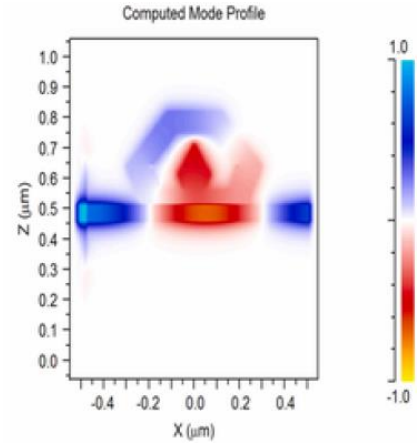

(C)

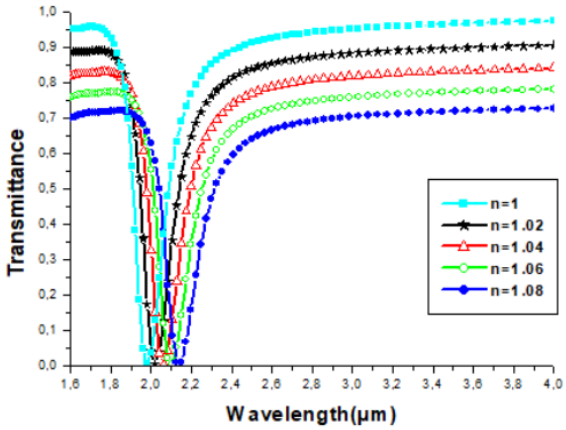

(d)

Figure IV.17 (a)*The transmission spectra of the MIM waveguide. (b) The contour profiles of field |Hz| of the resonator at 1.9826 μm, (c) for at 1.5 μm. (d)The transmission spectra of the structure for different refractive indices n.*

In our simulation, the TM polarized incident wave with electrical field components in the plane is directly coupled to the basic SPP mode [11]. The incident optical wave is converted into two parts, the transmitted wave and the reflected wave, by the resonator. A stable stationary wave can accumulate constructively in the resonator only when the following resonance condition is met [21]:

$$\Delta\varphi = 2\pi m, \quad m = 1,2, \ldots \tag{IV.3}$$

The resonance wavelength can be described as follows [22]:

$$\lambda_m = \frac{2L_{eff}n_{eff}}{m-\frac{\varphi_{ref}}{\pi}} \tag{IV.4}$$

Où L_{eff} is the actual resonator length and n_{eff} refers to the actual part of the SPP's effective refraction index , et φ_{ref} *is the phase-out of the SPP reflection on the metal wall of the resonator*.

IV.6.2 Geometric Optimization

IV.6.2.1 Influence of a the diamond cavity dimension on transmission spectrum and sensor sensitivity

We also conducted research on the performance of the geometry parameters in order to justify our design choices for this structure.

We began by investigating the diamond cavity dimension. Herein, the value of W is 50 nm, and L1 =600 nm, L2 =300 nm is fixed and uses symmetric parameters such as X Y and X1 =Y1 throughout this paper and to ensure the feasibility of the fabrication, we varied the length X Y= 90–110 nm with 10 nm steps (offered by the NIL (nanoimprint lithography) fabrication technique) and observed a slight shift in the resonant peak, as shown in Figure IV.18(a). Second, due to their sharpness and maximum transmission, we use the length X Y= 100 nm for the following analysis. As a result, in order to improve the properties of the plasmonic sensor, we investigated the effect of position g1 on the resonance wavelength shift in Figure IV.18(b). We consider g1 =50 nm to be the best value for surface plasmon propagation. Another important parameter to consider is the effect of X and Y lengths on the resonance wavelength, and we begin by using the following parameters: g1 =50 nm and X1 =Y1 =100 nm, while leaving the rest nchanged. The transmission spectra versus the dimensions of the HxTp as X Y= 150–210 nm with a range of 10 nm are shown in Figure IV.18(c). As we can see by increasing the lengths of X and Y, the peak's resonance wavelength shifts from 150 nm to 190 nm. We achieve two peaks in the nearinfrared (NIR) at 1505.8 nm, 1797.9 nm, and in the mid-IR at 3555.71, 3902.3 nm for 200, 210 nm, seeking to make this structure suitable for all ranges of optical communication and biomedical applications. During these shifts, we lose transmission power due to interactions between the surface plasmon polaritons SPPs and the increased lossy metallic part.

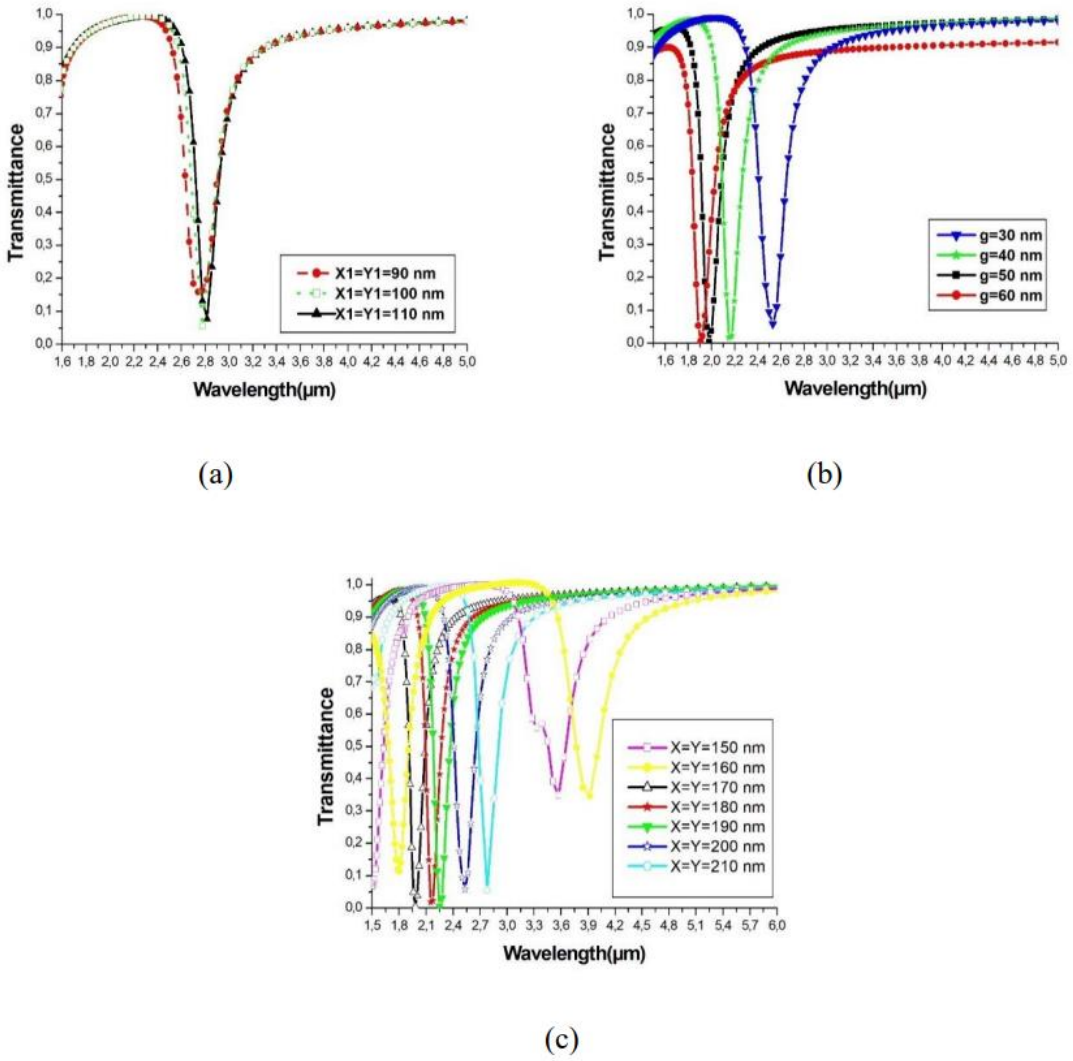

Figure IV.18 *(a) the transmission spectrum for different dimensions of diamond cavity X Y= 90–110 nm with a step of 10 nm. (b) the transmission spectra versus the position of the inner cavity with g1 =20–60 nm with a step of 10 nm. (c) the transmission spectra versus the dimension of h HxTp as X Y= 150–210 nm with a range of 10 nm.*

IV.6. 3 the Biomedical and Environment Applications of the Proposed Plasmonic Sensor

In part three, we look at the geometry of the proposed structure, which is composed of X1, Y1, g1, X, and Y. These structural variables control the resonance wavelength. The following section uses the sharper peak that occupies a narrower bandwidth in mid-IR from the preceding results, as illustrated in Figure IV 17(a). Since the mid-IR range is well-suited for biosensing as it encompasses the molecular vibrations that uniquely identify the biochemical building.

In addition, engineered mid-IR substrates with extremely high field enhancements at distinct resonance wavelengths enable the ultrasensitive IR detection of small amounts of

biomolecules. Thus, the sensing parameters are as follows: X1=Y1=100 nm and g1, X=Y, as 50 nm and 190 nm, respectively.

The proposed plasmonic sensor in biomedical applications has been studied. Using a 25% glucose solution in water changes the refractive index of water from nw = 1.3198 to ng = 1.3594, as Figure IV 19 (a) shows that we obtained a narrow, sharp peak with high transmission at the mid-IR range. A shift occurs as we change the RI of the surrounding medium, the sensitivity we abstained is 2329.2 nm/RIU. W carre out the reseach on the temper sensor, the dielectric of the structure is filled with ethanol material, the refractive index of ethanol material can be calculated as $n=n_0-dn/dT(T-T_0)$ (4)

Where T_0 as the ambient temperature at 200 C, $dn/dT = 3.94\times10^{-4}$, n_0 =1.36084, T is the ambient temperature from 100 to -100 with a step of 400C. As shown in Figure IV 19 (b), we achieve a sensitivity reach to 1.77 nm/C^0.

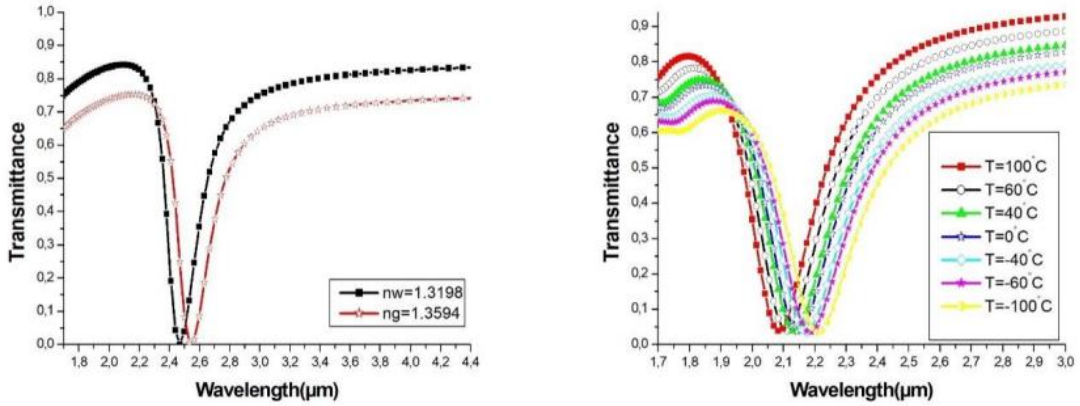

Figure IV 19 (a) *the peak of the transmission spectra versus the resonance wavelength for refractive index of the waternw=1.3198 and 25% solution of glucose in water as ng=1.3594, (b) the transmission spectra versus the resonancewavelength for refractive index of the temper ambient from T=100 to -100 with a step of 400C.*

To investigate all the potential of this structure, we studied the phenomenon theory of Fano resonance. As a fundamental resonant effect, the Fano resonance, which arises from the interference between a localized state and a continuum band [25], has been widely known in numerous physic systems. Unlike the Lorentzian resonance, the Fano resonance exhibits a typically sharp and asymmetric line profile, which has excellent critical applications in demultiplexing, plasmonic switch, and so on. Fano resonance profile promises a new application in sensors. Thus, optical components can use ultra-compact plasmonic structure, realizing Fano resonance in highly integrated optics [26].

As pointed out, we studied the phenomenon of Fano resonance by using a discontinuous waveguide with a distance of C, as shown in Figure IV 20 (a). First, we reduce the length g1 to 0 nm, and we increase the length C from 50 to 200 nm. The result shows that a Fano resonance occurs. However, as we increase the distance C from 0 to 50 nm, the peak becomes sharper and narrower till the optimum value with C=200 nm. We achieve a Fano resonance with high transmission and sharp bandwidth, as shown in Figure IV 20 (b). Moreover, this design has a potential application as switch ON (with g1=10nm and C=0 nm) and OFF (with g1=0nm and C=200 nm).

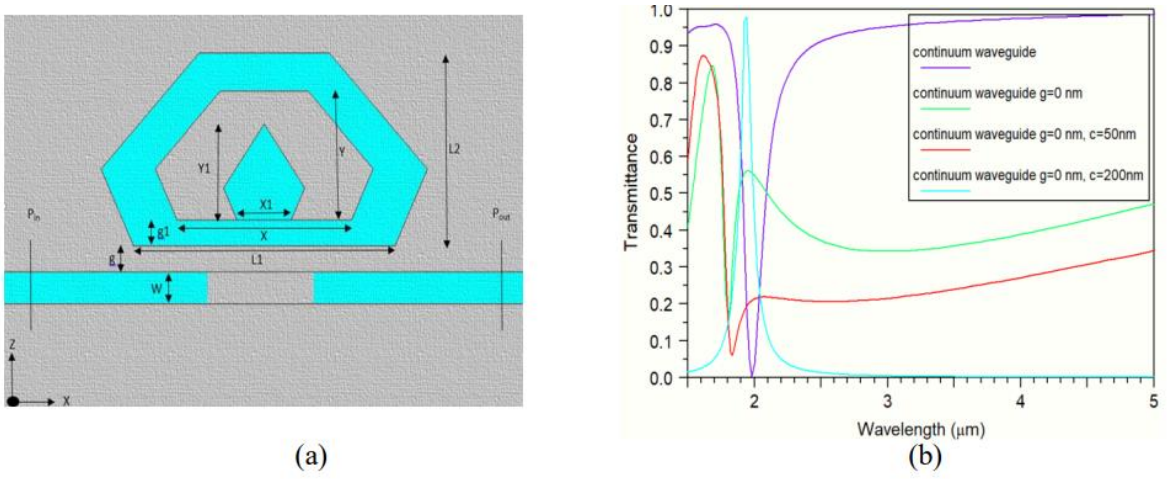

Figure IV 20 *(a) The schematic diagram of the proposed sensor structure with discontinue waveguide with a distance of C. (b) The transmission spectra versus the resonance wavelength for different states with continuum waveguide for g= 10–0 nm and discontinuewaveguide for g= 0 and C= 50, 200 nm.*

IV.7 Comparison of the proposed sensors with different designs of the literature based on plasmonic structures MIM

The following table shows a comparison of the sensitivity (S) for different MIM plasmonic sensors, with other works in the literature.

references	Sensitivity (nm/RIU)	year
[1] Nano-Rods in Hexagonal 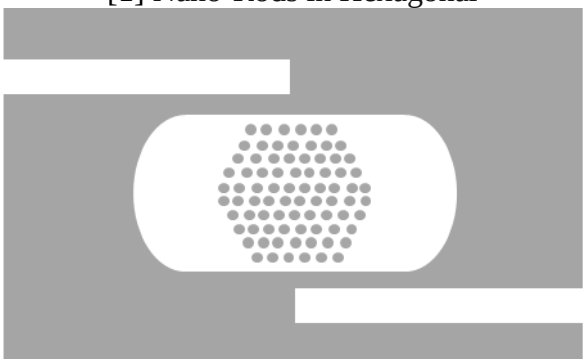	2610	2017
[2]Square Ring Metal-Insulator-Metal Waveguide-Based 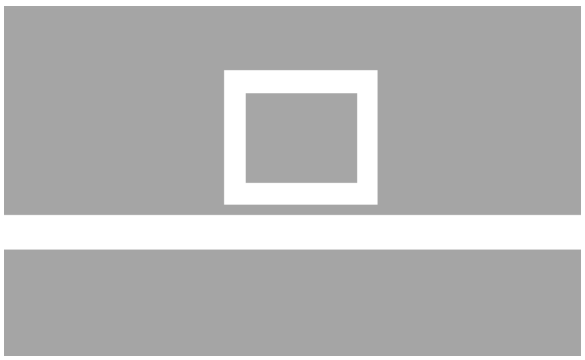	1496	2019
[3]Metal-Insulator-Metal Waveguide-Based two consecutive disk resonators 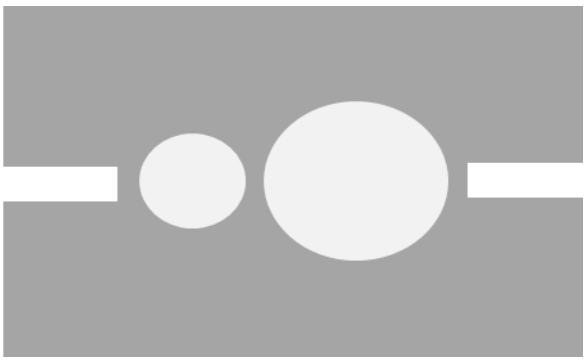	1500	2020

[4] Metal-Insulator-Metal Waveguide-Based Racetrack Integrated Circular 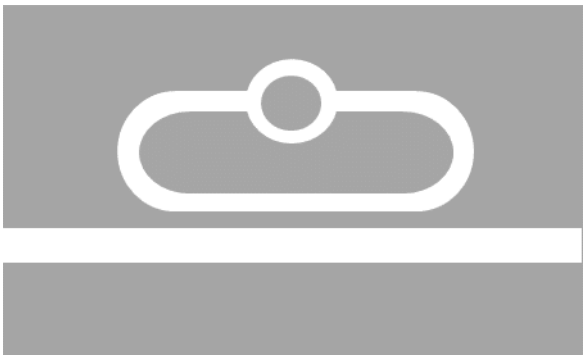	1400	2021
[5] ring-hexagonal resonator 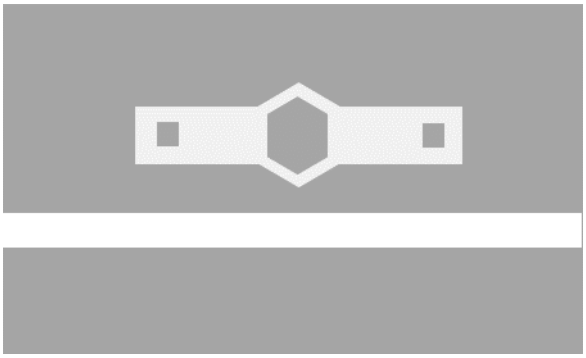	2115	2022
[6]a concentric-ring resonator 	1250	2023
[7] octagonal cavity resonator inside a square disk	2527.6	2023

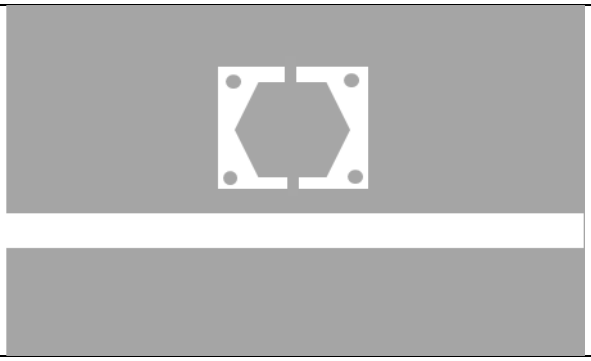		
[8] Trapezoidal-Shaped 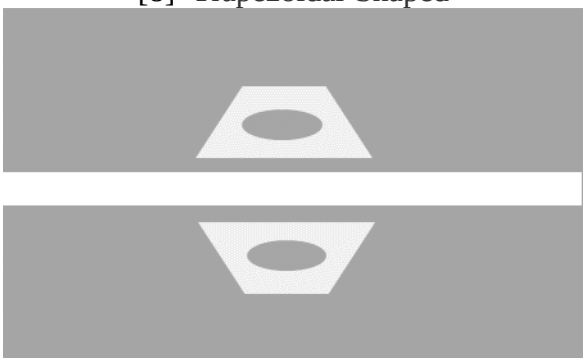	1328,57	2023
[9]**square split-ring cavity with a square center** 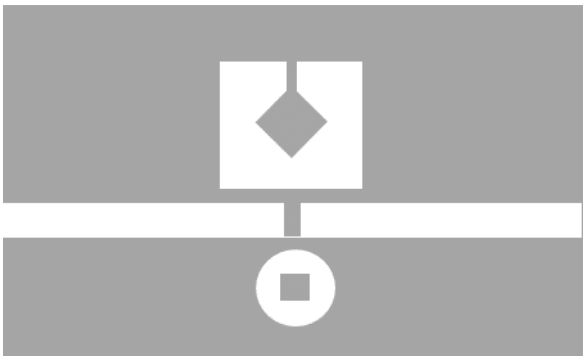	2453.33	2023
Our work **MIM Coupled With a Rectangular Cavity** [9] **MIM Waveguide with Notch Ring Resonator** [9] **MIM with a Notched Hexagonal Ring and a Stub** [9] **MIM with diamond resonator**[9]	3010 4508 2547 5155	2021 2021 2021 2022

Tableau IV. 1 *Comparison of the proposed sensors with different designs of the literature based on plasmonic structures MIM.*

IV.8 Conclusion

In this chapter, we have presented three proposals of RI nano-sensors with two-dimensional plasmonic structures using a metal-insulating-metal wave-guide (MIM). The Time Domain Finite Differences (FDTD) method integrated in the R-Soft commercial simulator is used to characterize all design variations.

The first proposed structure is a MIM waveguide coupled with a rectangular resonator for a near-infrared refraction index sensor. The transmission peak positions are linear in nature relative to the refractive index of the detected material, and can be easily manipulated by adjusting the length of the rectangular. In this structure, the maximum linear sensitivity is S = 1650 nm/RIU and S = 3010 nm/ RIU for mode 2 and mode 1 respectively, after optimization of structural parameters. Furthermore, when introducing another cavity inside the main rectangular, the senstivity is improved, making our proposed design an attractive candidate for a biosensor performance.

The second proposed structure is a MIM wave-guide coupled with Notch Ring Resonator. The positions of the transmission peaks have linear relations with the refraction index. Furthermore, in this structure, and after optimization of its structural parameters, the maximum linear sensitivity obtained is S = 4508 nm/RIU. This structure can also be used as a band cut sensor, as the positions of transmission peaks and bandwidth can be easily manipulated by adjusting the inner radius of the ring resonators and the rectangular distance. This performance makes our design proposal an attractive candidate for both a nanosensor and a band cutter.

Finally, the third proposed structure is a simple high-sensitivity medium-infrared plasmon refraction index sensor. Simplicity, detection sensitivity and transmission spectrum level that can be easily controlled by manipulating structural parameters are the main advantages of this structure. The designed MIM sensor (with diamond resonator) establishes a high transmission, with the same improved sensitivity of 5155 nm/RIU. As an example of application, we utilized the final structure: glucose biosensor, showing a sensitivity of 2329.3 nm/ RIU over an interval ranging from 0 to 300 g/L.

General conclusion

General conclusion

Surface plasmon resonance (SPR) has undoubtedly played a pivotal role in advancing emerging optical technologies. The unique characteristics of surface plasmons, encompassing the ability to confine light at dielectric-metal interfaces, have opened doors to a wide array of applications. These applications span a broad spectrum, encompassing fields such as biomolecule detection, optical enhancement, plasmonic solar cells, optical filters, and sensors, among others. Recent investigations have concentrated their efforts on the development of optical sensors founded upon plasmonic structures, particularly surface plasmon polaritons (SPP), incorporating metal-insulating-metal (MIM) waveguides for refractive index (RI) measurements.

The choice of MIM waveguides has been predicated upon their capacity to facilitate extensive propagation distances and profound field confinement, rendering them a favored platform for SPP waveguides. The manuscript at hand represents a valuable contribution to the ongoing exploration of MIM-based biosensors, meticulously tailored for RI measurements. Notably, refractive index is a foundational property interconnected with diverse parameters, thereby enabling the fabrication of sensors tailored for applications spanning temperature, pressure, humidity, DNA analysis, and the precise quantification of chemicals and proteins. The sensitivity of these sensors, that is, their capability to discern minute variations in refractive index, stands as a critical yardstick of their effectiveness.

To augment sensitivity, the strategic inclusion of MIM resonators emerges as a promising avenue. By introducing defect cavities into conventional MIM waveguides, the interaction length between surface plasmon polariton (SPP) modes and the target molecules within the active sensor region is significantly prolonged. This extension of interaction theoretically augments the sensitivity of the generated SPPs. Within the realm of MIM structures, the plasmonic resonator assumes a paramount role, exerting a profound influence on detection characteristics and device transmission. The core thrust of this work pertains to the meticulous design of plasmonic RI nano-sensors hinging on two-dimensional MIM waveguides constructed from silver, distinguished by diverse cavity geometries. The overarching objective is the optimization of both transmission and sensitivity within these nano-sensors.

The inaugural chapter serves as a foundational reservoir of theoretical insights encompassing surface plasmon resonance (SPR), optical coupling methodologies, and the fundamental attributes characterizing surface plasmon waves. Within the purview of plasmonics, gold and

silver reign supreme as the metals of choice, owing to their ability to sustain surface plasmons across the visible-near-infrared spectrum, a region where their dielectric permittivity assumes negative values. Furthermore, gold and silver exhibit minimal losses and correspondingly extensive propagation lengths within this spectral domain. Silver, in particular, distinguishes itself by boasting the closest plasmon resonance, thereby offering superior theoretical sensitivity. As such, it emerges as a more discerning choice for performance-driven applications when compared to gold.

The second chapter navigates through a compendium of applications rooted in surface plasmon resonance. These applications are systematically categorized into three overarching research themes: microscopic detection and surface interfaces, nano-photonic applications, and the domain of biomolecule detection. Furthermore, the chapter delves into the operative principles underpinning SPR effect sensors, in addition to elaborating upon their performance metrics, including sensitivity, resolution, and detection limits.

The third chapter introduces the simulation tool that forms the linchpin of this work, specifically FullWAVE. Leveraging the Finite-Difference Time-Domain (FDTD) algorithm, FullWAVE is uniquely tailored to facilitate in-depth investigations into two-dimensional plasmonic structures. The FDTD algorithm stands as a potent method for modeling electromagnetic phenomena within intricate and multifaceted structures, thereby serving as a powerful tool for the comprehensive exploration of plasmonic nano-sensors.

Bibliography

General introduction:

[1] M.I. Stockman, et al. « Roadmap on Plasmonics », J. Optics, vol. 20, p. 043001, 2018.

[2] F.Z. Zou, X. Pan, W. Luo, B. Yan, « Multiple-channel plasmonic filter based on metal-Insulator-Metal waveguide and fractal theory », Plasmonics, vol.12, pp. 1589–1594, 2017.

[3] M. Kwon, J. Shin, J.H. Lee, « Metal-insulator-silicon-insulator-metal waveguide splitters with large-arm separation », J. Lightwave Technology. vol.33, pp. 3843–3849, 2015.

[4] Z. Lu, R. Yang, R.A. Wahsheh, M.A.G. Abushagur, « Nanoplasmonic couplers and modulators based on metal-insulator-metal structures », Proceeding of SPIE 7604, Integrated Optics: Devices, Materials, and Technologies, vol. 7604, p.760419, 2010.

[5] M. Danaie, A. Geravand, « Design of low-cross-talk metal–insulator–metal plasmonic waveguide intersections based on proposed cross-shaped resonators », J. Nanophotonics, vol. 12, pp. 1-40, 2018.

[6] K. Li, M.I. Stockman, D.J. Bergman, « Self-similar chain of metal nano spheres as an efficient nanolens », Phys. Rev, vol. 91, pp. 227402-227405, 2003.

[7] S. Yu, S. Wang, T. Zhao, J. Yu, « Tunable plasmonic system based on a slotted side-coupled disk resonator and its multiple applications on chip-scale devices », Optik - International Journal for Light and Electron Optics, vol. 212, pp. 164748-164755, 2020.

[8] M. R. Rakhshani, « Refractive index sensor based on concentric triple racetrack resonators side coupled to metal–insulator–metal waveguide for glucose sensing », J. Optical Society of America B, vol. 36, pp. 2834-2842, 2019.

[9] P. Pfeifer, U. Aldinger, G. Schwotzer, S. Diekman, P. Steinrucke, « Real time sensing of specific molecular binding using surface plasmon resonance spectroscopy », Sensors and Actuators B: Chemical, vol. 54, pp. 166-175, 1999.

[10] T.S. Wu, Y.M. Liu, Z.Y. Yu, Y.W. Peng, C.G. Shu, H. Ye, « The sensing characteristics of plasmonic waveguide with a ring resonator », Optics. Express, vol. 22, pp. 7669–7677, 2014.

[11] J. Zhu, X. Huang, J. Tao, X. Jin, X. Mei, « Nanometeric plasmonic refractive index senor », Opt. Commun, vol. 285, pp. 3242–3245, 2012.

[12] X. Jin, X. Huang, J. Tao, X. Lin, Q. Zhang, « A novel nanometeric plasmonic refractive index sensor » , IEEE Transactions on Nanotechnology, vol. 9, pp. 134–137, 2010.

[13] A. Dolatabady, N. Granpayeh, V.F. Nezhad, « A nanoscale refractive index sensor in two dimensional plasmonic waveguide with nanodisk resonator », Opt. Commun, vol. 300, pp. 265–268, 2013.

[14] T. Wu, Y. Liu, Z. Yu, Y. Peng, C. Shu, H. He, « The sensing characteristics of plasmonic waveguide with a single defect », Opt. Commun, vol. 323, pp. 44–48, 2014.

Bibliography

Chapter I:

[1] W. L. Barnes, A. Dereux, T. W. Ebbesen, « Surface plasmon subwavelength optics », Nature, vol. 424, pp. 824–830, 2003.

[2] S. A. Guebrou, « Influence des plasmons de surface propagatifs sur la cohérence de systemes optiques », Thèse de Doctorat n.217, Université Claude Bernard-Lyon I, 2012.

[3] L. Tonks, I. Langmuir, « Oscillations in ionized gases », Phys. Rev, vol. 33, pp. 195–210, 1929.

[4] N. Ashcroft, N.D. Mermin, « Physique des Solides », EDP Sciences, Les Ulis, 2002.

[5] J. Proust, « Etudes, caractérisation et optimisation expérimentales de nano-capteurs plasmoniques », Thèse de Doctorat, Université de technologie Troyes, 2014.

[6] C. Kittel, « Introduction to solid state physics », 8Th Edition Wiley India Pvt. Limited, 2005.

[7] Thomas Lopez. « Conception, fabrication et caractérisation de lentilles planaires nano structurées dédiées aux capteurs d'images CMOS dans le proche-infrarouge ». Thèse de Doctorat, Université de Toulouse, 2016.

[8] P. Lecaruyer, M. Canva, J. Rolland, « Metallic film optimization in a surface plasmon resonance biosensor by the extended rouard method », Appl. Opt, vol. 46, pp. 2361–2369, 2007.

[9] P. B. Johnson, R. W. Christy, « Optical Constants of the Noble Metals », Phys. Rev. B, vol. 6, pp. 4370–4379, Décembre 1972.

[10] A. D. Rakic, A. B. Djurisic, J. M. Elazar, M. L. Majewski, « Optical properties of metallic films for vertical cavity optoelectronic devices », Appl. Opt, vol.37, pp. 5271-5283, Août 1998.

[11] WebElements, https://www.webelements.com, accessed March 2024l. 06-01-2021.

[12] http://www.webelements.com/silver/compounds.html. 06-01-2021.

[13] H. Raether, « Surface plasmons on smooth and rough surfaces and on gratings », Springer Tracts in Modern Physics, vol. 111, Springer, Berlin, Heidelberg, 1988.

[14] S. A. Maier, Plasmonics - Fundamentals and Applications », Springer, 2007

[15] E. A. Stern, R. A. Ferrell, « Surface plasma oscillations of a degenerate electron gas », Phys. Rev, vol. 120, pp. 130-136, 1960.

[16] X. Mao and M. Cada, "Optical Surface Plasmon in Semiconductors," in Advanced Photonics 2013.

[17] R. Gordon, A. G. Brolo, « Increased cut-off wavelength for a subwavelength hole in a real metal », Opt. Express, vol. 13, pp. 1933– 1938, 2005.

[18] E. Anemogiannis, E. N. Glytsis, T. K. Gaylord, « Determination of guided and leaky modes in lossless and lossy planar multilayer optical waveguides: reflection pole method and wavevector density method », J. Lightwave Technology, vol. 17, pp. 929–941, 1999.

Bibliography

Chapter II:

[1] Commercializing plasmonics, Editorial, Nature Photonics, vol. 9, p. 477, 2015.

[2] Focusing on applications, Editorial, Nature Nanotechnology, vol. 10, p. 1, 2015.

[3] Cesar Clavero, « Plasmon-induced hot-electron generation at nanoparticle/metal-oxide interfaces for photovoltaic and photocatalytic devices », Review, Nature Photonics, vol. 8, pp. 95-103, 2014.

[4] Pierre Viste, « Brevets en plasmonique : les tendances depuis 20 ans », Photoniques, vol. 90, pp. 19-20, 2018.

[5] W. L. Barnes, bv Surface plasmon-polarition lenght scales: a route to sub-wavelenght optics », Journal of Optics A, vol. 8, pp. 87-93, 2006.

[6] D. Courjon et C. Bainier, « Le Champ proche optique : Théorie et applications », edité chez Springer, Paris, 2001.

[7] S. Bozhevolnyi, A.Boltasseva, T. Søndergaard, T. Nikolajsen, K. Leosson, « Photonic bandgap structures for long-range surface plasmon polaritons », Optics Communications, vol. 250, pp. 328-333, 2005.

[8] Benoit Rogez, « Excitation électrique locale de nanostructures plasmoniques par la pointe d'un microscope à effet tunnel », Thèse de doctorat, Université Paris Sud - Paris XI, 2014.

[9] C-V. Tapor, M. Puiu, C. Bala, « Strategies for Surface Design in Surface Plasmon Resonance (SPR) Sensing», Biosensors, vol, 13,pp. 465, 2023.

[10] RD. Al Bostami, WH. Abuwatfa, GA. Husseini, « Recent Advances in Nanoparticle-Based Co-Delivery Systems for Cancer Therapy. », Nanomaterials (Basel), vol, 15, pp. 2672, 2022

[11] R.C. Jorgenson, S.S. Yee, « A fiber-optic chemical sensor based on surface plasmon resonance », Sensors and Actuators B: Chemical, vol. 12, pp. 213–220, 1993.

[12] R.C. Jorgenson, « Surface plasmon resonance based bulk optic and fiber optic sensors », Ph.D. Dissertation, University of Washington, Seattle, WA, USA, 1993.

[13] D. Sarid, « Long-Range Surface-Plasma Waves on Very Thin Metal Films », Phys. Rev. Lett, vol. 47, pp. 1927–1930, 1981.

[14] S. A. Maier, H. A. Atwater, « Plasmonics: Localization and guiding of electromagnetic energy in metal/dielectric structures », J. Appl. Phys., vol. 98, p. 011101, Juillet 2005.

[15] C. Billaudeau. « Guidage optique dans les cristaux plasmoniques 1D et 2D ». Thèse de doctorat en Physique Atomique, Université Paris Sud - Paris XI, 2007.

[16] B. Liedberg, C. Nylander, I. Lundström, « Biosensing with surface plasmon resonance-How it all started », Biosensors and Bioelectronics, vol. 10, pp. i-ix, 1995.

[17] R.W. Wood, « On a remarkable case of uneven distribution of light in a diffraction grating spectrum », Phil. Mag, vol. 4, pp. 396–402, 1902.

[18] U. Fano, « The theory of anomalous diffraction gratings and of quasi-stationary waves on metallic surfaces (sommerfeld's waves) », J. Opt. Soc. Am, vol. 31, pp. 213–222, 1941.

[19] R.A. Ferrell, « Predicted radiation of plasma oscillations in metal films », Physical Review, vol. 111, pp. 1214–1222, 1958.

[20] A. Otto, « Excitation of nonradiative surface plasma waves in silver by the method of frustrated total reflection », Z. Phys, vol. 216, pp. 398– 410, 1968.

[21] E. Kretschmann, H. Raether, « Radiative decay of non radiative surface plasmons excited by light », Z. Naturforsch. A, vol. 23, pp. 2135–2136, 1968.

[22] M. Chamtouri, « Etude exhaustive de la sensibilité des Biopuces plasmoniques structurées intégrant un réseau rectangulaire 1D : effet de la transition des plasmons localisés vers les plasmons propagatifs », Thèse de doctorat en Physique, Université Paris Sud - Paris XI; Université de Tunis El Manar, 2013.

[23] B. Liedberg, C. Nylander, I. Lundstrom, « Surface plasmon resonance for gas detection and biosensing », Sens. Actuators, vol. 4, pp. 299–304, 1983.

[24] M. ZEKRITI, « Traitement théorique des capteurs à base de la résonance des plasmons de surface en configuration bimétallique », Thèse de doctorat en Physique, Université MOHAMMED V- AGDAL – Rabat, 2013.

[25] **N.** Miura, M. Sasaki, K.V. Gobi, C. Kataoka, Y. Shoyama, « Highly sensitive and selective surface plasmon resonance sensor for detection of sub-ppb levels of benzo [a] pyrene by indirect competitive immunoreaction method », Biosensors and Bioelectronics, vol. 18, pp. 953-959, 2003.

[26] K. Hegnerová, M. Bocková, H. Vaisocherová, Z. Krištofiková, J. Říčný, D. Řípová, J. Homola, « Surface plasmon resonance biosensors for detection of Alzheimer disease biomarker », Sensors and Actuators B: Chemical, vol. 139, pp. 69-73, 2009.

[27] N. MAALOULI, « Développement d'un banc plasmonique en goutte et conception de nouvelles interfaces appliquées à la biodétection », Thèse de doctorat en Optique et Lasers, Université de Lille 1, 2012.

[28] J. Zhu, X. Huang, J. Tao, X. Jin, X. Mei, « Nanometeric plasmonic refractive index senor », Opt. Commun, vol. 285, pp. 3242–3245, 2012.

Bibliography

Chapter III:

[1] P. Berini, « Bulk and surface sensitivities of surface plasmon waveguides », New J. Phys, vol. 10, pp. 105010-105046, 2008.

[2] D. Arbel, M. Orenstein, « Plasmonic modes in W-shaped metal-coated silicon grooves », Opt. Express, vol. 16, pp. 3114-3119, 2008.

[3] L. Dobrzynski, A. Akjouj, B. Djafari-Rouhani, J.O. Vasseur, M. Bouazaoui, J.P. Vilcot, H. AlWahsh, P. Zielinski, J.P. Vigneron, « Simple nanometric plasmon multiplexer », Phys. Rev. E, vol. 69, pp. 035601-035603, 2004.

[4] J. A. Dionne, L.A. Sweatlock, H.A. Atwater, A. Polman, « Planar metal plasmon waveguides: frequency-dependent dispersion, propagation, localization, and loss beyond the free electron model », Phys. Rev. B, vol. 72, pp. 075405-075415, 2005.

[5] Z. Yu, G. Veronis, S. Fan, M.L. Brongersma, « Gain-induced switching in metal-dielectric-metal plasmonic waveguides », Appl. Phys. Lett, vol. 92, p. 041117, 2008.

[6] RSoft Design Group, Inc, « FullWAVE 6.1User Guide », license 16847214, 1999-2008.

[7] A. Noual, Y. Pennec, A. Akjouj, B. Djafari-Rouhani, L. Dobrzynski, « Nanoscale plasmon waveguide including cavity resonator », J. Phys. Condens. Matter, vol. 21, p. 375301, 2009.

[8] A. Noual, A. Akjouj, Y. Pennec, B. Djafari-Rouhani, L. Dobrzynski, « Modeling of two-dimensional nanoscale Y-bent plasmonic waveguides with cavities for demultiplexing of the telecommunication wavelengths », New Journal of Physics, vol. 11**,** p. 103020, 2009.

[9] RSoft Design Group, Inc, « BandSolve 4.1 User Guide », license 16847214, 1999-2008.

[10] F. Bougriou, « Etude théorique des matériaux à bandes interdites photoniques bidimensionnels: Applications dans le domaine du guidage optique et la détection », Thèse de doctorat, Université Constantine 1, 2013.

[11] A. Harhouz, « Contribution à l'étude et la conception des capteurs à base de cristaux photoniques », Thèse de doctorat, Université Mohamed Boudiaf - M'sila, 2017.

[12] K.S.Yee, « Numerical solution of initial boundary value problems involving Maxwell's equations in isotropic media », IEEE Trans. Antennas and propagation, vol. 14, pp. 302-307, 1966.

[13] A. Taflove, M. Brodwin, « Numerical solution of steady-state electromagnetic scattering problems using the time-dependent Maxwell's equations », IEEE transactions on microwave theory and techniques, vol. 23, pp. 623-630, 1975.

[14] X. Wu ,X. Bao ,J. Shen, X. Chen, H. Cui, « Evaluation of Void Defects behind Tunnel Lining through GPR forward Simulation », Sensors, vol. 22, pp. 970, 22022,.

[15] A. Taflove, « The Finite-Difference Time-Domain Method », Norwood, MA: Artech House Inc, 1995.

[16] O. Bouleghlimat, « Etude des cristaux photoniques anisotropes pour l'application dans l'optique intégrée », Thèse de doctorat, Université Mohamed Boudiaf - M'sila, 2016.

[17] J. P. Berenger, « Three-dimensional perfectly matched layer for the absorption of electromagnetic waves », J. Comput. Phys, vol. 127, pp. 363-379, 1996.

[18] M. Moukhtari, « Contribution à L'étude et La Conception Des Cavités à Cristaux Magneto Photoniques », Thèse de doctorat en Electronique, Université Mohamed Boudiaf - M'sila, 2018.

[19] C. Kittel, « Physique de l'état solide », 8e éd., Paris : Dunod, 2007.

[20] R. A. Ammar, « Génération des plasmons polaritons de surface en configuration de Kretschmann », Journal of Advanced Research in Science and Technology, vol. 5, pp. 829-833, 2018.

[21] H. Ben salah, A. Hocini, M.N. Temmar, D. Khedrouche, « Design of mid infrared high sensitive metal-insulator-metal plasmonic sensor », Chinese Journal of Physics, vol. 61, pp. 86- 97, 2019.

[22] M.R. Rakhsani, M.A. Mansouri-Birjandi, « High-sensitivity plasmonic sensor based on metal- insulator-metal waveguide and hexagonal-ring cavity », IEEE Sens. J,vol. 16, pp. 3041–3046, 2016.

[23] W. Wu, J. Yang, J. Zhang, J. Huang, D. Chen, H. Wang, « Ultra-high resolution filter and optical field modulator based on a surface plasmon polariton », Opt. Lett, vol. 41, pp. 2310-2313, 2016.

[24] Y. Yu, J. Si, Y. Ning, M. Sun, X. Deng, « Plasmonic wavelength splitter based on a metal-insulator-metal waveguide with a graded grating coupler », *Opt. Lett*, vol. 42, pp. 187–190, 2017.

[25] F. Lu, Z. Wang, K. Li, A. Xu, « A plasmonic triple-wavelength demultiplexing structure based on MIM waveguide with side-coupled nanodisk cavities », IEEE Transactions on Nanotechnology, vol. 12, pp. 1185–1190, 2013.

[26] R. Grover, T.A. Ibrahim, T.N. Ding, Y. Leng, L.-C. Kuo, S. Kanakaraju, K. Amarnath, L.C. Calhoun, P.-T. Ho, « Laterally coupled InP-based single-mode microracetrack notch filter », IEEE Photonics Technology Letters, vol. 15, pp. 1082-1084, 2003.

[27] H. Lu, X. Liu, D. Mao, « Plasmonic analog of electromagnetically induced transparency in multi-nano resonatorcoupled waveguide systems », Phys. Rev. A, vol. 85, pp. 053803-053809, 2012.

[28] P.B. Johnson, R. W. Christy, « Optical constants of the noble metals », Phys. Rev. B, vol. 12, pp. 4370–4379, 1972.

[29] R. Zafar, M. Salim, « Enhanced figure of merit in fano resonance based plasmonic refractive index sensor », IEEE Sensors Journal, vol. 15, pp. 6313–6317, 2015.

[30] S.L. Xiang, G.H. Xu, « Tooth-shaped plasmonic waveguide filters with nanometeric sizes », Opt. Lett, vol. 33, pp. 2874-2876, 2008.

[31] S. Ghorbani, M. A. Dashti, M. Jabbari, « Plasmonic nano-sensor based on metal dielectric-metal waveguide with the octagonal cavity ring », Laser Phys, vol. 28, pp. 066208-066213, 2018.

[32] A. Noual, « Modélisation des structures nano plasmoniques et photoniques.Applications aux phénoménes de filtrage et à la conception de capteurs bioplasmoniques », Thèse de Doctorat, Université de Lille1, 2010.

[33] J. Zhu, X. Huang, J. Tao, X. Jin, X. Mei, « Nanometeric plasmonic refractive index senor », Opt. Commun, vol. 285, pp. 3242–3245, 2012.

[34] Q. Zhang, X.G. Huang, X.S. Lin, J. Tao, X.P. Jin, « A subwavelength coupler-type MIM optical filter », Optics Express, vol. 17, pp. 7549-7554, 2009.

Bibliography

Chapter IV:

[1] A. Lobnik, M. Turel, Š.K. Urek, « Optical chemical sensors: Design and applications », Advances in Chemical Sensors: Edited by Prof. Wen Wan, p. 358, 2012.

[2] P. Mehrotra, « Biosensors and their applications – Areview », Journal of Oral Biology and Craniofacial Research, vol. 6, pp. 153-159, 2016.

[3] Z. Madadi, K. Abedi, G. Darvish, M. Khatir, « An infrared narrowbandplasmonic perfect absorber as a sensor », Optik, vol. 183, pp. 670–676, 2019.

[4] T. S. Wu, Y. M. Liu, Z. Y. Yu, Y. W. Peng, C. G. Shu, H. Ye, « The sensing characteristics of plasmonic waveguide with a ring resonator », Opt. Express, vol. 22, pp. 7669–7677, 2014.

[5] M.R. Rakhshani, M.A. Mansouri-Birjandi,, « Utilizing the Metallic Nano-Rods in Hexagonal Configuration to Enhance Sensitivity of the Plasmonic Racetrack Resonator in Sensing Application », Plasmonic, vol. 12, pp. 999-1006, 2017.

[6] X. Jin, X. Huang, J. Tao, X. Lin, Q. Zhang, « A novel nanometeric plasmonic refractive index sensor », IEEE Transactions on Nanotechnology, vol. 9, pp. 134–137, 2010.

[7] Y. X. Huang, Y. Y. Xie, W. L. Zhao, H. J. Che, W. H. Xu, X. Li, J. C. Li, « A plasmonic refractive index sensor based on a MIM waveguide with a side-coupled nanodisk resonator », IEEE 20th International Conference on Embedded and Real-Time Computing Systems and Applications, Chongqing, China, 2014, pp. 1-5, 2014.

[8] T. Wu, Y. Liu, Z. Yu, Y. Peng, C. Shu, H. He, « The sensing characteristics of plasmonic waveguide with a single defect », Opt. Commun, vol. 323, pp. 44–48, 2014.

[9] M. J. Al-mahmod, R. Hyder, M. Z. Islam, « Numerical studies on a plasmonic temperature nanosensor based on a metal-insulator-metal ring resonator structure for optical integrated circuit applications », Photonics and Nanostructures - Fundamentals and Applications, vol. 25, pp. 52–57, 2017.

[10] Y. F.C. Chau, C.T.C. Chao, H.J. Huang, Y. C. Wang, H. P. Chiang, M.N.S.M. Idris, Z. Masri, C.M. Lim, « Strong and tunable plasmonic field coupling and enhancement generating from the protruded metal nanorods and dielectric cores », Results in Physics, vol. 13, p. 102290, 2019.

[11] P. K. Wei, Y. C. Huang, C. C. Chieng, F. G. Tseng, W. Fann, « Off-angle illumination induced surface plasmon coupling in subwavelength metallic slits », Opt. Express, vol. 13, pp. 10784–10794, 2005.

[12] A. Dolatabady, N. Granpayeh, V.F. Nezhad, « A nanoscale refractive index sensor in two dimensional plasmonic waveguide with nanodisk resonator », Opt. Commun, vol. 300, pp. 265–268, 2013.

[13] M. R. Rakhshani, M. A. Mansouri-Birjandi, « High-sensitivity plasmonic sensor based on metal-insulator-metal waveguide and hexagonal-ring cavity », IEEE Sensors Journal, vol. 16, pp. 3041-3046, 2016.

[14] J. Yin, J. Tian, R. Yang, « Investigation of the transmission properties of a plasmonic MIM waveguide coupled with two ring resonators », Materials Research Express, vol. 6, p. 035018, 2018.

[15] J. Chen, Y. Li, Z. Chen, J. Peng, J. Qian, J. Xu, Q. Sun, « Tunable resonances in the plasmonic split-ring resonator », IEEE Photonics Journal, vol. 6, pp. 1-6, 2014.

[16] Y. Y. Xie, Y. X. Huang, W. L. Zhao, W. H. Xu, C. He, « A Novel Plasmonic Sensor Based on Metal–Insulator–Metal Waveguide with Side-Coupled Hexagonal Cavity », IEEE Photonics Journal, vol. 7, pp. 1-2, 2015.

[17] T. Wu, Y. Liu, Z. Yu, Y. Peng, C. Shu, H. He, « The sensing characteristics of plasmonic waveguide with a single defect », Optics Communications, vol. 323, pp. 44-48, 2014.

[18] H. Zhao, X. G. Guang, J. Huang, « Novel optical directional coupler based on surface plasmon polaritons », Physica E: Low-dimensional Systems and Nanostructures, vol. 40, pp. 3025-3029, 2008.

[19] S. H. Kwon, « Deep Subwavelength-Scale Metal–Insulator–Metal Plasmonic Disk Cavities for Refractive Index Sensors », IEEE Photonics Journal, vol. 5, pp. 4800107-4800107, 2013.

[20] Z. Guo, K. Wen, Q. Hu, W. Lai, J. Lin, Y. Fang, « Plasmonic multichannel refractive index sensor based on subwavelength tangent-ring metal–insulator–metal waveguide », Sensors, vol. 18, p. 1348, 2018.

[21] Q. Zhang, X. G. Huang, X. S. Lin, J. Tao, X. P. Jin, « A subwave length coupler-type MIM optical filter », Optics Express, vol. 17, pp. 7549–7555, 2009.

[22] L. Chen, Y. Liu, Z. Yu, D. Wu, R. Ma, Y. Zhang, H. Ye, « Numerical analysis of a near-infrared plasmonic refractive index sensor with high figure of merit based on a fillet cavity », Optics Express, vol. 24, pp. 9975–9983, 2016.

[23] W. Yang, Y. F. Chou Chau, S. C. Jheng, « Analysis of transmittance properties of surface plasmon modes on periodic solid/outline bowtie nanoantenna arrays », Physics of Plasmas, vol. 20, p. 064503, 2013.

[24] S. Ghorbani, M. Sadeghi, Z. Adelpour, « A highly sensitive and compact plasmonic ring nano-biosensor for monitoring glucose concentration », Laser Physics, vol. 30, pp. 026204-026209, 2020.

[25] J. Pan, S. Qianhan, L. Zheng, G. Wang, F. Chen, « Super High Sensitivity Plasmonic Temperature Sensor Based on Square Ring Shape Resonator with Nanorods Defects», Optical and Quantum Electronics, 2021.

[26] N. Amoosoltani, N. Yasrebi, A. Farmani, A. Zarifkar, « A plasmonic nano-biosensor based on two consecutive disk resonators and unidirectional reflection less propagation effect », IEEE Sensors Journal, vol. 20. pp. 9097-9104, 2020.

[27] M. A. Butt,A. Andrzej Kaźmierczak, N. L. Kazanskiy, S. N. Khonina, « Metal-Insulator-Metal Waveguide-Based Racetrack Integrated Circular Cavity for Refractive Index Sensing Application», Electronics, vol. 10, pp. 1419, 2021.

[28] F. Aghaei, H. Bahador, High sensitivity metal-insulator-metal sensor based on ring-hexagonal resonator with a couple of square cavities connected», Physica Scripta, pp. 97, pp. 065508. 2022.

[29] F. Chen, W.X. Yang, « Nanosensor and slow light based on quintuple Fano resonances in a metal insulator metal waveguide coupled with a concentric-ring resonator », Journal of the Optical Society of America B,vol. 40, p. 736-742, 2023.

[30] M.A, Haque, R. Rahad,A.K.M. Rakib,S.S. Sharar, R.H. Sagor ,« Plasmonic sensor for rapid detection of water adulteration in honey and quantitative measurement of lactose concentration in solution», Results in Physics ,vol 51, p. 106733, 2023.

[31] Ghanavati, M. and M.A. Karami, « Ellipsoid Defect in Trapezoidal-Shaped Cavities Coupled to Multi-resonance Plasmonic Metal–Insulator-Metal Waveguide Toward Ultrasensitive Temperature Sensor», Plasmonics, vol. 18, p. 1047-1057, 2023.

[32] R. Zhang, H. Tian, Y. Liu, S. Cui, «Multiple Fano Resonances in a Metal Insulator Metal Waveguide for Nano-Sensing of Multiple Biological Parameters and Tunable Slow Light », Photonics,vol 10**,** 2023.

[33] H**.** Bahri, S. Mouetsi, A. Hocini, H. Ben salah. «A high sensitive sensor using MIM waveguide coupled with a rectangular cavity with Fano resonance», Opt Quantum Electron, vol. 53, pp. 332, 2021.

[34] H**.** Bahri, A. Hocini, S. Mouetsi, A. Hocini, H. Ben salah « Glucose Sensing on Plasmonic Nanostructures Using MIM Waveguide with Notch Ring Resonator», ECS J Solid State Sci Technol, vol. 10, pp. 071015. 2021

[35] H. Ben salah, A. Hocini, H**.** Bahri, N. Melouki « High Sensitivity Plasmonic Sensor Based on Metal Insulator Metal Waveguide Coupled with a Notched Hexagonal Ring Resonator and a Stub », ECS J Solid State Sci Technol, vol. 10, pp. 071030. 2021

[31] H. Bahri, S.Mouetsi, A.Hocini, H. Ben Slah S. Ingebrandt, V. Pachauri, M. Hamani, «, A high-sensitivity biosensor based on a metal-insulator-metal diamond resonator and application for biochemical and environment detections », Optik, vol, 271, pp. 170083, 2022.

Publications

1. Bahri H, Hocini A, Mouetsi S, Ben Salah H. Glucose Sensing on Plasmonic Nanostructures Using MIM Waveguide with Notch Ring Resonator. ECS Journal of Solid State Science and Technology. 2021/07/23 2021;10(7):071015.
2. Bahri H, Mouetsi S, Hocini A, Ben Salah H. A high sensitive sensor using MIM waveguide coupled with a rectangular cavity with Fano resonance. Optical and Quantum Electronics. 2021;53(6).
3. Ben Salah H, Hocini A, Bahri H, Melouki N. High Sensitivity Plasmonic Sensor Based on MetalInsulatorMetal Waveguide Coupled with a Notched Hexagonal Ring Resonator and a Stub. ECS Journal of Solid State Science and Technology. 2021;10(8).
4. Bahri H, Hocini A, Bensalah H, et al. A high-sensitivity biosensor based on a metal insulator metal diamond resonator and application for biochemical and environment detections. Optik. 2022/12/01/ 2022;271:170083.
5. Bensalah H, Hocini A, Bahri H. Design and Analysis of a Mid-Infrared Ultra-High Sensitive Sensor Based on Metal-Insulator-Metal Structure and Its Application for Temperature and Detection of Glucose. Progress In Electromagnetics Research M. 2022;112:81-91.
6. Bensalah H, Bahri H, Hocini A, Zegaar I, Ingebrandt S, Pachauri V. Design of a plasmonic sensor based on a nanosized structure for biochemical application. Journal of Physics: Conference Series. 2022;2240(1).
7. Zegaar I, Hocini A, Khedrouche D, Ben Salah H, bahri H. Plasmonic stop-band filter based on a MIM waveguide coupled with cavity resonators. Journal of Physics: Conference Series. 2022;2240(1).
8. Bensalah H, Hocini A, Bahri H, Khedrouche D, Ingebrandt S, Pachauri V. A plasmonic refractive index sensor with high sensitivity and its application for temperature and detection of biomolecules. Journal of Optics. 2023/09/01 2023;52(3):1035-1046.

International Communications

- H. Bahri, A. Hocini, S. Mouetsi, H. Bensalah. « High sensitivity sensor based on the Fano resonance ». 6th International Conference on Nanoscience and Nanotechnology (ICONN 2021), SRM IST, Chennai.

- Ben salah H, hocini abdesselam, Bahri H, Imane Zegaar « Design nanosize structure based on plasmonic biosensor for biochemical application ». Twenty-second International Summer School VEIT. 20 – 24 September 2021, Sozopol, Bulgaria

- Imane Zegaar, Ben salah H, hocini abdesselam, Bahri H, « Plasmonic band-pass filter based MIM waveguide couple with a cavity resonator » Twenty-second International Summer School VEIT. 20 – 24 September 2021, Sozopol, Bulgaria

- Hocine BAHRI, Souheil MOUETSI, Abdsselam HOCINI, Sven INGEBRANDT, Vivek PACHAURI, Hocine BEN SLAH, « A high-sensitivity biosensor based on metal–insulator–metal and rectangular resonator for biochemical detection.

The first international conference on electronics, artificial intelligence and new technologies ICEAINT-2021 8- 9 December 2021. University Larbi Ben M'hidi, Oum El Bouaghi, Algeria

doctoral thesis*: "Design of nanosized plasmonic structure for Biosensing applications"*
Presented by*: *Bahri Hocine*
Supervised by*: *Prof. Mouetsi Souheil and Prof. HOCINI Abdesselam*

Abstract

Surface Plasmon polaritons (SPPs) are surface electromagnetic waves propagating along a metal-dielectric interface and have great potential applications in the realization of highly integrated optical circuits due to their capability to overcome the diffraction limit of light. The introduction of cavities with defects in the conventional metal-insulator-metal (MIM) waveguide ensured a longer interaction between the SPP modes produced and the molecules under test presented in the active region of the sensor. In all MIM structures, the plasmon resonator is the critical part that influences the detection and transmission characteristics of the devices.

In this context, this thesis aims the study and design of plasmonic nano-sensors based on two-dimensional MIM waveguides made of silver for metal, for refractive index measurements (RI), for integrated optics application. The goal is to optimize the sensitivity and the transmission of these nano-sensors according to the physical and geometric parameters. To do this, we focus in our study on three concepts of RI nano-sensors with MIM plasmonic structures. The first structure concerns a MIM based waveguide plate coupled by a hexagonal shaped ring resonator for a near infrared refractive index sensor. In this structure, the maximum linear sensitivity is S = 2220 nm / RIU and S = 3010 nm / RIU for mode 2 and mode 1 respectively. In the second structure, we propose a MIM waveguide coupled to intersected double cavity ring resonators for a refractive index sensor. In this structure, and after optimization of its structural parameters, the maximum linear sensitivity obtained is S = 4508 nm / RIU. The third structure concerns a simple design of mid infrared high sensitive metal-insulator-metal plasmonic sensor. In this structure, and after optimization of its structural parameters, the maximum linear sensitivity obtained is S = 5155 nm / RIU. In the three concepts of RI nano-sensors; the simplicity, the sensitivity of detection and the level of the transmission spectrum which can be easily controlled by manipulating the structural parameters; are the main advantages of these structures.

Keywords: *Surface plasmon polariton (SPP) – Metal – insulator – metal (MIM) waveguide - Refractive index sensor – FDTD.*

الملخص

بولاريتون البلازمون السطحي (SPP) عبارة عن موجات كهرومغناطيسية سطحية تنتشر على طول واجهة معدنية عازلة ولها تطبيقات محتملة كبيرة في صنع دوائر ضوئية متكاملة للغاية نظرًا لقدرتها على التغلب على محدودية انحراف الضوء. كفل إدخال التجاويف التي بها عيوب في الدليل الموجي MIM تفاعلًا أطول بين أوضاع SPP المنتجة والجزيئات قيد الاختبار المعروضة في المنطقة النشطة من المستشعر. في جميع هياكل MIM ، يعتبر مرنان البلازمونيك هو الجزء الحاسم الذي يؤثر على خصائص الكشف والإرسال للأجهزة.

في هذا السياق ، تهدف هذه الأطروحة إلى دراسة وتصميم مستشعرات النانو البلازمية بناءً على أدلة موجية ثنائية الأبعاد (MIM) المكونة من الفضة للمعدن لقياسات معامل الانكسار (RI) للتطبيق في البصريات المتكاملة. الهدف هو تحسين حساسية هذه المستشعرات النانوية ونقلها وفقًا للمعايير الفيزيائية والهندسية. لهذا ، استندنا في دراستنا إلى ثلاثة مفاهيم لمستشعرات النانو RI مع هياكل البلازمونيك. يقدم الهيكل الأول؛ لوحة دليل موجي قائمة على MIM مقترنة بمرنان حلقة سداسية الشكل لمستشعر معامل الانكسار القريب من الأشعة تحت الحمراء. في هذا الهيكل، يكون الحد الأقصى للحساسية الخطية S = 3010 nm / RIU وS = 2220 nm / RIU للوضع 2 والوضع 1 على التوالي. يقدم الهيكل الثاني ؛ دليل موجي MIM مقترن بمرنان حلقة تجويف مزدوجة متقاطعة لجهاز استشعار معامل الانكسار. في هذا الهيكل، وبعد تحسين المعلمات الهيكلية، يكون الحد الأقصى للحساسية الخطية التي تم الحصول عليها هوS = 4508 nm / RIU للوضع 2 والوضع 1 على التوالي. يقترح الهيكل الثالث تصميم بسيط لمستشعرMIM بلازمونيك عالي الحساسية للأشعة تحت الحمراء المتوسطة. في هذا الهيكل، وبعد تحسين المعلمات الهيكلية، يكون الحد الأقصى للحساسية الخطية التي تم الحصول عليها هو S= 5155 nm/RIU. في المفاهيم الثلاثة لمستشعرات النانو RI ؛ بساطة وحساسية الكشف ومستوى طيف الإرسال الذي يمكن التحكم فيه بسهولة عن طريق معالجة المعلمات الهيكلية ؛ هي المزايا الرئيسية لهذه الهياكل.

الكلمات المفتاحية : *بولاريتون البلازمون السطحي(SPP) - دليل موجي معدن- عازل- معدن (MIM)– مستشعر معامل الانكسار .FDTD.*